



저작자표시-비영리-변경금지 2.0 대한민국

이용자는 아래의 조건을 따르는 경우에 한하여 자유롭게

- 이 저작물을 복제, 배포, 전송, 전시, 공연 및 방송할 수 있습니다.

다음과 같은 조건을 따라야 합니다:



저작자표시. 귀하는 원저작자를 표시하여야 합니다.



비영리. 귀하는 이 저작물을 영리 목적으로 이용할 수 없습니다.



변경금지. 귀하는 이 저작물을 개작, 변형 또는 가공할 수 없습니다.

- 귀하는, 이 저작물의 재이용이나 배포의 경우, 이 저작물에 적용된 이용허락조건을 명확하게 나타내어야 합니다.
- 저작권자로부터 별도의 허가를 받으면 이러한 조건들은 적용되지 않습니다.

저작권법에 따른 이용자의 권리는 위의 내용에 의하여 영향을 받지 않습니다.

이것은 [이용허락규약\(Legal Code\)](#)을 이해하기 쉽게 요약한 것입니다.

[Disclaimer](#)

**Doctor of Philosophy**

**Development of one-step and fast manufacturing  
process for stable superhydrophobic surface using  
laser beam machining under silicone oil on  
metals and ceramics**

The Graduate School of the University of Ulsan

School of Mechanical Engineering

**Dinh The Hung**

Development of one-step and fast manufacturing  
process for stable superhydrophobic surface using  
laser beam machining under silicone oil on  
metals and ceramics

Supervisor: Professor Doo-Man Chun

A Dissertation

Submitted to the Graduate School of the University of Ulsan in Partial  
Fulfillment of the Requirements for the Degree of  
Doctor of Philosophy

by

**Dinh The Hung**

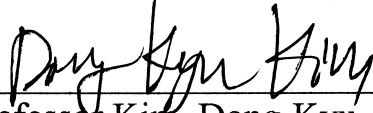
School of Mechanical Engineering

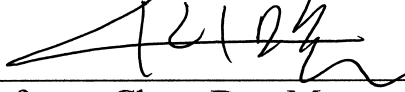
University of Ulsan, South Korea

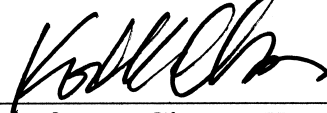
August 2021

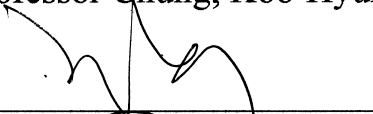
**Development of one-step and fast manufacturing  
process for stable superhydrophobic surface using  
laser beam machining under silicone oil on  
metals and ceramics**

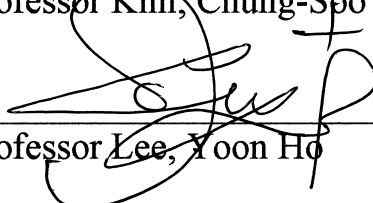
This certifies that the thesis of Dinh The Hung is approved

  
\_\_\_\_\_  
Committee Chairman: Professor Kim, Dong-Kyu

  
\_\_\_\_\_  
Committee Member: Professor Chun, Doo-Man

  
\_\_\_\_\_  
Committee Member: Professor Chung, Koo-Hyun

  
\_\_\_\_\_  
Committee Member: Professor Kim, Chung-Soo

  
\_\_\_\_\_  
Committee Member: Professor Lee, Yoon Ho

School of Mechanical Engineering

University of Ulsan, South Korea

August 2021

Dinh The Hung 의  
공학박사 학위 논문을 인준함

심사위원장 김동규

심사위원 천두만

심사위원 정구현

심사위원 김충수

심사위원 이윤희



울산대학교 대학원

2021년 08월

# Acknowledgments

First and foremost, I am extremely grateful to my supervisor, Prof. Doo-Man Chun, for his invaluable advice, support, and patience during my Ph.D. study. His immense knowledge and plentiful experience have encouraged me in all the time of my academic research and my daily life.

Besides my advisor, I would like to thank the rest of my thesis committee: Professors Dong-Kyu Kim, Koo-Hyun Chung, Chung-Soo Kim, and Yoon Ho Lee for their encouragement, insightful comments that helped me to further improve my dissertation.

I would like to thank all the members of the Hybrid Manufacturing Technology Lab. It is their kind help and support that made my study and life in Korea a wonderful time.

Finally, I would like to express my gratitude to my parents, my wife, and my sister. Without their tremendous understanding and encouragement in the past few years, it would be impossible for me to complete my study.

# Abstract

Recently, a number of publications using laser fabrication superhydrophobic surfaces have increased. After laser fabrication, the surface exhibits hydrophilicity, so it is necessary to combine with other methods to create a superhydrophobic surface. As a result, laser combined with heat treatment was chosen to fabricate the superhydrophobic surface because this post-process doesn't need chemical treatment or complex equipment. With this post-process, two kinds of materials as titanium, soda-lime glass were chosen for the fabrication of superhydrophobic surfaces. And the effect of laser power, step size, and pattern design on wettability were investigated. However, taking a long time for heat treatment as for 6 hours for titanium, 48 hours for soda-lime glass is one of the most disadvantages. Therefore, developing a new, simple, and fast process for the fabrication of superhydrophobic surfaces is essential. This new process used laser beam machining under silicone oil for fabricating superhydrophobic on various materials. In detail, with the new process, the study also reported the influence of changing laser parameters such as laser power, scan speed, step size, pattern design (grid, line-patterned), and silicone oil height during the fabrication process. Besides, the stability and robustness of the surface fabrication in the two processes (new process and post-process) to be used for evaluating the quality of the surface were also investigated. The stability of the superhydrophobic surface was tested by an aging test – put in the ambient air for a long time. Meanwhile, the robustness of the superhydrophobic surface was checked by scotch tape test. Finally, some potential applications were reported as water bouncing, water adhesion, self-cleaning, water position, controlling of water moving with different shapes (maze, circle, zigzag).

# Contents

<b>Acknowledgments</b> .....	i
<b>Abstract</b> .....	ii
<b>Contents</b> .....	iii
<b>List of Figures</b> .....	vi
<b>List of Tables</b> .....	xii
<b>List of Abbreviations</b> .....	xiii
<b>Chapter 1: Introduction of superhydrophobicity</b> .....	1
1.1 Superhydrophobic surface.....	2
1.2 Laser beam machining .....	5
1.3 Research motivations and objectives.....	7
1.4 Thesis organization .....	9
<b>Chapter 2: Fabrication superhydrophobic on titanium surface by using laser beam machining and heat treatment</b> .....	11
2.1 Background.....	12
2.2 Materials and methods .....	13
2.3 Results .....	16
2.3.1 Surface morphology.....	16
2.3.2 Wettability .....	19
2.3.3 Stability .....	26
2.4 Discussion.....	29
2.4.1 Effect of the laser power and step size on wettability .....	29
2.4.2 Mechanism.....	32



2.5 Potential applications .....	34
2.6 Summary.....	35
<b>Chapter 3: Fabrication superhydrophobic on glass surface by using laser beam machining and heat treatment .....</b>	<b>36</b>
3.1 Background.....	37
3.2 Experiment .....	38
3.2.1 Fabrication methods .....	38
3.2.2 Surface analysis .....	40
3.3 Results .....	43
3.3.1 Wettability .....	43
3.3.2 Transparency .....	46
3.3.3 Stability and robustness .....	50
3.4 Discussion.....	53
3.4.1 Effect of step size and laser power on wettability and transmittance .	53
3.4.2 Mechanism.....	55
3.5 Potential applications .....	59
3.6 Summary.....	61
<b>Chapter 4: Fabrication superhydrophobic on metals and ceramics surface by using laser beam machining under silicone oil.....</b>	<b>62</b>
4.1 Background.....	63
4.2 Experiment method.....	64
4.2.1 Materials and chemical element .....	64
4.2.2 Fabrication method .....	64
4.3 Results .....	67

4.3.1 Surface morphology .....	67
4.3.2 Wettability .....	70
4.3.3 Isotropic and anisotropic .....	74
4.3.4 Stability and robustness .....	75
4.4 Discussion.....	79
4.4.1 Effect of laser power on wettability .....	79
4.4.2 Effect of viscosity on wettability.....	82
4.4.3 Wettability with different materials.....	83
4.4.4 Compare the robustness between new process and post-process .....	85
4.4.5 Mechanism.....	87
4.5 Potential applications .....	91
4.6 Summary.....	94
<b>Chapter 5: Conclusion .....</b>	<b>95</b>
<b>Reference .....</b>	<b>99</b>
<b>Appendices .....</b>	<b>105</b>
Appendix A: Credits & Copyright Permissions.....	105
Appendix B: The confocal microscope with a different parameter when using laser beam fabrication under silicone oil .....	106
Appendix C: Contact angle and the sliding angle at different parameters....	108
Appendix D: Summary CA and SA of samples when using laser fabrication under silicone oil .....	111

# List of Figures

Figure 1. Superhydrophobicity in nature [1].....	2
Figure 2. The contact angle on the (A) smooth surface and (B) rough surface. ..	3
Figure 3. The applications of superhydrophobic surfaces [11]. .....	4
Figure 4. Various patterns are prepared through femtosecond laser microfabrication [19]. .....	5
Figure 5. Many papers were published in the last ten years under the topic nanosecond laser, picosecond laser, femtosecond laser with superhydrophobic taken from Web of Science. ....	6
Figure 6. Schematic images of (a) the laser beam machining system, and (b) pattern design.....	14
Figure 7. Definition of the parallel and perpendicular directions for the line pattern.....	16
Figure 8. Confocal microscopy images of the grid-patterned samples with a step size of 100, 200, 300 $\mu$ m at a laser power of 1, 2, 3W.....	17
Figure 9. Confocal microscopy images of the line-patterned samples with a step size of 100, 200, 300 $\mu$ m at a laser power of 1, 2, 3W.....	18
Figure 10. Images of water droplet contact angle: (a) initial stages (area with red color around), and after heat treatment for line-patterned samples (b) parallel direction (area with blue color around) (c) perpendicular direction (area with grey color around).....	21
Figure 11. Measurement of the contact angle and sliding angle of line-patterned samples with two directions: parallel direction (blue color) and perpendicular direction (red color) at a laser power of 1, 2, and 3W.....	22

Figure 12. Measurement of contact angle (blue color) and sliding angle (red color) of grid-patterned samples at a laser power of 1W; 2W; and 3W.....	24
Figure 13. The sliding angle of the line-patterned sample at laser power 3W with a 200 $\mu$ m step size: (a) parallel direction, and (b) perpendicular direction.....	25
Figure 14. Contact angle and sliding angle for the line pattern 35 days after heat treatment.....	27
Figure 15. Contact angle and sliding angle for the grid pattern 35 days after heat treatment.....	28
Figure 16. Effect of step size and laser power on wettability.....	29
Figure 17. Effect of grid-patterned microstructure on the wetting transition with SA.....	30
Figure 18. Effect of line-patterned microstructure on the wetting transition from the isotropic state to the anisotropic state.....	31
Figure 19. Top-view (a–d) field emission scanning electron microscopy (FESEM) images and (e–h) enlarged images of laser-machined surfaces with different step sizes 50, 300 $\mu$ m for grid pattern, and 50, 300 $\mu$ m for line pattern, respectively.....	33
Figure 20. Performance of superhydrophobic titanium surface: (a) water adhesion, (b) water bouncing with grid pattern, (c) water bouncing with line pattern – perpendicular direction, and (d) water bouncing with line pattern – parallel direction.....	34
Figure 21. Schematic of (a) the laser-beam machining system, and (b) a laser-beam path (grid pattern).....	39
Figure 22. FESEM images of a sample with 0.4W laser power and 200 $\mu$ m of step size.....	41

Figure 23. Confocal microscope images of the laser-processed surfaces at 200 $\mu$ m step size and different laser power a) 0.2, b) 0.3, c) 0.4, d) 0.5W. ....	41
Figure 24. Confocal microscope images of the laser-processed surfaces at 0.4W laser power and different step size a) 150, b) 200, c) 250, d) 300, e) 350 $\mu$ m. ....	42
Figure 25. Confocal microscope images of the laser-processed surfaces with (a) different powers at 200 $\mu$ m step size, and (b) different step sizes at 0.4W of laser power. ....	42
Figure 26. Contact angle images of (a) flat glass and a sample fabricated with 0.4W laser power and 200 $\mu$ m of step size, (b) before heat treatment, and (c) after heat treatment. ....	43
Figure 27. Contact and sliding angle of samples after heat treatment. ....	45
Figure 28. Transmittance results of unprocessed glass and laser-fabricated glass at different laser power and step sizes. ....	47
Figure 29. Top view of real images at different step sizes and laser powers. ....	48
Figure 30. Schematic image of light interactions with different surface structures. ....	49
Figure 31. Contact and sliding angle of samples after 8 weeks in ambient air since laser fabrication and surface heat treatment. ....	50
Figure 32. (a) Schematic of the scotch tape test for evaluating the stability and durability of the superhydrophobic glass surface, and (b) CA and SA results on the sample with laser power 0.4W - 200 $\mu$ m step size after the tape test. ....	52
Figure 33. (a) CA and SA results, and (b) transmittance at 400nm and 700 nm of light wavelength at the visible spectrum of all samples with different step sizes and laser power. ....	54
Figure 34. XRD results of soda-lime glass: (I) flat bare glass, (II) laser-ablated glass before heat treatment, and (III) laser-ablated glass after heat treatment. ...	56

Figure 35. FTIR spectra of soda-lime glass (a) before heat treatment, and (b) after heat treatment. .... 58

Figure 36. Performance of superhydrophobic glass surface: (a) water adhesion, (b) self-cleaning, (c) water bouncing, and (d) water position. .... 60

Figure 37. Schematic images of (a) the laser beam machining system, (b) pattern design, and (c) detail process for fabrication of superhydrophobic surface..... 66

Figure 38. FESEM images of the copper surface at 7.5W laser power, 0.75mm silicone oil height, 100 $\mu$ m step size, and 10mm/s scan speed..... 67

Figure 39. Confocal microscopy images of the copper surface with 10mm/s scan speed, 7.5W laser power, 0.75mm silicone oil height, and different step sizes a) 100, b) 200, c) 300, d) 400 $\mu$ m..... 68

Figure 40. CA and SA at same laser power of 7.5W with different silicone oil height (0.25, 0.5, 0.75, 1mm), step size (100, 200, 300, 400 $\mu$ m), and scan speed (10, 20, 50, 100, 200, 300mm/s). .... 71

Figure 41. CA and SA at same silicone oil height of 1mm with different laser power (2.5, 5, 7.5, 10W), step size (100, 200, 300, 400 $\mu$ m) and scan speed (10, 20, 50, 100, 200, 300mm/s)..... 73

Figure 42. The contact angle and the sliding angle at 7.5W laser power, 100, 200, and 300 $\mu$ m step size, 10mm/s scan speed, and 0.75mm silicone oil height. .... 74

Figure 43. CA and SA after laser fabrication (blue color), after 21 days (orange color), and after 80 days (grey color). .... 75

Figure 44. Schematic of the scotch tape test for evaluating the robustness of the superhydrophobic on the copper surface. .... 76

Figure 45. The CA and SA on the superhydrophobic copper surface after twenty cycles of tape test..... 78

Figure 46. Effect of burr height and step size on wettability. .... 79

Figure 47. The values of CA and SA following the increase of viscosity of silicone oil by using laser beam machining fabrication under silicone oil with 7.5W laser power, 100 $\mu$ m step size, 10mm/s scan speed, and 0.75mm silicone oil height. .... 83

Figure 48. a) CA and SA of a superhydrophobic surface by using laser fabrication under silicone oil with different materials, and b) water bouncing on a different superhydrophobic surface. .... 84

Figure 49. Compare the CA and SA of superhydrophobic copper surface between new process (laser beam machining under silicone oil), and post-process (laser and heat treatment) after 5 cycles tape test. .... 86

Figure 50. FESEM of copper surfaces with (a) laser under silicone oil, and (b) laser in air. .... 87

Figure 51. XRD results on unfabricated, only laser, and laser under silicone oil with Copper, Titanium, and Sapphire. .... 89

Figure 52. FTIR spectra of the only laser, and laser under silicone oil with Copper, Titanium, and Sapphire. .... 90

Figure 53. Performance of superhydrophobic copper surface: (a) water adhesion, (b) water bouncing, (c) self-cleaning. .... 92

Figure 54. Controlling of water moving following different shapes. .... 93

Figure 55. Confocal microscopy images of the samples at 7.5W laser power, 100 $\mu$ m step size, 0.75mm silicone oil height and different scan speeds a) 10, b) 20, c) 50, d) 100, and e) 200mm/s. .... 106

Figure 56. Confocal microscopy images of the samples at 10mm/s scan speed, 100 $\mu$ m step size, 0.75mm silicone oil height, and different laser powers a) 5, b) 7.5, and c) 10W. .... 107

Figure 57. Confocal microscopy images of the samples at 10mm/s scan speed, 7.5W laser power, 100 $\mu$ m step size, and different silicone oil heights a) 0.25, b) 0.5, c) 0.75, and d) 1mm. .... 107

Figure 58. CA and SA on copper surfaces at 0.25mm silicone oil height with different laser power (2.5, 5, 7.5, 10W), step size (100, 200, 300, 400 $\mu$ m), and scan speed (10, 20, 50, 100, 200, 300mm/s)..... 108

Figure 59. CA and SA on copper surfaces at 0.5mm silicone oil height with different laser power (2.5, 5, 7.5, 10W), step size (100, 200, 300, 400 $\mu$ m), and scan speed (10, 20, 50, 100, 200, 300mm/s)..... 109

Figure 60. CA and SA on copper surface at 0.75mm silicone oil height with different laser power (2.5, 5, 7.5, 10W), step size (100, 200, 300, 400 $\mu$ m), and scan speed (10, 20, 50, 100, 200, 300mm/s)..... 110



## List of Tables

Table 1. The parameter by using laser fabrication on titanium surface. ....	15
Table 2. Energy-dispersive X-ray spectroscopy (EDS) results on burrs before and after heat treatment. ....	33
Table 3. Composition of the soda-lime glass.....	39
Table 4. The process parameters by using laser beam machining and heat treatment.....	40
Table 5. EDS results on burr and non-fabrication area of the soda-lime glass surface. ....	57
Table 6. The average of burr height following different conditions.....	69
Table 7. The distribution of CA and SA following the change of laser power, step size, and scan speed. ....	81
Table 8. Time for laser fabrication with a 5x5mm <sup>2</sup> area.....	82
Table 9. EDS results of copper, titanium, and sapphire materials.....	89
Table 10. The presence of CA and SA following the change of laser power (2.5, 5, 7.5, 10W), step size (100, 200, 300, 400μm), scan speed (10, 20, 50, 100, 200, 300mm/s), and silicone oil height (0.5, 0.75, 1mm). ....	111

## List of Abbreviations

N°	Short name	Full name
1	CA	Contact angle
2	SA	Sliding angle
3	WDCA	Water droplets contact angle
4	Ti	Titanium
5	Cu	Copper
6	SUS	Stainless steel
7	Al	Aluminum
8	FESEM	Field Emission Scanning Electron Microscopy
9	XRD	X-ray diffraction
10	EDS	Energy-dispersive X-ray spectroscopy
11	FTIR	Fourier transform infrared spectrometer

**Chapter 1:**  
**Introduction of**  
**superhydrophobicity**

## 1.1 Superhydrophobic surface

A superhydrophobic surface is a surface on which a water droplet can easily move, and in nature, it can present through some animals and leaves as shown in Figure 1.

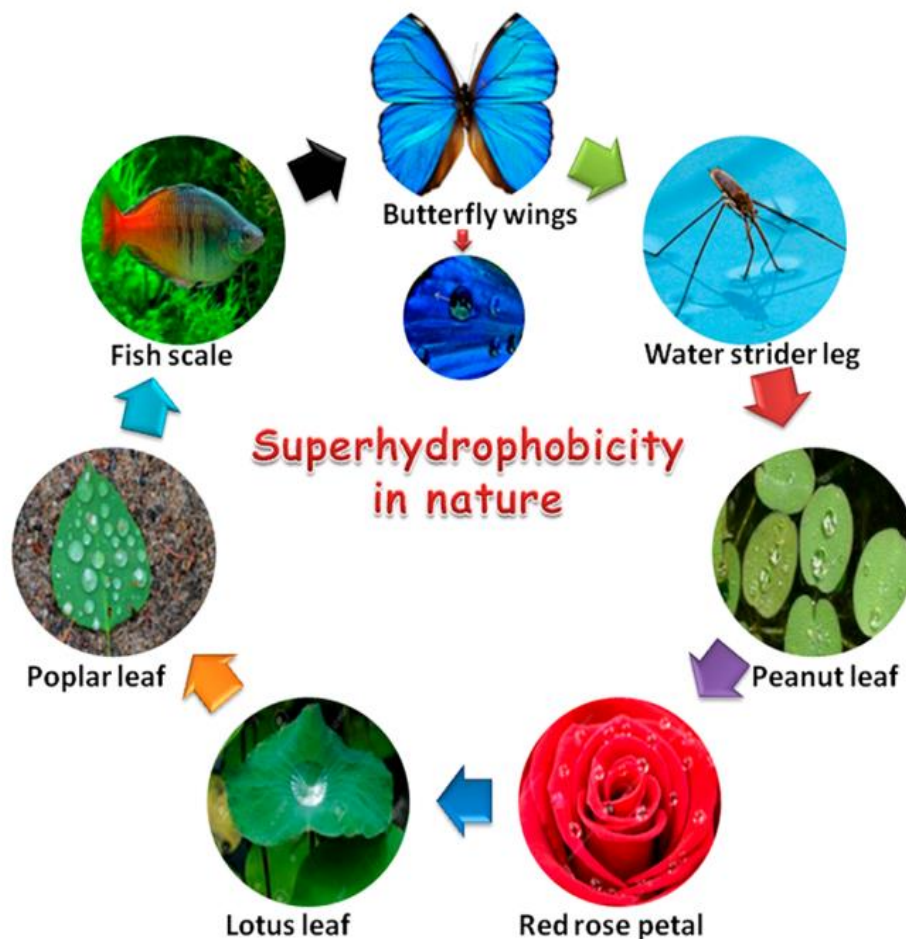


Figure 1. Superhydrophobicity in nature [1].

In particular, the superhydrophobic surface was defined through the angle between liquid, solid, and air. This angle was divided into two kinds of angles as a high contact angle ( $CA > 150^\circ$ ) and a small sliding angle ( $SA < 10^\circ$ ). In normal cases, for making a superhydrophobic surface, the rough surface and low surface energy are required as shown in Figure 2.

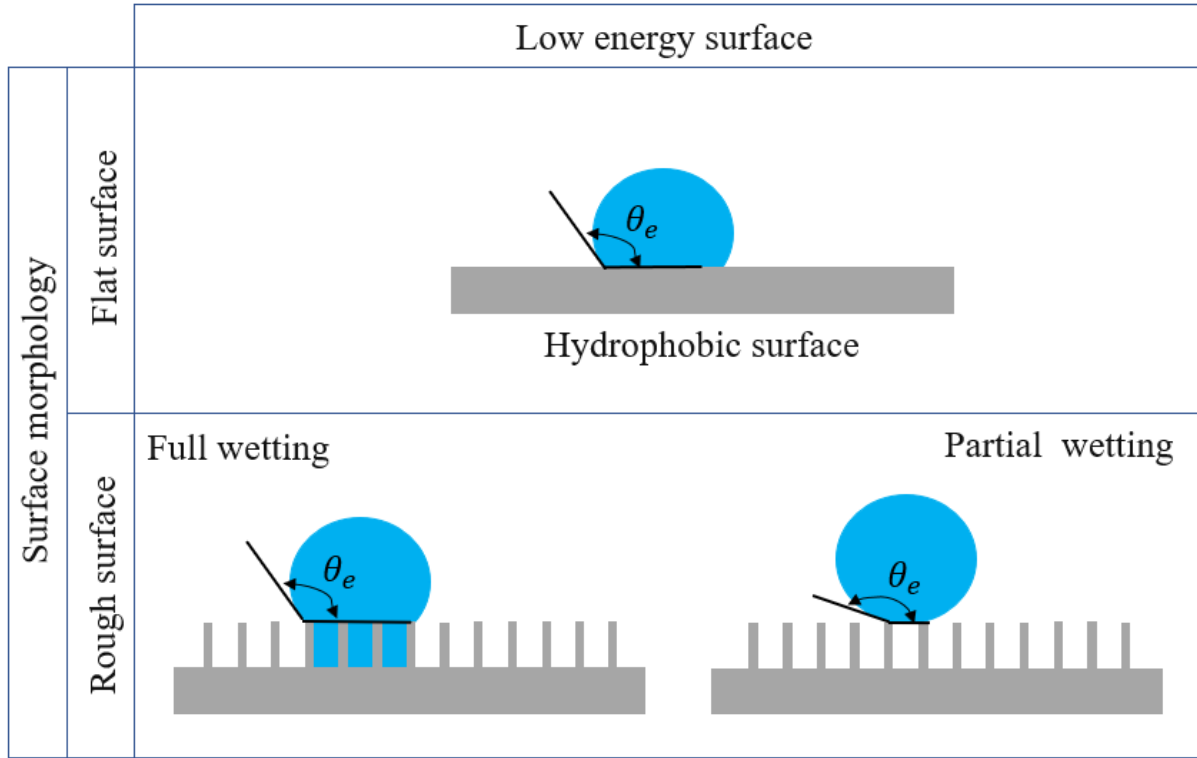


Figure 2. The contact angle on the (A) smooth surface and (B) rough surface.

With a rough surface, the Cassie-Baxter model (partial wetting) and the Wenzel model (full wetting) can be used for explanation of the wetting states [2,3] while the Young model can be used for smooth (or flat) surface [4]. The wettability on a smooth surface that follows Young's model can be described by using equation (1). While equations (2), and (3) were used to describe the wettability of the rough surface follow Wenzel and Cassie-Baxter's model, respectively.

$$\cos\theta = \frac{\gamma_{SA} - \gamma_{SL}}{\gamma_{LA}} \quad (1)$$

$$\cos\theta_w = r\cos\theta_e \quad (2)$$

$$\cos\theta_c = \varphi_1\cos\theta_e - \varphi_2 \quad (3)$$

where  $\theta_e$  is the equilibrium water droplet contact angle on a flat surface,  $r$  is a roughness factor equal to the actual surface divided by the geometric surface,  $\theta_w$

is the water droplet contact angle in the full wetting state on a rough surface,  $\theta_c$  is the water droplet contact angle in the partial wetting state on a rough surface,  $\varphi_1$  is the area fraction of the water-solid area to the projected area, and  $\varphi_2$  is the area fraction of the water-air area to the projected area,  $\theta$  is the water droplet contact angle in the smooth surface,  $\gamma_{SA}, \gamma_{SL}, \gamma_{LA}$  are the surface energies of the solid against air, solid against liquid, and liquid against air, respectively.

Based on the characteristic of superhydrophobic surface on which water droplets can move easily, this kind of surface has many applications such as self-cleaning [5], water collection [6], anti-icing [7], antibacterial [8], oil-water separation [9], water purification [10] so on as shown in Figure 3. There are many applications for superhydrophobic surface exists, however, the way to create this kind of surface is still attractive and alluring for researchers. And a new process to make a superhydrophobic surface should be simple, take short time, more stable, and more robust than the old one, and it can apply widely in the industry, these requirements are always a challenge for researchers.



Figure 3. The applications of superhydrophobic surfaces [11].

Recently, numerous studies on superhydrophobic surfaces have been reported. A superhydrophobic surface was achieved by the fabrication of micro/nanometer-scale rough structures [12] by different methods, such as coating [13], chemical etching [14], laser texturing [15–17], UV irradiation [18], and so on. All of these techniques required either special equipment or complex process control. Among these techniques, laser beam machining was the most prominent because it could be set up easily, economically, and friendly to the environment, and it can easily apply to the industry.

## 1.2 Laser beam machining

Laser machining has been used widely because of its precision, easy setup, and great effectiveness for many patterning as shown in Figure 4.

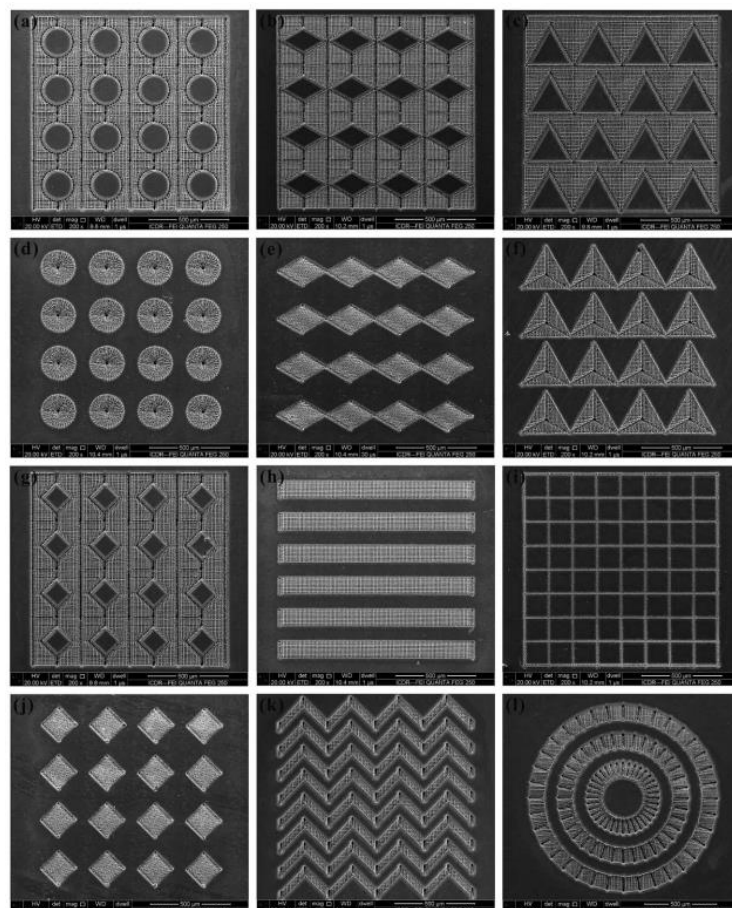


Figure 4. Various patterns are prepared through femtosecond laser microfabrication [19].

There are three main kinds of laser sources such as nanosecond, picosecond, and femtosecond laser, which were used in many research facilities and industries. The number of published papers under the topic of using the laser (nanosecond, picosecond, and femtosecond laser) to create superhydrophobic surfaces has been increased year by year, detailed as shown in Figure 5. In these published papers, mainly researchers use femtosecond and nanosecond laser. However, in the case of using laser for creating a superhydrophobic surface, researchers still need to do several processes after the laser fabrication step such as heat treatment [20,21], put a long time in the air (more than 10 days) [17,22–24], heating in the dark environment [25], storing in vacuum environment [26,27], chemical coating [11,12 ]. Moreover, these techniques can apply to only one or two materials. Besides, when using a laser beam fabrication superhydrophobic surface, the roughness of the surface was an important key for the fabrication of a superhydrophobic surface. Moreover, to control the surface roughness, it is necessary to pay attention to some parameters as laser power, step size, scan speed, environment, and properties of materials [30–33].

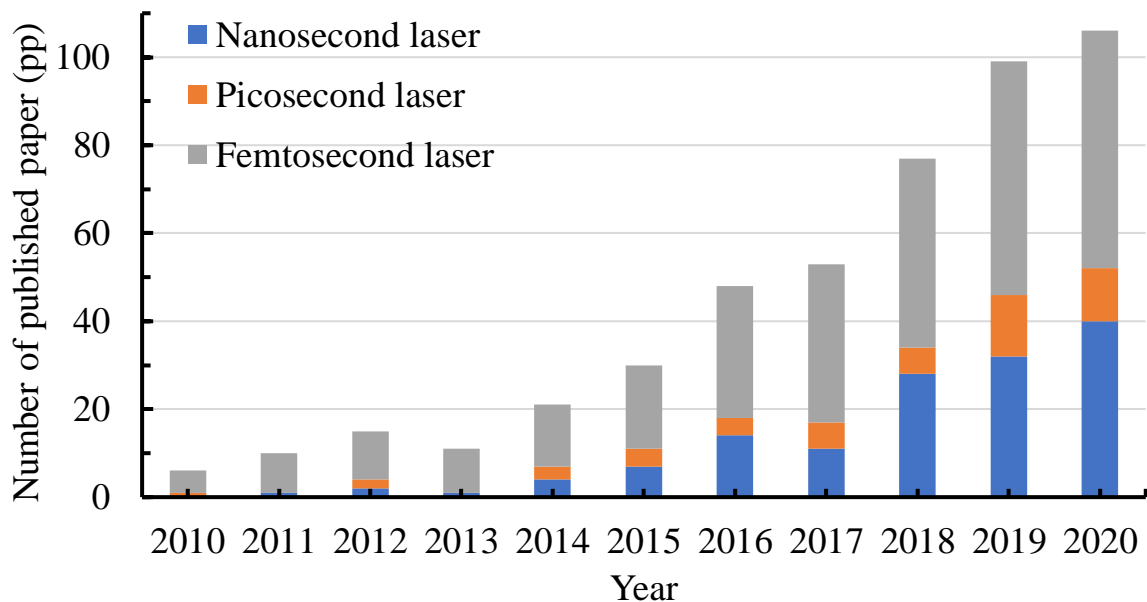


Figure 5. Many papers were published in the last ten years under the topic nanosecond laser, picosecond laser, femtosecond laser with superhydrophobic taken from Web of Science.



In other studies, some researchers have tried to use only nanosecond pulsed laser without any chemical to create an easy fabrication and remove the effect of an unwanted chemical on the surface. However, immediately after fabrication using nanosecond pulsed laser, the pattern showed a hydrophilic surface and became a superhydrophobic surface after being put under ambient conditions for a long time (several days or months) [34–36]. Other researchers used laser beam machining on the substrate surface, such as a laser to create microstructures, then they applied a chemical on these microstructures [29,37,38] or placed the microstructures into a high vacuum for several hours to make the superhydrophobic surfaces [39–41].

### **1.3 Research motivations and objectives**

As a member of a Hybrid Manufacturing Technology Lab, in the past, we already developed a post-process for making superhydrophobic surfaces without chemicals, no complicated equipment, and high contact angle ( $CA > 170^\circ$ ). This post-process included the laser and heat treatment process, which meant, the samples with micro/nanostructure surface were firstly fabricated by using a nanosecond laser machining then the samples were put in the oven for several hours to become a superhydrophobic surface and after the heat treatment process, the hydrophobic group will appear on the sample's surface. With this post-process, a number of researches on many kinds of materials as copper, aluminum, stainless steel, and sapphire have been conducted and published. However, in these publications, the researchers only focused on changing the step size with metals or changing the laser power with ceramic - sapphire. That meant, application of the post-process on titanium, and glass has not been studied. In addition, titanium and glass are common materials and can be easily encountered in daily life with many applications and especially in biomedical applications. For these reasons, research on superhydrophobicity on titanium and glass was conducted in this study. However, the heat treatment process in post-process

would take a very long time from several hours (6 hours) for titanium to few days (two days or 48 hours) for glass. Not only that, the post-process even contained two separated steps to fabricate a sample to a superhydrophobic surface. In order to surmount these disadvantages, it is necessary to develop a new process that takes short time and should be a single process. As a result, we have succeeded in developing a new process that fabricates superhydrophobic surfaces within few seconds or few minutes. This new process is called laser beam machining under silicone oil. And the effect of manufacturing conditions such as silicone oil height, step size, scan speed, and laser power are investigated. Furthermore, a simple comparison of surface robustness was carried out between this new process and post-process by a tape test. The mechanism of wettability changing from hydrophilic to superhydrophobic by using laser beam machining under silicone oil was explained as well. Furthermore, some applications such as self-cleaning, difficult shapes were proposed in this study.

The simple technique using nanosecond laser beam machining under silicone oil can be a good candidate to apply in manufacturing and industry due to the following reasons:

- The fabrication time is short (reduce from few hours or few days of post-process to few minutes or few seconds).
- The new process created a more robust and stable surface than the post-process.
- No toxic chemical is required.
- The new process can be applied on many kinds of materials such as titanium, copper, aluminum, stainless steel, sapphire, and glass to make superhydrophobic surfaces.
- Application for big fabrication areas and even for many difficult patterning shapes.

Additionally, the results could provide a useful guide to select the proper laser power, step size, silicone oil height, and scan speed for controlling wettability and fabrication time with many metals and ceramics substrates.

## **1.4 Thesis organization**

The thesis's structure will be divided into 5 chapters as below:

**Chapter 1** focuses on the literature review including the definition of superhydrophobic surface, some applications, and how to make a superhydrophobic surface. Next, a review about using laser beam machining for the fabrication of superhydrophobic surfaces will be mentioned. The final part will describe the motivation, and the objectives, and the thesis organization.

**Chapter 2** describes the fabrication of superhydrophobic on titanium surface by using laser beam machining and heat treatment. Besides, the effect of different laser power, step sizes on surface wettability was investigated. In addition, it was shown clearly the effect of pattern design between grid-pattern and line pattern on the CA and SA. And the stability of the samples after a long time put in the air was measured. Final some potential applications also are mention in this chapter.

**Chapter 3** describes the fabrication of superhydrophobic on soda-lime glass surface by using laser beam machining and heat treatment. The chapter points out some effects of laser power, step size on wettability and transparency. And the stability and robustness on the surface of the samples were also investigated. Finally, some potential applications were shown in this chapter.

**Chapter 4** describes the fabrication of superhydrophobic on metals and ceramics materials surface by using laser beam machining under silicone oil. Among all materials mentioned in this study, copper was the main material to be used for all checking processes. While titanium, stainless steel, aluminum,

sapphire, and glass were checked with a typical condition for the fabrication of a superhydrophobic surface. The effect of laser power, step size, scan speed, and silicone oil height with grid-patterned were investigated. With the laser beam machining under silicone oil, the isotropic and anisotropic behavior on the surface with line-patterned was presented. The stability and robustness of the superhydrophobic surface also were checked. With silicone oil, the effect of viscosity was one of the key factors to the superhydrophobic surface, so the viscosity was also investigated. A comparison of robustness between surface fabricated by laser beam machining under silicone oil and surface fabricated by laser beam machining and heat treatment was presented. Finally, some potential applications were shown in this chapter.

**Chapter 5** summarizes several outstanding results from the post-process (laser and heat treatment) and the new process (laser beam machining under silicone oil) was mentioned in this chapter.

**Chapter 2:**  
**Fabrication**  
**superhydrophobic on**  
**titanium surface by using**  
**laser beam machining and**  
**heat treatment**

## 2.1 Background

Numerous studies on superhydrophobic surfaces have been reported. A superhydrophobic surface has been achieved by the fabrication of micro/nanometer-scale rough structures [12] through different methods, such as coating [13], laser texturing [17], UV irradiation [18], and so on. These techniques all require either special equipment or complex process control. Some researchers have tried only laser beam machining without any chemicals for the easy fabrication and removal of unwanted properties of chemicals on the surface. However, immediately after laser surface texturing, the surface was hydrophilic, and the surface became a superhydrophobic surface after a long time (several days or months) under ambient conditions. On the other hand, laser surface texturing for wetting modification has been extensively studied in different materials as metal [42], polymers [43], or ceramics [44]. In these materials, titanium is a common material that can easily meet in daily life with many special conventional properties. Titanium and its alloys can have much application in the biomedical [5,6], aerospace industry [47] because of its lightweight, low elasticity, high specific strength, corrosion resistance. With these characteristic, wide applications, especially in biomedical application, titanium and its alloys were many researchers choose for checking superhydrophobic surfaces. Some researchers used laser beam machining on a titanium surface, such as an ultrashort picosecond laser [48] or laser micromachining, to create microstructures, and then they applied a toxic chemisorption post-process on these microstructures [37] or placed the microstructures in ambient air for 30 days to make the surfaces hydrophobic [17]. Previous studies have mainly focused on how to produce superhydrophobic metallic surfaces or changing the wetting behavior from hydrophilicity to superhydrophobicity on metals when using laser beam machining.

Recently, a solution combining nanosecond pulsed laser and heat treatment to prevent the usage of toxic chemicals and long fabrication time has been reported to form superhydrophobic copper [20], titanium [20], and aluminum grid-patterned surfaces [21]. However, research has focused mainly on the change in wetting behavior on only grid-patterned surfaces. The effects of pattern design and laser power on the superhydrophobicity of metal surfaces, which also plays an important role in optimization of fabrication time as well as the performance of superhydrophobic surfaces in industry and manufacturing, have not been studied yet. In this research, the effect of the microstructure based on pattern design, laser power, and step size on superhydrophobicity was studied. The obtained results could provide a useful guide to select the proper laser power, step size, and pattern design for various purposes in the efficiency of process, fabrication time, and specified applications such as control of the moving direction of a water droplet with a lined pattern design.

## **2.2 Materials and methods**

Titanium sheets (99.5% purity, Nilaco Corporation, Tokyo, Japan) with a 0.5mm thickness were used in the experiments. A Q-switched Nd: YAG 355-nm UV nanosecond pulsed laser (Awave355-3W20K, Advanced Optowave Ronkonkoma, NY 11779) and a focusing lens with 5 $\mu$ m beam spot size were used. Figure 6a shows a schematic image of the nanosecond pulsed laser system. Laser beam machining was performed with grid and line patterns (Figure 6b) because it is easy to fabricate. Besides, the grid pattern surface has an isotropic wetting state it means, the CA and SA are the same for the x and y measurement direction, while the line pattern shows the anisotropic wetting state – it means the values of CA and SA following two-direction x and y will difference. And the process parameters are summarized in Table 1. The laser power was studied from 1 to 3W, and the step size was studied from 50 to 300 $\mu$ m. Three samples for each condition were produced for reproducibility.

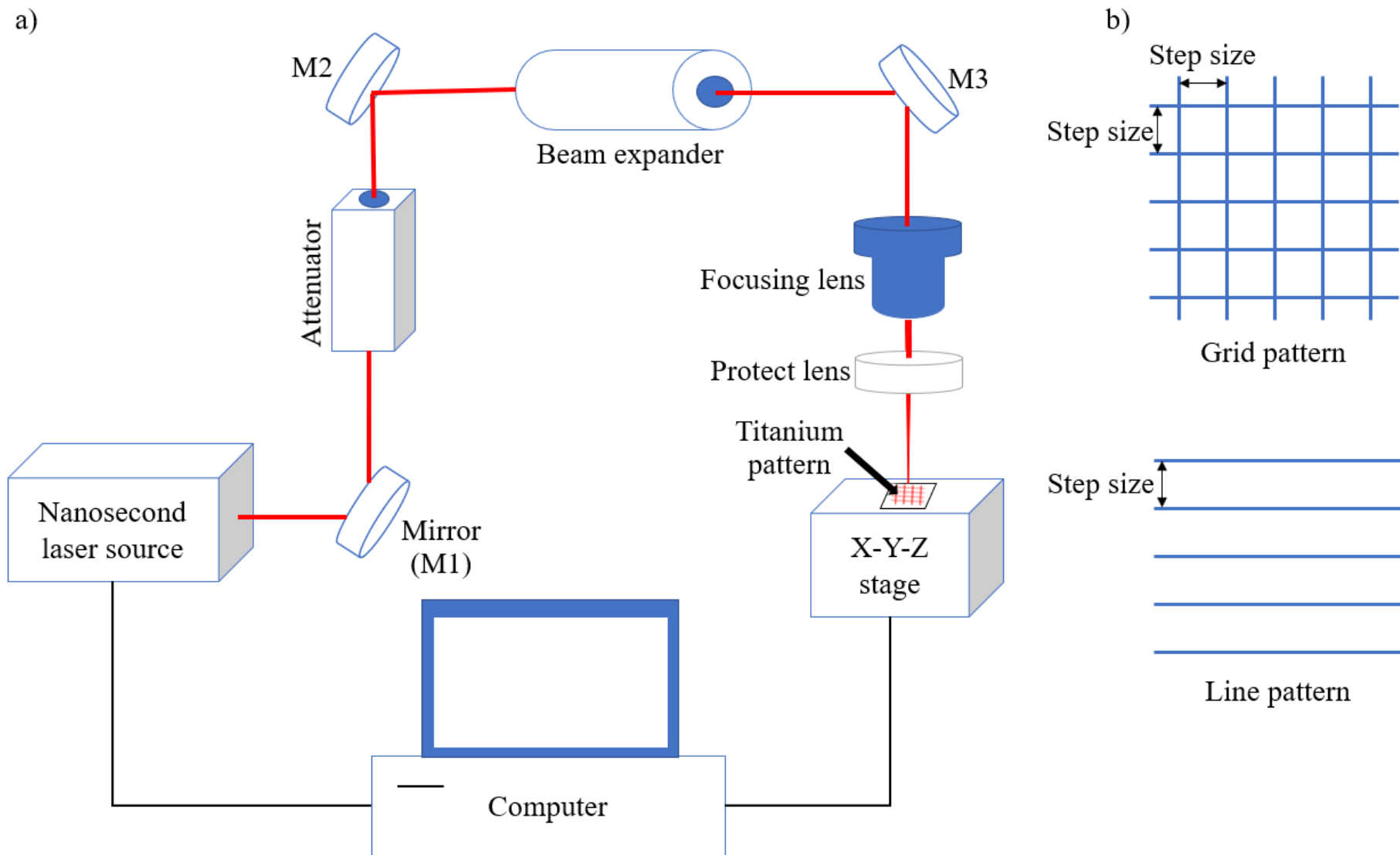


Figure 6. Schematic images of (a) the laser beam machining system, and (b) pattern design.



Table 1. The parameter by using laser fabrication on titanium surface.

<b>Name of Parameter</b>	<b>Value</b>
Pulse frequency (kHz)	20
Pulse duration (ns)	20
Stage speed (mm/s)	1
Laser power (W)	1, 2, 3
Step size ( $\mu\text{m}$ )	50, 100, 150, 200, 250, 300
Number of samples	3

After laser beam machining, the samples were put in an oven at 200°C for a 6 hours heat treatment. The samples were then cooled naturally in ambient air for 2 hours, and the contact angles on samples were measured by a contact angle meter (SmartDrop SDLab-200TEZD, Femto Fab, Seongnam, Korea) to evaluate the wettability of the samples. The CA of each sample was measured one time with a 11  $\mu\text{L}$  volume of water because the water droplet could be easily placed on a titanium surface. A three-dimensional (3D) laser scanning confocal microscope (VK-X200 series, Keyence, Osaka, Japan), a field emission scanning electron microscopy (FESEM, JSM-6500F, Jeol Co., Tokyo, Japan), and energy-dispersive X-ray spectroscopy (point EDS, JSM-6500F, Jeol Co., Tokyo, Japan) were used to analyze the surface structure. Commonly, a water droplet placed on the grid pattern exhibits isotropic wetting behavior, while one placed on the line pattern shows isotropic and anisotropic, parallel and perpendicular directional wetting, as shown in Figure 7.

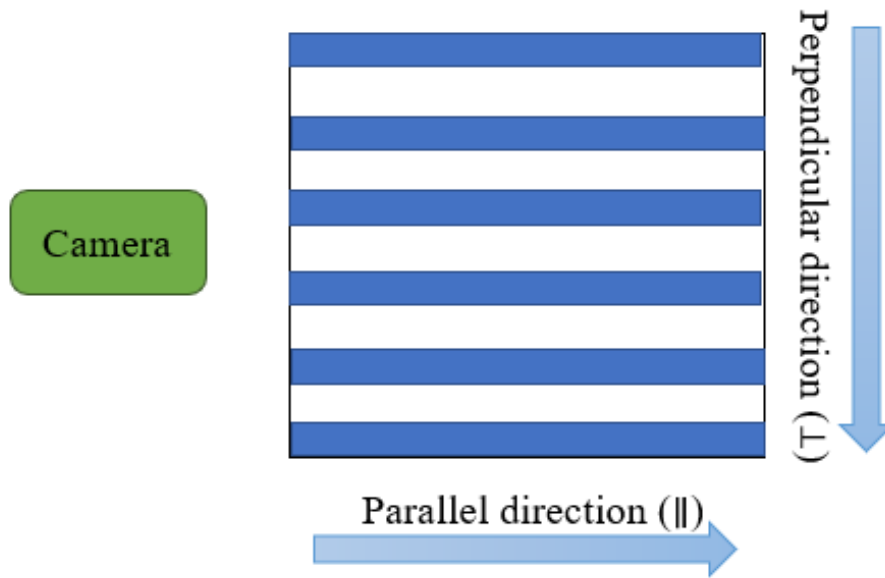


Figure 7. Definition of the parallel and perpendicular directions for the line pattern.

## 2.3 Results

### 2.3.1 Surface morphology

The two-dimensional (2D) and 3D images of the laser-machined surfaces with different laser powers, step sizes, and pattern designs were observed by 3D confocal microscopy as shown in Figures 8 and 9. The grid and line patterns were clearly fabricated by nanosecond pulsed laser. Nonfabricated flat areas between the grid and line patterns were also observed.

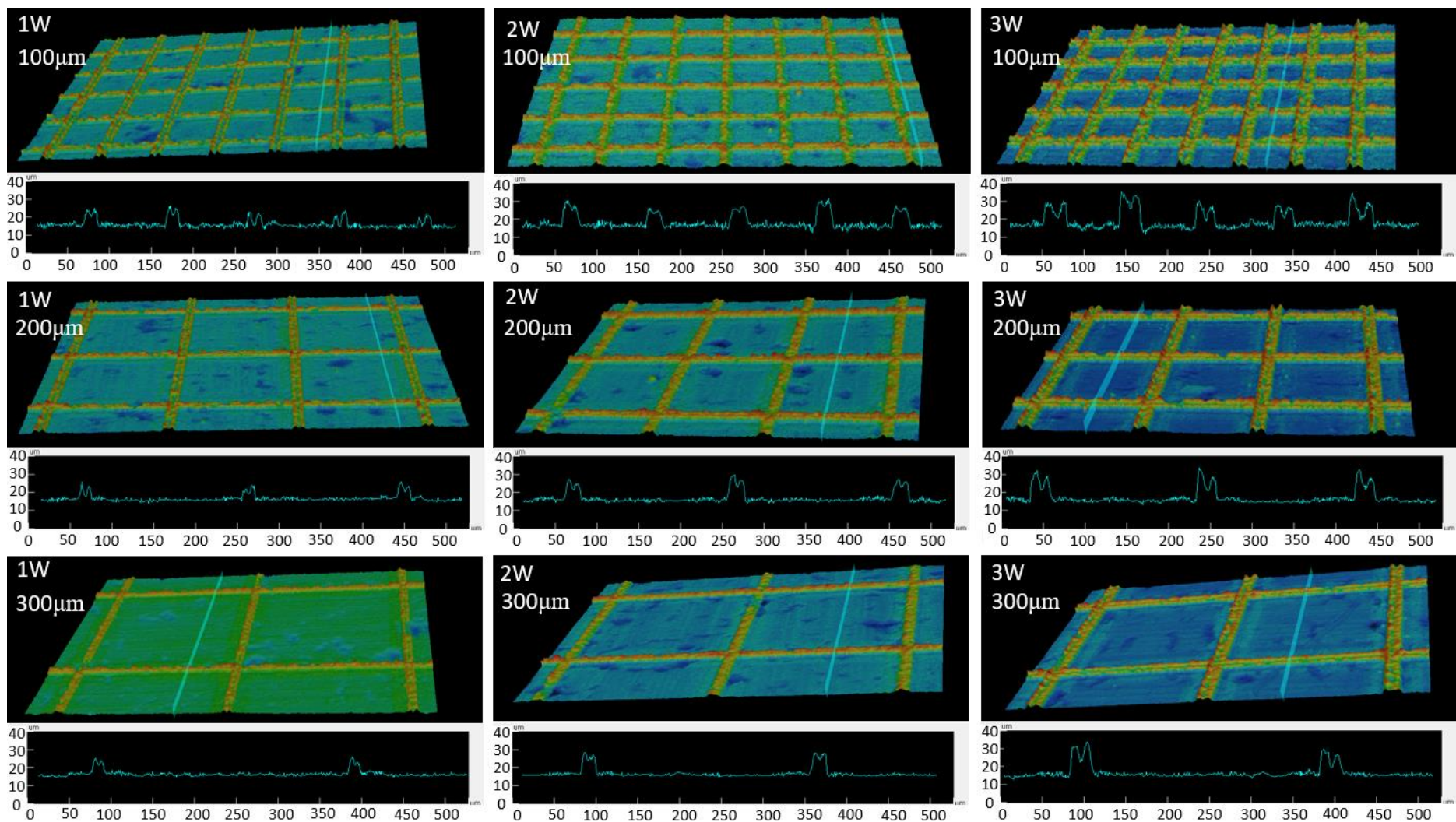


Figure 8. Confocal microscopy images of the grid-patterned samples with a step size of 100, 200, 300 μm at a laser power of 1, 2, 3W.

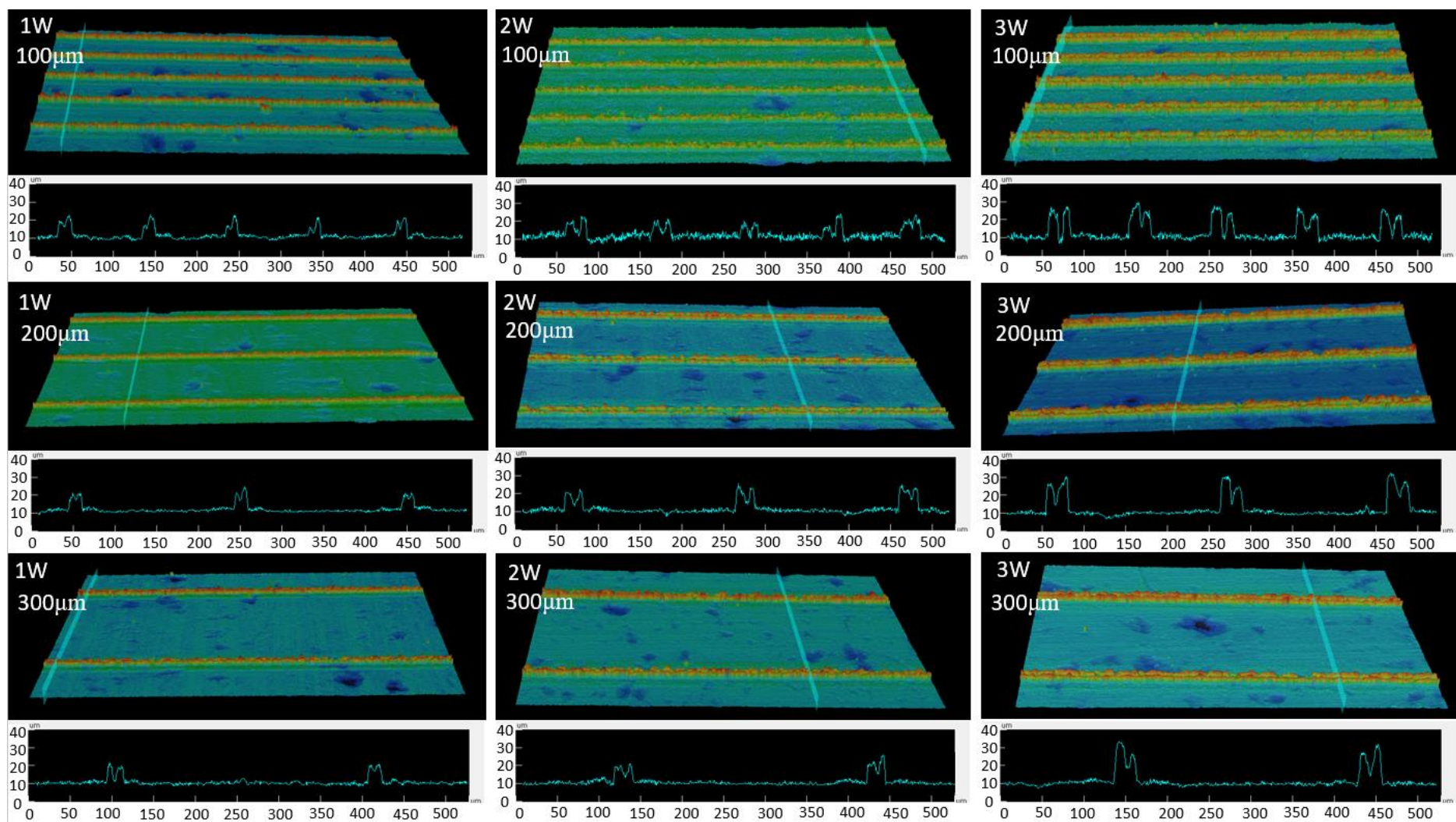


Figure 9. Confocal microscopy images of the line-patterned samples with a step size of 100, 200, 300 μm at a laser power of 1, 2, 3W.

Figures 8 and 9 show the typical grid and line pattern structures measured by 3D confocal microscopy. Burrs around laser machined areas were clearly observed. The height and width of the burr increased as the laser power increased. The average heights of the burrs in grid patterns were approximately  $9.94 \pm 1.7\mu\text{m}$  at 1W,  $10.95 \pm 0.8\mu\text{m}$  at 2W, and  $15.81 \pm 0.5\mu\text{m}$  at 3W, while the line patterns were approximately  $9.83 \pm 2.7\mu\text{m}$  at 1W,  $12.97 \pm 3.25\mu\text{m}$  at 2W, and  $18.09 \pm 3.2\mu\text{m}$  at 3W. The average widths were approximately  $22.27 \pm 4.5\mu\text{m}$  at 1W,  $24.38 \pm 0.85\mu\text{m}$  at 2W, and  $29.22 \pm 0.95\mu\text{m}$  at 3W for grid pattern, and those for the line patterns were approximately  $18.73 \pm 2.5\mu\text{m}$  at 1 W,  $25.56 \pm 2.5\mu\text{m}$  at 2W, and  $29.54 \pm 3.5\mu\text{m}$  at 3W.

### 2.3.2 Wettability

The typical images of CA before and after heat treatment are shown in Figure 10 for line-patterned samples at 3W laser power and step size change from 50 to  $300\mu\text{m}$ . Before heat treatment, all samples showed the CAs less than  $90^\circ$  (hydrophilic), as shown in Figure 10a, but the samples became superhydrophobic surfaces after heat treatment, as shown in Figure 10b, and c.

Figure 11 showed the change in wetting state on line-patterned surfaces with laser power and step size. When the laser power decreased, the critical step size also changed. The critical step size was the point where the wetting state of the surface tended to change from isotropic to anisotropic behavior. From the difference of contact angles ( $\Delta\text{CA}$ ) between two directions (parallel and perpendicular to the line patterns), isotropicity and anisotropicity were defined [49]. The calculation of  $\Delta\text{CA}$  was performed using the following equation:

$$\Delta\text{CA} = |\text{CA}_\perp - \text{CA}_\parallel| \quad (4)$$

If  $\Delta\text{CA} < 10^\circ$ , then the material is called isotropic; if  $\Delta\text{CA} > 10^\circ$ , then it is called anisotropic. When the laser power increased from 1W to 2W and then to 3W, the

critical step size changed from 150  $\mu\text{m}$  to 200 $\mu\text{m}$  and then to 250 $\mu\text{m}$  for the contact angle difference, respectively, as shown in Figure 11. The laser power at 3W did not show any differences between the parallel direction and perpendicular direction for all step sizes smaller than 250 $\mu\text{m}$ . At a 300 $\mu\text{m}$  step size of line-patterned samples with 3W, the contact angles following the parallel direction and perpendicular direction showed a clear difference. At 2W with a 250 $\mu\text{m}$  step size, there was a clear difference in CA between the two directions, as there was at 1W with a 200 $\mu\text{m}$  step size. The more the step size increased, the larger was the difference between the CA of the two directions. Decreasing laser power did not have an effect at a small step size (especially at 50 and 100 $\mu\text{m}$ ); however, at a large step size (from 150 to 300 $\mu\text{m}$  in this research), the difference between the parallel and perpendicular directions was large, especially at a 300 $\mu\text{m}$  step size for all laser powers. Additionally, the anisotropic behavior was clear in the sliding angle results. For example, with a laser power of 2W at 250 $\mu\text{m}$  step size, the sliding angle exhibited along the parallel direction but did not show along the perpendicular direction. The contact angles and sliding angles following the perpendicular direction were always greater than those following the parallel direction. Following the parallel direction, a water droplet can easily move on the surfaces because there is no barrier along the moving direction of the water droplet; along the perpendicular direction, the burr acted as a barrier, which prevented the movement of the water droplet, and the water droplet was more difficult to move than along the parallel direction.

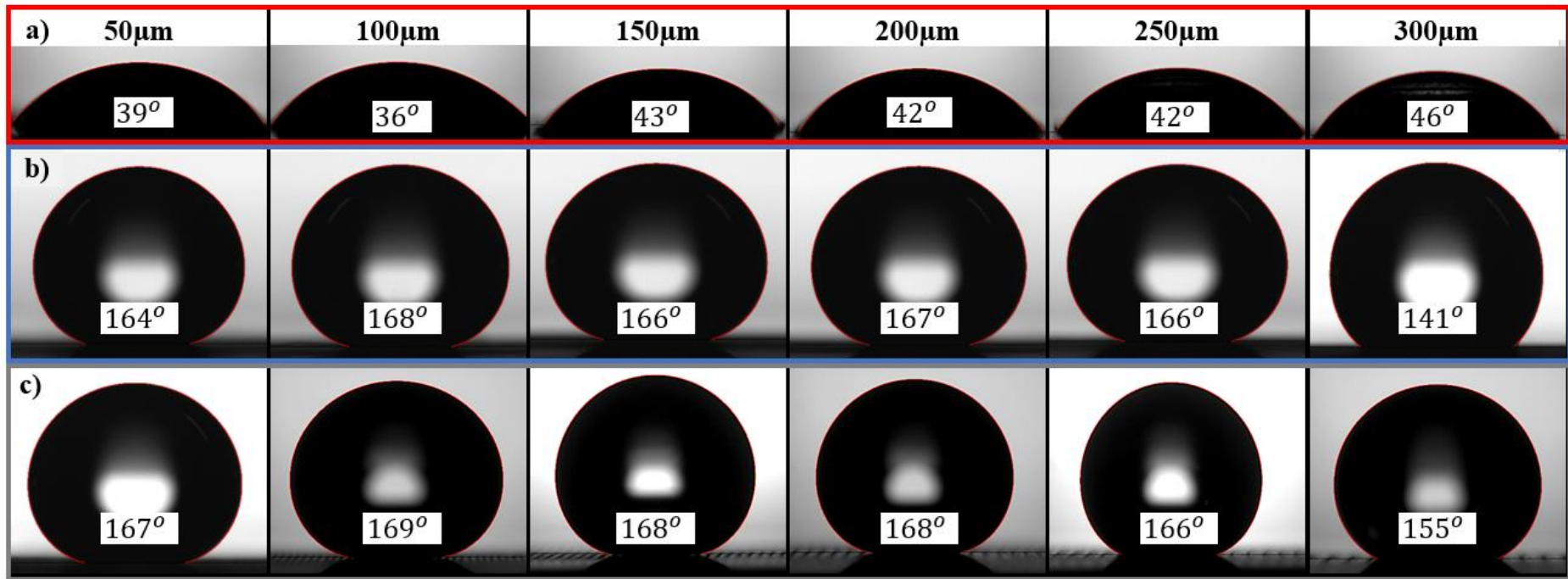


Figure 10. Images of water droplet contact angle: (a) initial stages (area with red color around), and after heat treatment for line-patterned samples (b) parallel direction (area with blue color around) (c) perpendicular direction (area with grey color around).

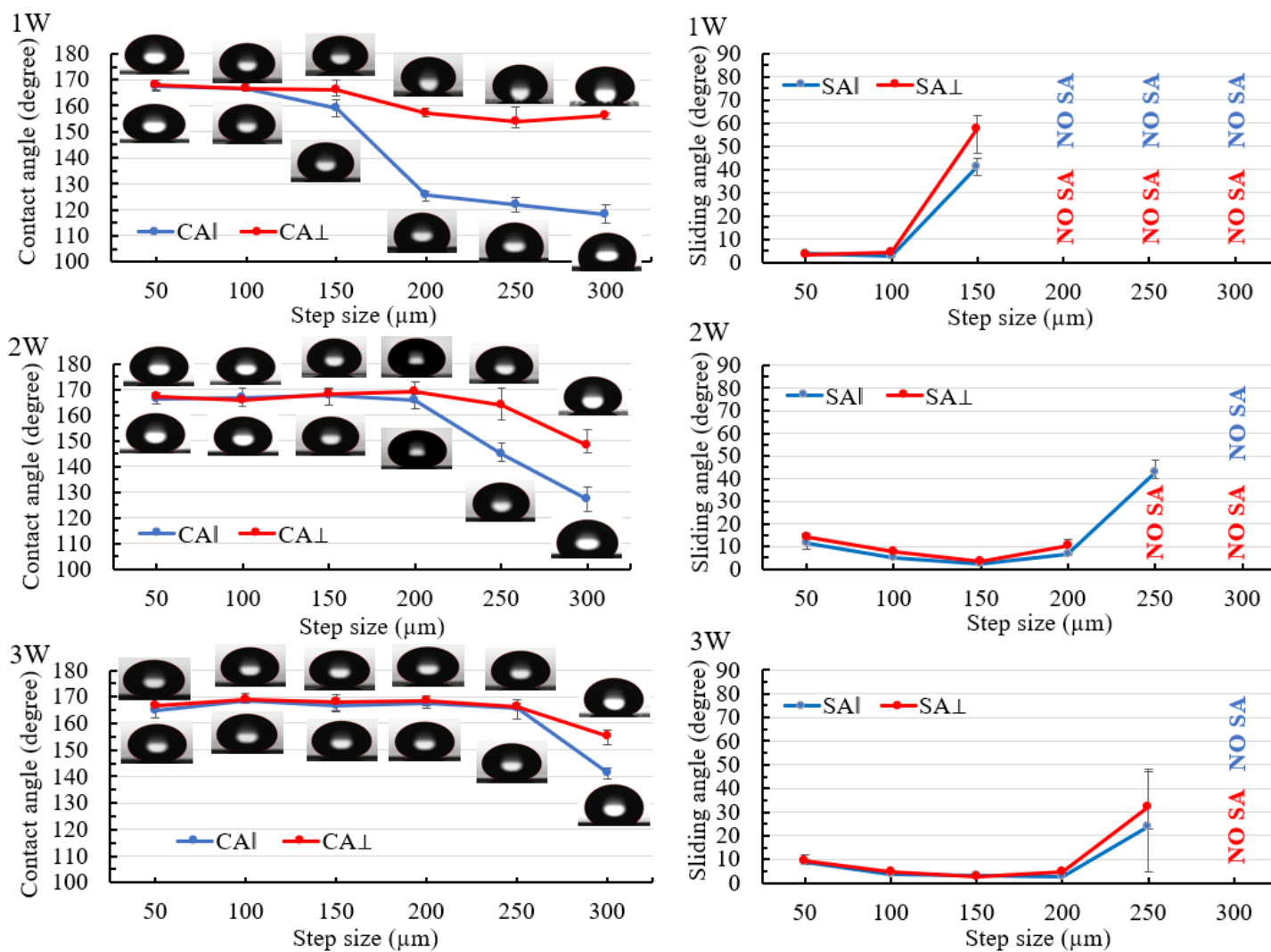


Figure 11. Measurement of the contact angle and sliding angle of line-patterned samples with two directions: parallel direction (blue color) and perpendicular direction (red color) at a laser power of 1, 2, and 3W.



Figure 12 shows the contact angle and sliding angle for the grid pattern. Similar to line-patterned samples, when the laser power changed, the critical step size, where the wetting state tended to change, also changed. The grid-patterned samples included two critical step sizes where the “lotus effect” wetting state, which has  $CA > 150^\circ$  and  $SA < 10^\circ$ , changed to the wetting state which has  $CA > 150^\circ$  and  $SA > 10^\circ$ , and the wetting state, which has  $CA > 150^\circ$  and  $SA > 10^\circ$ , changed to the “Petal effect” wetting state which has  $CA > 150^\circ$  and no SA. From the values of sliding angle, the wetting state of the grid-patterned samples was defined. If the sliding angle was smaller than  $10^\circ$ , the surface showed a lotus effect. If the sliding angle was greater than  $10^\circ$ , the surface might not show any lotus effect or petal effect. The surface showed the petal effect when there was no sliding angle. In Figure 12, when the laser power increased from 1 to 2W, the critical step size, where the wetting state changed from the lotus effect wetting state, changed from 150 to 250 $\mu\text{m}$ . At 2 and 3W, all step sizes showed a contact angle of approximately  $165^\circ$  and sliding angle smaller than  $10^\circ$ , except at the 300 $\mu\text{m}$  step size at 2W, the SA was  $32^\circ$ . At 1W with a 300 $\mu\text{m}$  step size, there was no SA, and CA was  $157 \pm 1.3^\circ$ . At 200- $\mu\text{m}$  and 250 $\mu\text{m}$  step size for 1W, the SA was greater than  $10^\circ$ .

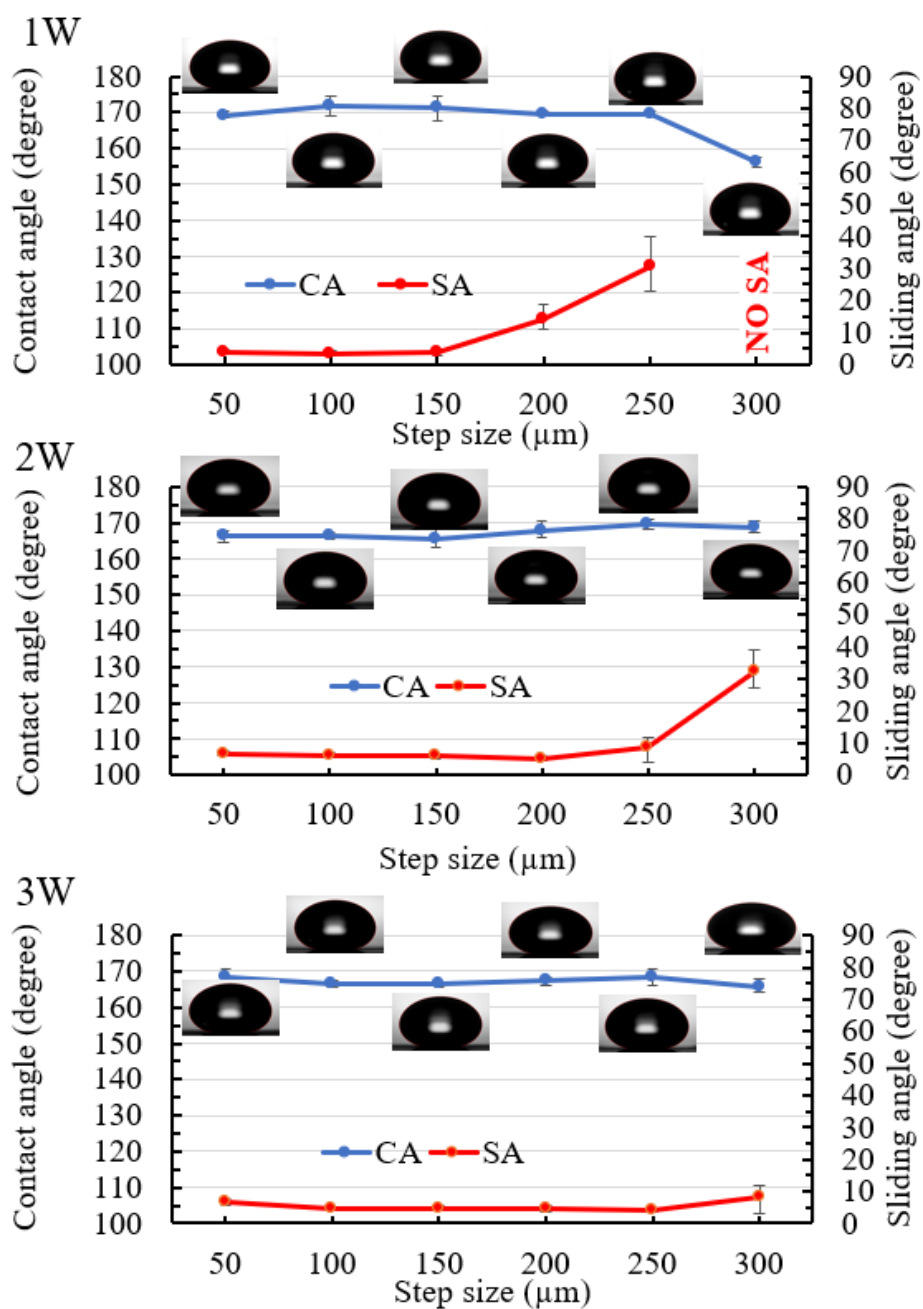


Figure 12. Measurement of contact angle (blue color) and sliding angle (red color) of grid-patterned samples at a laser power of 1W; 2W; and 3W.

The images of sliding angle on the titanium surfaces were shown in Figure 13 for line patterns of a  $200\mu\text{m}$  step size at 3W laser power. The substrate was tilted at a speed of  $1.6^\circ/\text{s}$ , and the water droplet started sliding at approximately  $7^\circ$  for the parallel direction and  $10^\circ$  for the perpendicular direction. In this study, several step sizes did not have a sliding angle when tilting to  $90^\circ$ ; even when tilting manually to  $180^\circ$ . The water droplet might contact the hydrophilic surface and show a strong attraction to this surface. Therefore, the water droplet cannot move off the surface. To illustrate the case where the surfaces do not have a sliding angle, we assume that their sliding angles approach  $180^\circ$ .

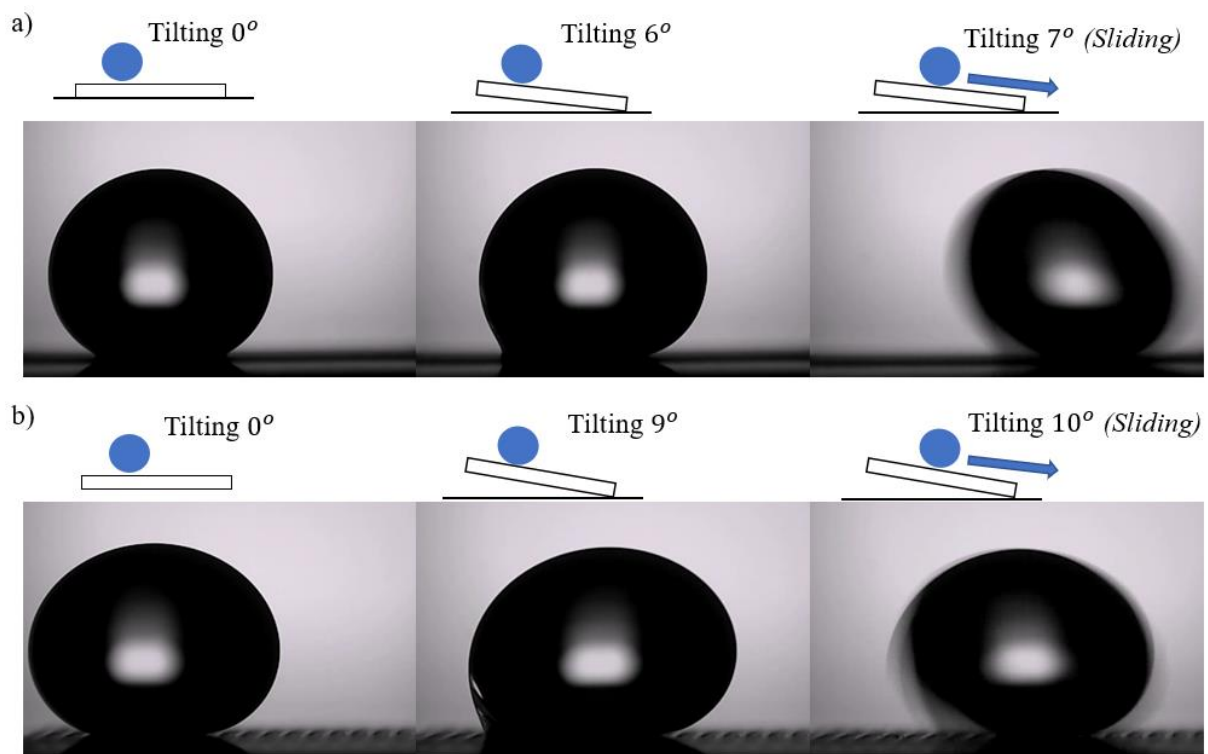


Figure 13. The sliding angle of the line-patterned sample at laser power 3W with a  $200\mu\text{m}$  step size: (a) parallel direction, and (b) perpendicular direction.

### 2.3.3 Stability

After heat treatment, all samples were put in ambient air for 35 days. Wettability measurements were then performed again for all samples, as shown in Figures 14 and 15. With the grid pattern, after 35 days, the contact angle increased from  $1^\circ$  to  $6^\circ$  and the sliding angle was smaller than  $10^\circ$ . Especially at a laser power of 1W with a step size of  $300\mu\text{m}$ , the sliding angle was greater than  $30^\circ$ , which was two times larger than just after heat treatment, and the contact angle increased from  $156^\circ$  to  $162^\circ$ . As shown in Figure 14, line-patterned samples showed behavior similar to the grid pattern. The contact angle increased and sliding angles decreased to less than  $5^\circ$  or  $10^\circ$  at several step sizes compared to their values just after heat treatment. Of special note, several samples that had no sliding angle just after heat treatment now showed a sliding angle, indicating superhydrophobicity, with the sliding angle improving over time.

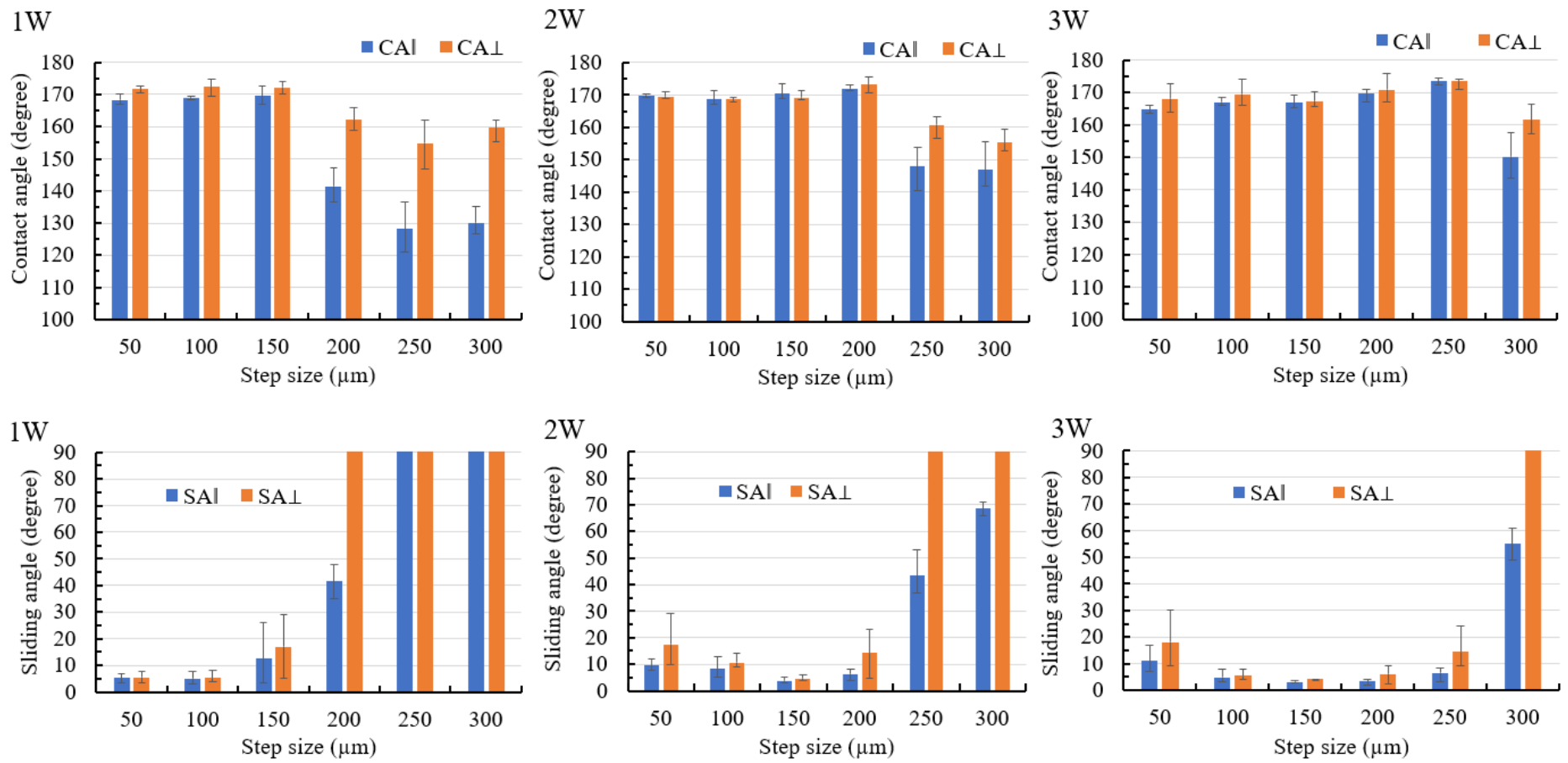


Figure 14. Contact angle and sliding angle for the line pattern 35 days after heat treatment.

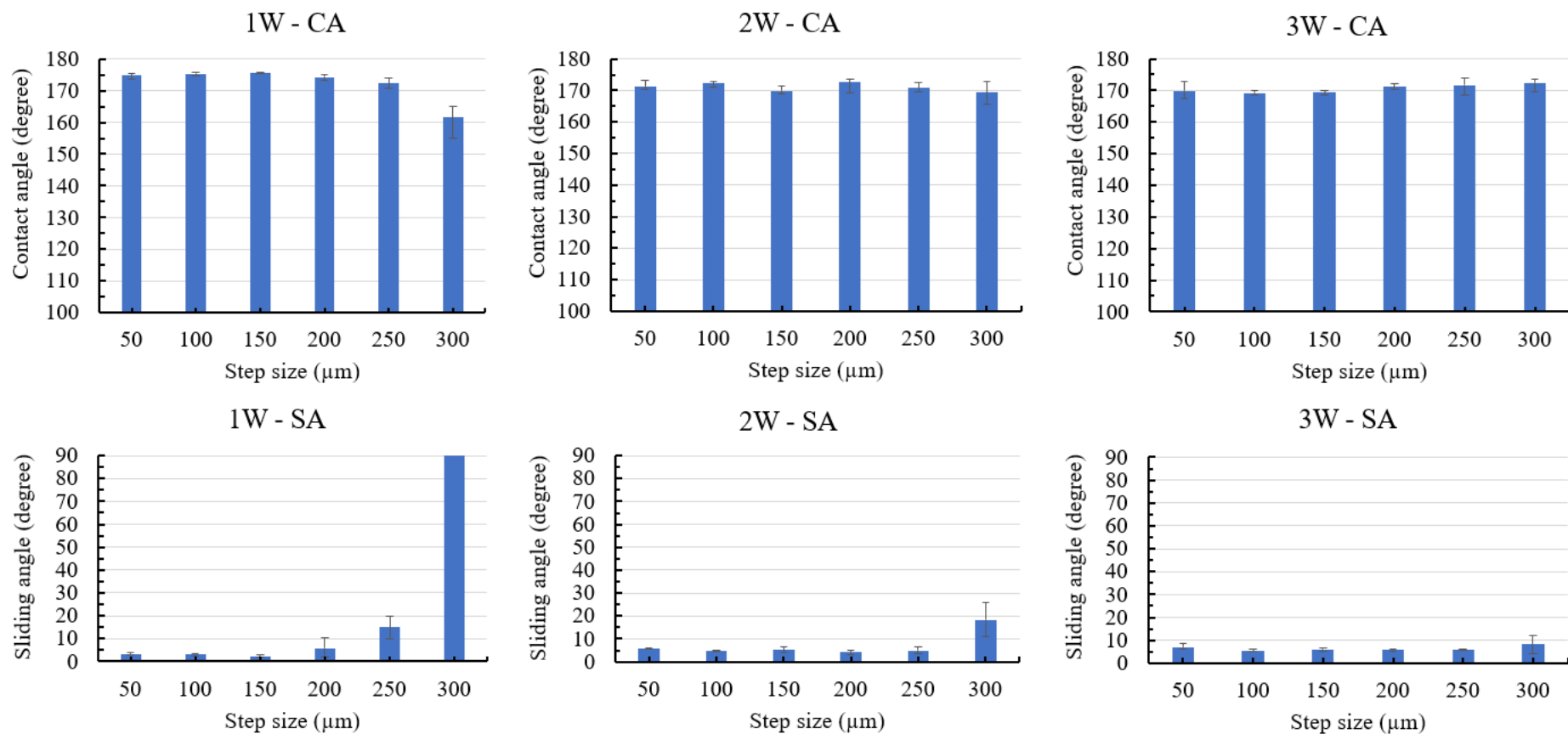


Figure 15. Contact angle and sliding angle for the grid pattern 35 days after heat treatment.

## 2.4 Discussion

### 2.4.1 Effect of the laser power and step size on wettability

Increasing the laser power from 1 to 3W and changing the step size from 50 to 300 $\mu\text{m}$  affected the surface wettability of the grid-patterned surface and the line-patterned surface as shown in Figure 16. The height of the burr increased when increasing the laser power from 1 to 3W. The dimension of microburrs affected the wettability as well as the critical step size. At a small step size (examples: 50, 100 $\mu\text{m}$ ), microburrs still supported the water droplet, but at a big step size (200, 250, 300 $\mu\text{m}$ ), the water droplet might penetrate between the microburrs, and the water droplet could touch on the flat surface. Therefore, a pinning effect was observed, which resulted in isotropic to anisotropic behavior transition of the line-patterned surfaces and the SA change of the grid-patterned surfaces.

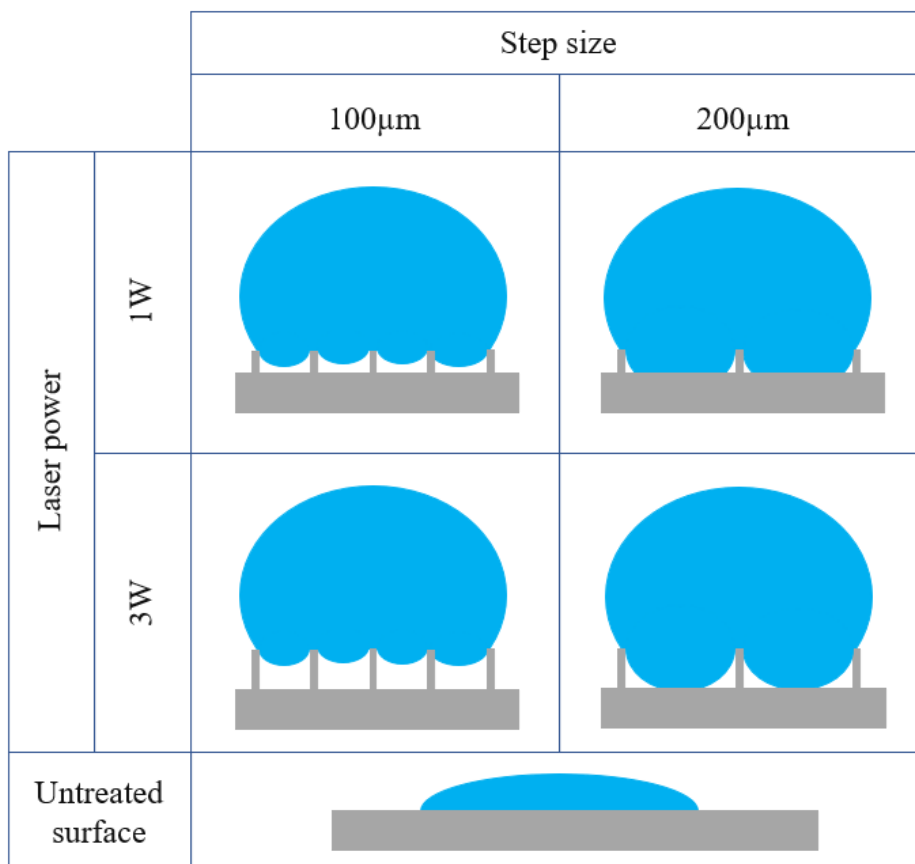


Figure 16. Effect of step size and laser power on wettability.

The contact angles of all samples were greater than  $160^\circ$ , except samples at 1W laser power with  $300\mu\text{m}$  step size. The burr height at 1W laser power was the lowest and the step size of  $300\mu\text{m}$  was the biggest. Therefore, the water droplet could not be supported by burrs and it affected the contact angle and sliding angle. The variation of the sliding angle of the grid-patterned samples showed a clear effect on the decrease in laser power. The values of the sliding angles can be divided into three regions ( $\text{SA} \leq 10^\circ$ ,  $10^\circ < \text{SA} < 180^\circ$ , and No SA) as shown in Figure 17. This result is helpful for other researchers to choose a proper laser power and step size to fabricate the desired superhydrophobic surfaces for specific applications.

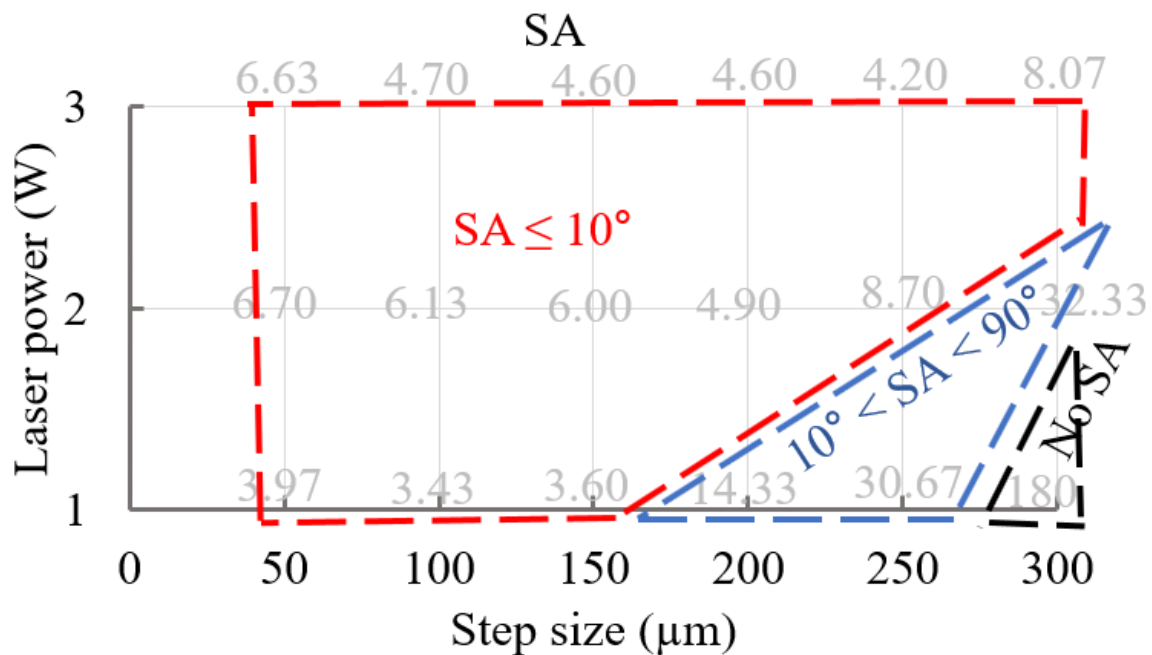


Figure 17. Effect of grid-patterned microstructure on the wetting transition with SA.

With the line pattern, the contact angle decreased when the laser power changed from 3 to 1W while the sliding angle increased and did not have a sliding angle at a large step size ( $200 - 300\mu\text{m}$ ). At a small step size ( $50 - 100\mu\text{m}$ ), when decreasing the laser power, the values of the contact angle and sliding angle show a small difference. When decreasing the laser power with the line samples, the



contact angle showed clearly anisotropic behavior at a large step size (200 - 300  $\mu\text{m}$  at 1W, 250 - 300  $\mu\text{m}$  at 2W, and 300 $\mu\text{m}$  at 3W). These results could provide a useful guide to select the proper values of laser power, step size, and pattern design to produce a contact angle larger than  $160^\circ$  and a sliding angle smaller than  $10^\circ$ .

With the same laser power, the grid-patterned samples showed CAs and SAs better than the line-patterned samples. For good superhydrophobicity and isotropicity, the grid pattern was better. However, for control of water direction applications, the line pattern can be utilized more effectively. The laser power and step size show a clear change in the anisotropy in Figure 18. Figure 18 shows two regions with  $\Delta\text{CA} < 10^\circ$  and  $\Delta\text{CA} > 10^\circ$  related to the isotropic wetting state and anisotropic wetting state, respectively. It is a useful guide for selecting the isotropicity or anisotropic wetting state based on the laser power and step size values. In addition, SAs can be controlled by line patterns.

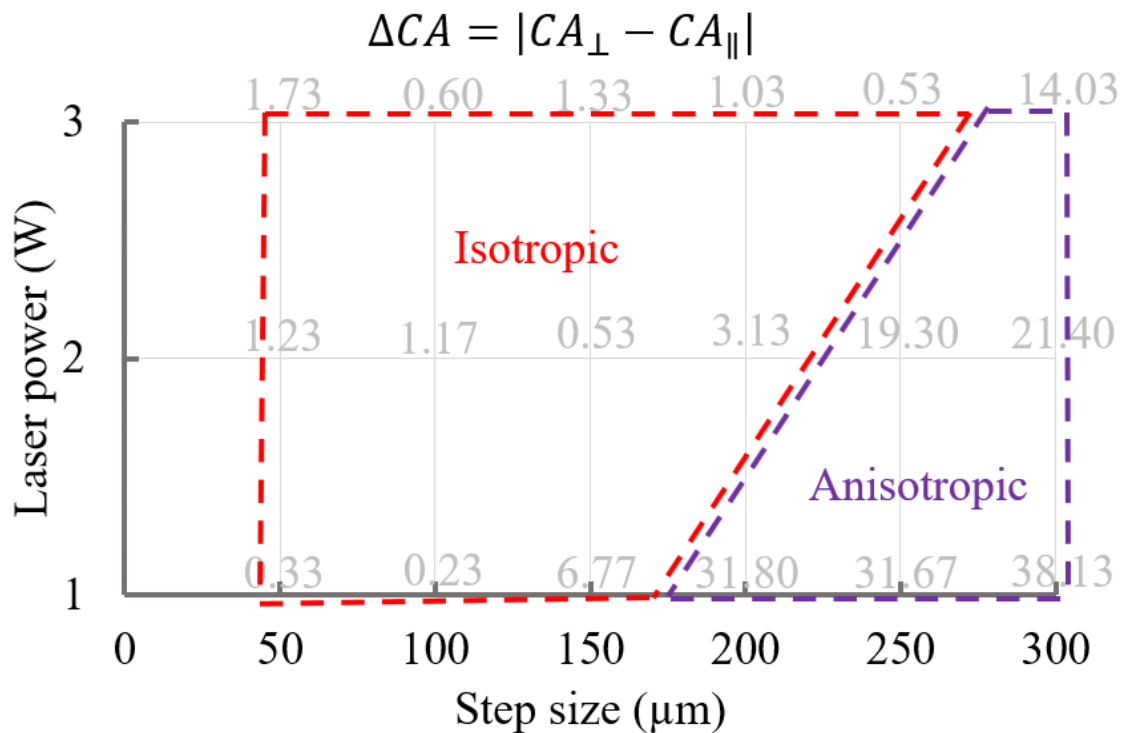


Figure 18. Effect of line-patterned microstructure on the wetting transition from the isotropic state to the anisotropic state.

## 2.4.2 Mechanism

The phenomena of wetting transition on the titanium surfaces from hydrophilic become superhydrophobic surfaces after heat treatment time could be interpreted by investigation of surface chemistry as well as surface morphology. The surface structures of titanium were nano-micro hierarchical structures after laser beam machining and there was no clear change before and after heat treatment. The fabricated paths make clear structures on titanium surfaces as shown in Figures 8, 9, and 19. The superhydrophobicity on the titanium surface was increased as heat treatment time was increased. The results of EDS showed that the atomic ratio of elements on the burr was changed before and after the heat treatment as shown in Table 2. After heat treatment, the wettability of all samples changed from a hydrophilic surface to a superhydrophobic surface. From the results of EDS, the amount of carbon content on the burr was increased regardless of step size and pattern. This result is similar to other researcher's results. The mechanism was reported as organic absorption of hydrophobic groups ( $-\text{CH}_3$ ) [17,32,50]. And this organic absorption can happen in the air, but heat treatment can accelerate the organic adsorption. Therefore, nano-micro hierarchical structures by laser beam machining and low-energy surface by organic adsorption could make the surface superhydrophobic.

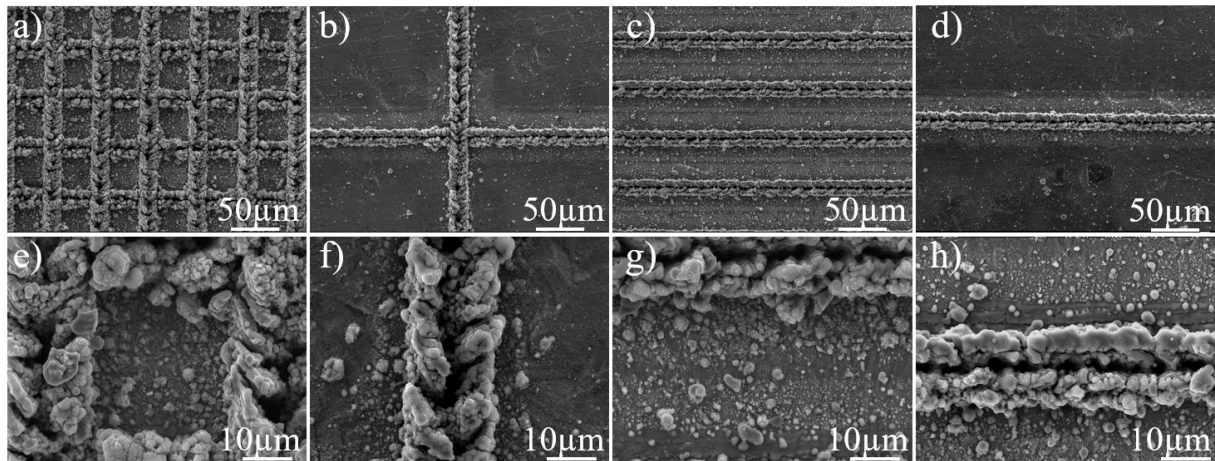


Figure 19. Top-view (a–d) field emission scanning electron microscopy (FESEM) images and (e–h) enlarged images of laser-machined surfaces with different step sizes 50, 300 μm for grid pattern, and 50, 300 μm for line pattern, respectively.

Table 2. Energy-dispersive X-ray spectroscopy (EDS) results on burrs before and after heat treatment.

Element (atomic %)	Line pattern				Grid pattern			
	Step size		Step size		Step size		Step size	
	50 μm		300 μm		50 μm		300 μm	
	before	after	before	after	before	after	before	after
C	6.51	7.33	6.43	9.35	5.67	7.6	7.33	8.35
O	68.26	68.51	47.95	64.52	62.96	63.62	56.95	65.94
Ti	25.23	24.16	45.62	26.12	31.37	28.79	35.72	25.71
C/Ti	0.26	0.30	0.14	0.36	0.18	0.31	0.16	0.32
O/Ti	2.71	2.84	1.05	2.47	2.01	2.63	1.25	2.52

## 2.5 Potential applications

The samples fabricated with a 50 $\mu$ m step size and 1W laser power for grid pattern of titanium surfaces showed superior superhydrophobic performance while for line pattern the step size 100 $\mu$ m, and 2W laser power was chosen for laser fabrication surface as shown in Figure 20. The sample showed low adhesion through with a 10 $\mu$ L volume of water touch on the surface. In addition, water droplets with 10 $\mu$ L volume were dropped from a height of 7cm onto these surfaces with the tilting angle of 4 $^\circ$  and water droplet bouncing was clearly observed for grid pattern and line pattern follow two directions. This demonstrates the good stability of superhydrophobic surfaces fabricated by laser beam machining and heat treatment.

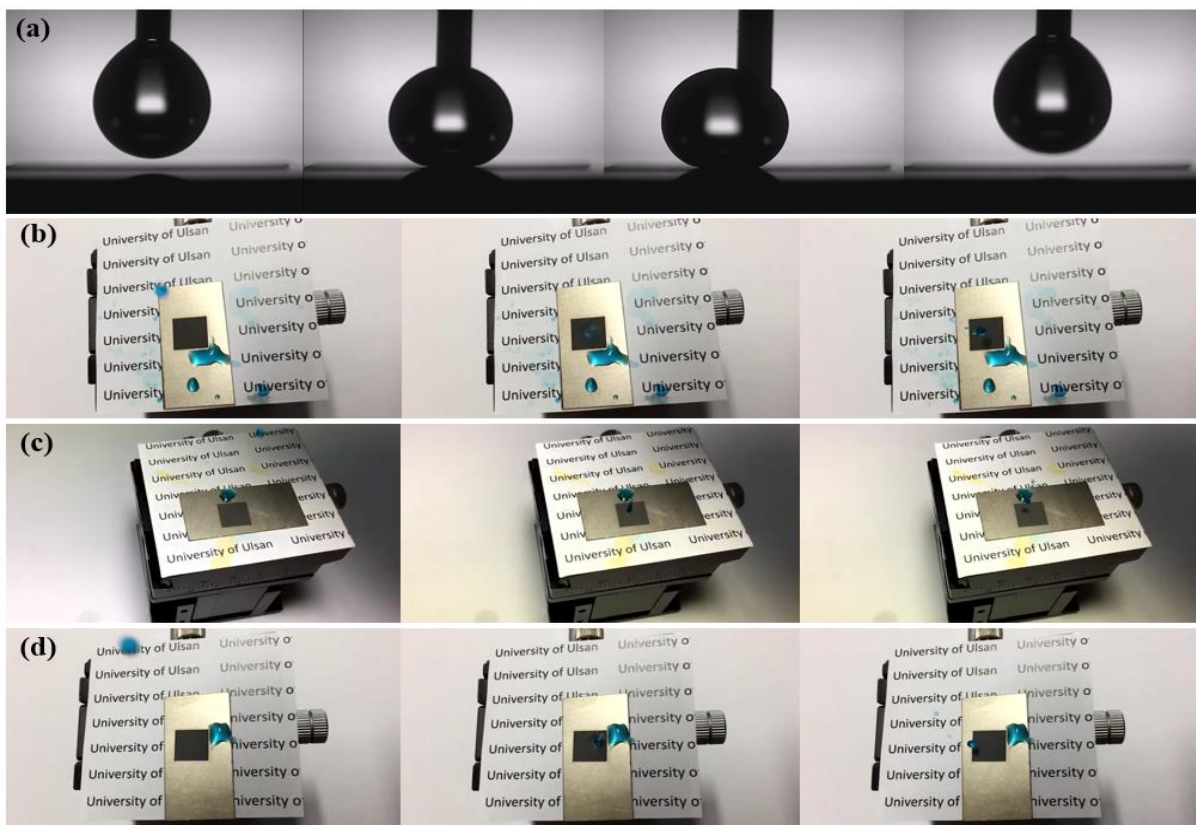


Figure 20. Performance of superhydrophobic titanium surface: (a) water adhesion, (b) water bouncing with grid pattern, (c) water bouncing with line pattern – perpendicular direction, and (d) water bouncing with line pattern – parallel direction.

## 2.6 Summary

This study developed a method to produce a superhydrophobic surface on titanium with no toxic chemicals and with a short time fabrication. The effects of microstructure and step size on superhydrophobicity were investigated. At the same laser power, the grid pattern showed better CA and SA than the line pattern. When decreasing laser power in line-patterned samples, the critical step size for the isotropic to anisotropic transition region was reduced from a large to a smaller step size. The anisotropic behavior was clearly observed at 1W with a 200 $\mu$ m to 300 $\mu$ m step size. With decreasing laser power in the grid-patterned samples, the critical step size for the lotus effect and petal effect region was reduced. The obtained results could provide a useful guide to select proper fabrication parameters for the fabrication of desired superhydrophobic surfaces. For a high-quality superhydrophobic surface and isotropicity, the grid pattern was a good candidate. To make a superhydrophobic surface with strong anisotropic behavior to control the water direction, the line pattern is preferred.

**Chapter 3:**  
**Fabrication**  
**superhydrophobic on glass**  
**surface by using laser beam**  
**machining and heat**  
**treatment**

### 3.1 Background

A variety of methods of fabricating superhydrophobic surfaces are now available, including laser machining [15,16], layer-by-layer assembly [51], and chemical etching [14]. Among them, laser machining has been used widely because of its precision and effectiveness for patterning on various material substrates. Besides, many types of materials can be used in fabricating superhydrophobic surfaces such as metals (copper, aluminum, titanium) [20,32,52], ceramics (glass and sapphire) [53,54], polymers [43,55], and silicon [56]. Among these materials, glass is a unique material with high transmittance, low-cost with a variety of applications encountered in daily life such as windows (vehicles, buildings, etc.), display panels for electronic (mobile monitors, etc.), military purpose, telecommunications, and biomedical [57]. With many advantages, the glass was chosen to fabricate a superhydrophobic surface. Any glass with nanoscale or microscale roughness on its surface can become superhydrophobic, and considerable research efforts have been devoted to improving fabrication methods, such as plasma etching [58], coating [59–61], and laser machining combined with chemical coating [62–64]. However, these methods require multi-step procedures, toxic chemicals, or additional complex processes for pattern fabrication. Moreover, fabricating superhydrophobic glass surfaces in parallel with keeping their high transparency is still a big challenge for researchers. In fact, to enhance the superhydrophobicity, the roughness of the surface should be increased; however, such an increase, on another side, reduces the transmittance of light due to the light scattering. This paradox is always a difficult problem for researchers to create both superhydrophobic and transparent surfaces. Up to the present, some researchers have achieved the result of good transmittance and superhydrophobic but in these processes need to high temperatures such as 550°C [65], and 1100°C [66]. In these research, the CA on

glass surface smaller than  $164^\circ$ . Besides, it is pointed out that the CA of glass tends to reduce after being put in the air for a long time (42 days) [67].

In this study, we focus on a facile method to make a superhydrophobic glass surface with CA higher  $170^\circ$  by controlled fabrication areas, low environmental impact, no chemical usage, acceptable transparency, stability in the air for a long time, and ease of application to the bio-medical field. The results show that the fabrication of a transparent superhydrophobic surface can be realized with laser-beam machining and simple heat treatment and without the use of additional chemical coatings. The fabricated superhydrophobic surface exhibited stability after 8 weeks in ambient air. In addition, we investigated the effects of step sizes and laser power on superhydrophobicity and transmittance. A study of the effects of process parameters during fabrication can provide guidelines and a reference for controlling the wettability and transparency of glass surfaces.

## **3.2 Experiment**

### **3.2.1 Fabrication methods**

A Q-switched Nd: YAG 355nm ultraviolet nanosecond pulse laser (Awave 355-3W 20KHz, Advanced Optowave, Ronkonkoma, NY, USA) was used with optics and a 3-axis translation stage, as shown in Figure 21a. A laser source provided a laser beam, and an attenuator controlled the laser power. A beam expander was used to increase the beam diameter, and the laser light was converged by a focusing lens to ablate on the substrate. Beam position was controlled using a 3-axis translation stage.



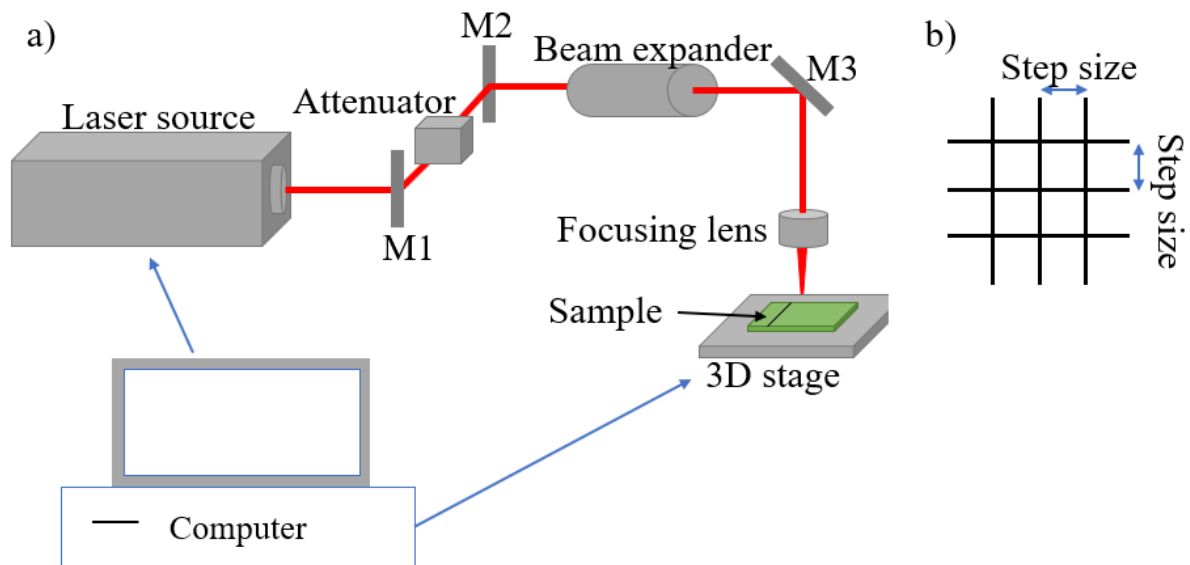


Figure 21. Schematic of (a) the laser-beam machining system, and (b) a laser-beam path (grid pattern).

A commercially available soda-lime glass with a thickness of 1mm (Microscope slides 7101, Henso Labware Manufacturing, Hangzhou, China) was used. The chemical composition of the glass is supplied in Table 3.

Table 3. Composition of the soda-lime glass

Oxide	SiO <sub>2</sub>	Na <sub>2</sub> O	K <sub>2</sub> O	CaO	MgO	Al <sub>2</sub> O <sub>3</sub>	Fe <sub>2</sub> O <sub>3</sub>
wt. %	72.00	14.50	0.30	7.05	3.95	1.65	0.06

The effects of laser power and step sizes on superhydrophobicity and transparency were recorded, and the process parameters are summarized in Table 4. The beam path was a grid pattern, as shown in Figure 21b, and the fabrication area was  $5 \times 5\text{mm}^2$ . After laser-beam machining, all samples were put in a commercial oven for 48 hours at 240°C. All samples were then cooled at room temperature for an hour to permit an examination of wettability and transmittance.

Table 4. The process parameters by using laser beam machining and heat treatment.

<b>Name of Parameter</b>	<b>Value</b>
Power (W)	0.2; 0.3; 0.4; 0.5
Pulse Frequency (kHz)	20
Scanning speed (mm/s)	1
Step size ( $\mu\text{m}$ )	150; 200; 250; 300; 350
Number of samples	5

### 3.2.2 Surface analysis

The surface structure was analyzed by a 3D laser scanning confocal microscope (VK-X200 series, Keyence, Osaka, Japan), and by a field emission scanning electron microscopy (SEM, JSM-6500F, Jeol Co., Tokyo, Japan). Figure 22 shows the SEM images taken at a laser power of 0.4W and a step size of 200 $\mu\text{m}$ . While Figure 23-25 shows the images from a confocal microscope with the samples fabricated at different laser powers and step sizes. All samples showed burrs and redeposited materials around the channels. The average burr heights were obtained from 20 measurements of each sample. The average burr heights of samples with 0.5W and 0.4W of laser power were approximately 4.8 $\mu\text{m}$  and 2.5 $\mu\text{m}$ , respectively. The average burr heights of samples taken at lower laser powers (0.3W and 0.2W) were smaller than 1 $\mu\text{m}$ . The wettability of samples was assessed by measuring the CA and SA with 9 $\mu\text{L}$  water droplets using a contact angle meter (SmartDrop, FemtoFab, Korea). The volume of water was 9 $\mu\text{L}$  because a water droplet of 8 $\mu\text{L}$  could not be easily separated from the needle to the surface due to low adhesion on the surface. The SA was measured when the surface was moved at a speed of 1.6°/s. The transmittance values of the fabricated glass surface were measured using an ultraviolet-visible-near infrared spectrophotometer with a visible spectrum range from 380nm to 750nm.

Energy-dispersive X-ray spectroscopy (EDS, JSM-6500F, Jeol Co., Tokyo, Japan), high-resolution X-ray diffraction (XRD, Bruker D8 Discovery), and Fourier-transform infrared spectroscopy (FTIR, Varian 670-IR, Varian Inc., USA) were used to analyze the chemical composition of the fabricated glass surface.

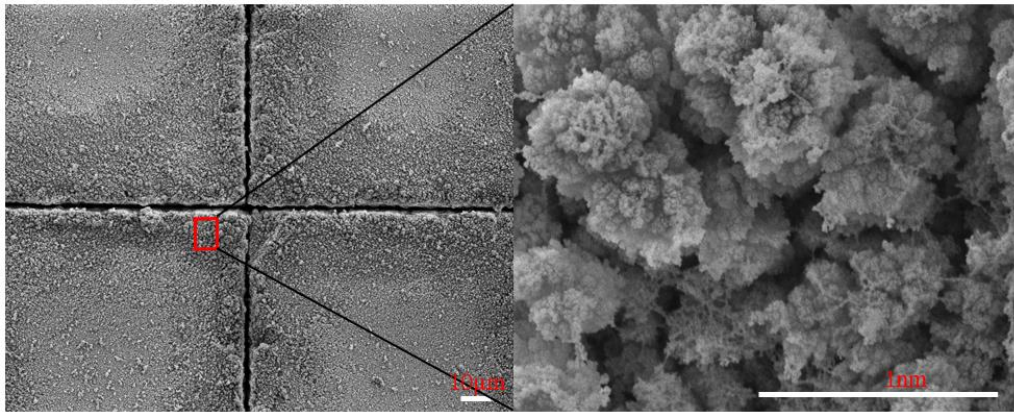


Figure 22. FESEM images of a sample with 0.4W laser power and 200µm of step size.

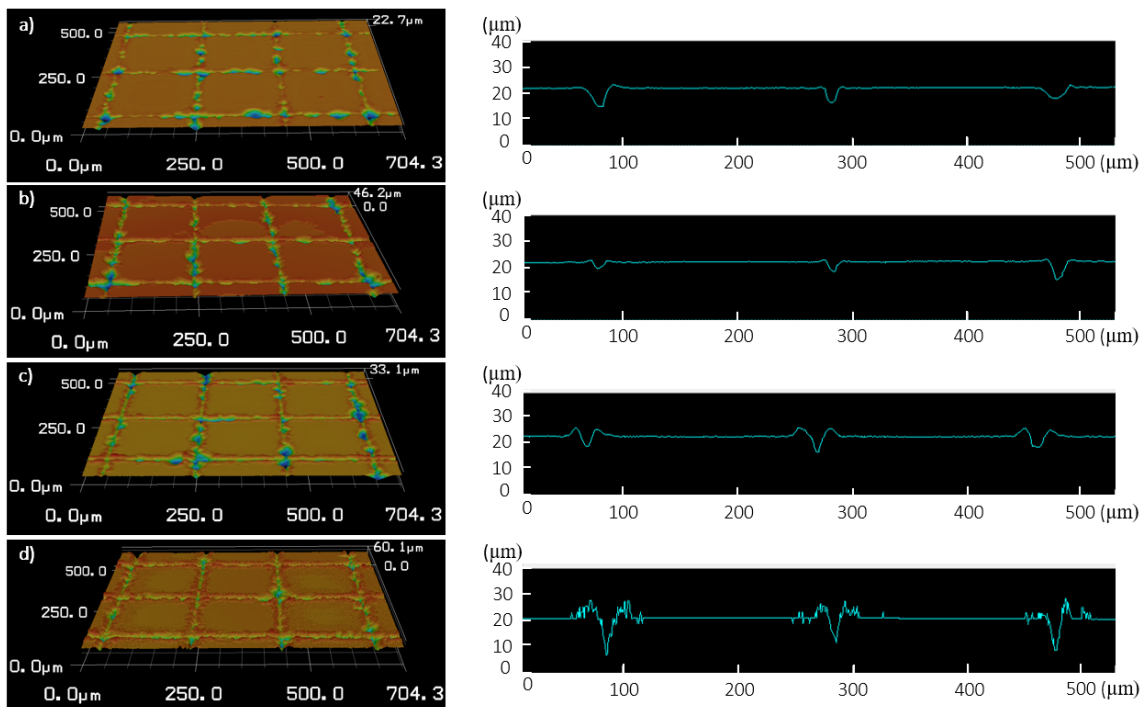


Figure 23. Confocal microscope images of the laser-processed surfaces at 200µm step size and different laser power a) 0.2, b) 0.3, c) 0.4, d) 0.5W.

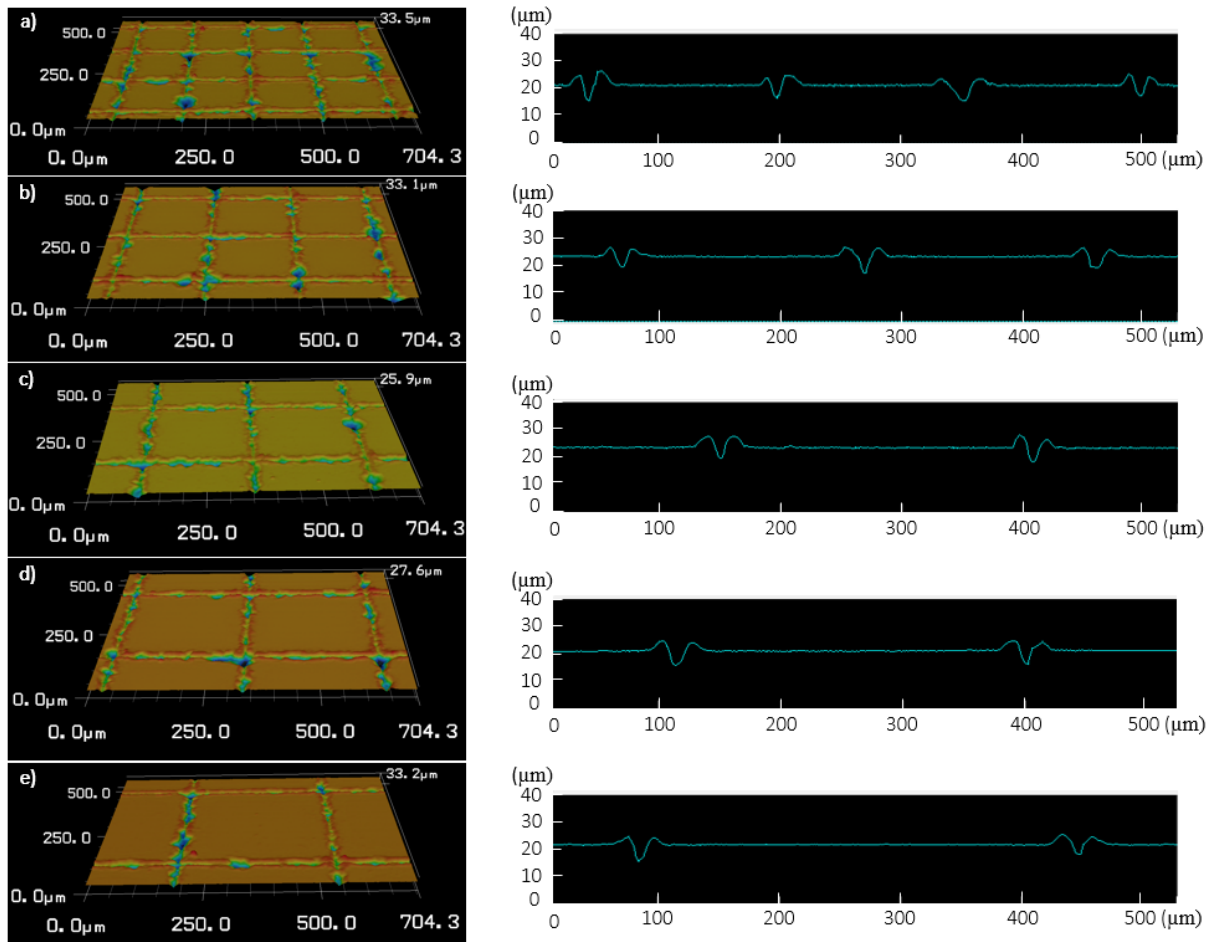


Figure 24. Confocal microscope images of the laser-processed surfaces at 0.4W laser power and different step size a) 150, b) 200, c) 250, d) 300, e) 350 $\mu\text{m}$ .

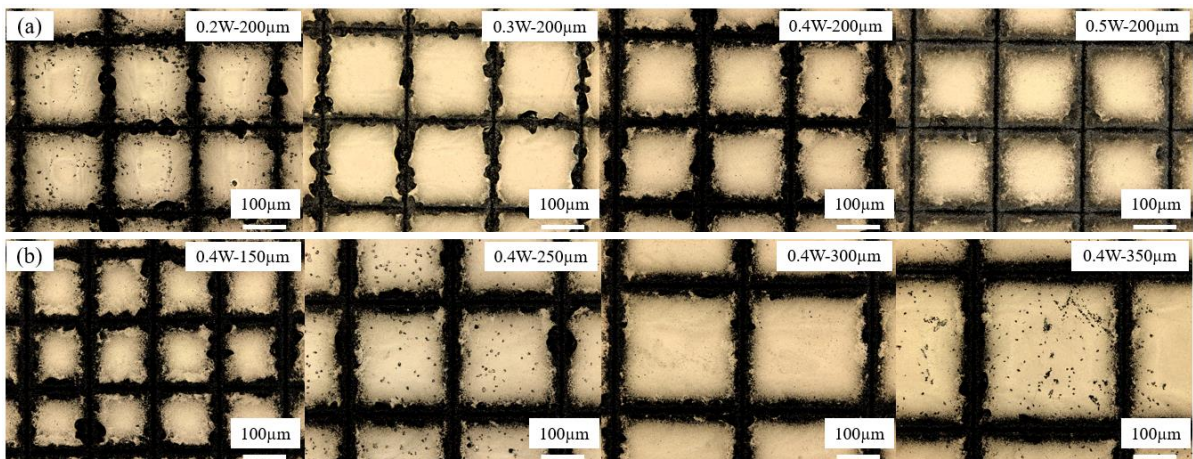


Figure 25. Confocal microscope images of the laser-processed surfaces with (a) different powers at 200 $\mu\text{m}$  step size, and (b) different step sizes at 0.4W of laser power.

### 3.3 Results

#### 3.3.1 Wettability

The flat bare glass surface is hydrophilic, with a CA of  $46^\circ$  as shown in Figure 26a. In Figure 26, the CAs were measured on the 3 different surfaces, including a flat glass surface, a surface before heat treatment (or just after laser fabrication), and a surface after heat treatment (or after laser fabrication and heat treatment). The laser-machined surface before heat treatment showed approximately  $20^\circ$  of CA. However, the surface became superhydrophobic with a CA larger than  $170^\circ$  after heat treatment.

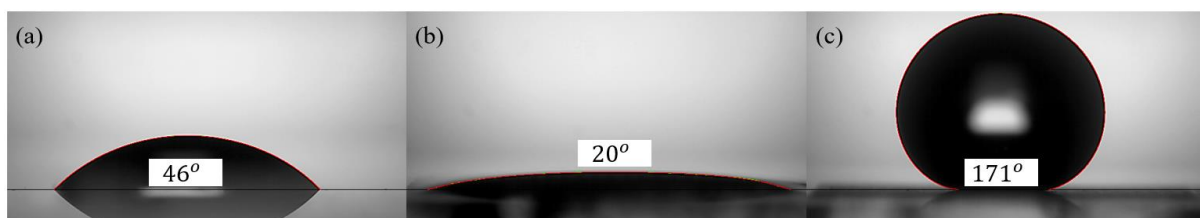


Figure 26. Contact angle images of (a) flat glass and a sample fabricated with 0.4W laser power and  $200\mu\text{m}$  of step size, (b) before heat treatment, and (c) after heat treatment.

In this study, we examined the effects of process parameters by changing the laser power and the step size. The laser power changed from 0.2W to 0.5W. Step size was increased from  $150\mu\text{m}$  to  $350\mu\text{m}$ . Just after laser-beam machining but before heat treatment, all glass surfaces became more hydrophilic compared with bare flat glass, with contact angles smaller than  $20^\circ$  and no sliding angles. After the samples were stored in ambient air for 8 weeks, all samples showed a CA of approximately  $21^\circ$  and no SA. This phenomenon differed greatly from the effects of laser-ablated metals. Nanosecond-laser-ablated metals such as copper, stainless steel, aluminum, and titanium become superhydrophobic or showed an

increased CA after several weeks in ambient air. In addition, heat treatment at 100°C or 200°C to the laser-ablated metals accelerated the wettability transition from several weeks to several hours. The mechanism for such wettability transition from hydrophilic surface to the superhydrophobic surface of laser-ablated metals was explained as organic absorption or reduction [5,8]. However, the laser-ablated glass could not become superhydrophobic after heat treatment at 200°C for 24 hours. These results indicated that the wettability transition of laser ablation and heat treatment on the glass surface was relatively slower than the ones of metals. Hence, the laser-ablated glass for superhydrophobic surfaces required a higher temperature and longer heat treatment time than metals. After heat treatment for 48 hours at 240°C, all samples became superhydrophobic, with a CA greater than 150°. As shown in Figure 27, all samples fabricated with 0.4W and 0.5W of laser power exhibited a high CA ( $> 170^\circ$ ) and small SA ( $< 10^\circ$ ), which are adequate for self-cleaning applications. Samples fabricated with 0.2W and 0.3W of laser power and small step size (150 $\mu$ m) had a high CA ( $> 170^\circ$ ) and small SA ( $< 10^\circ$ ). However, with a relatively large step size (200 $\mu$ m to 350 $\mu$ m), the samples did not show a small SA ( $> 10^\circ$ ). The SA increased with a step size.

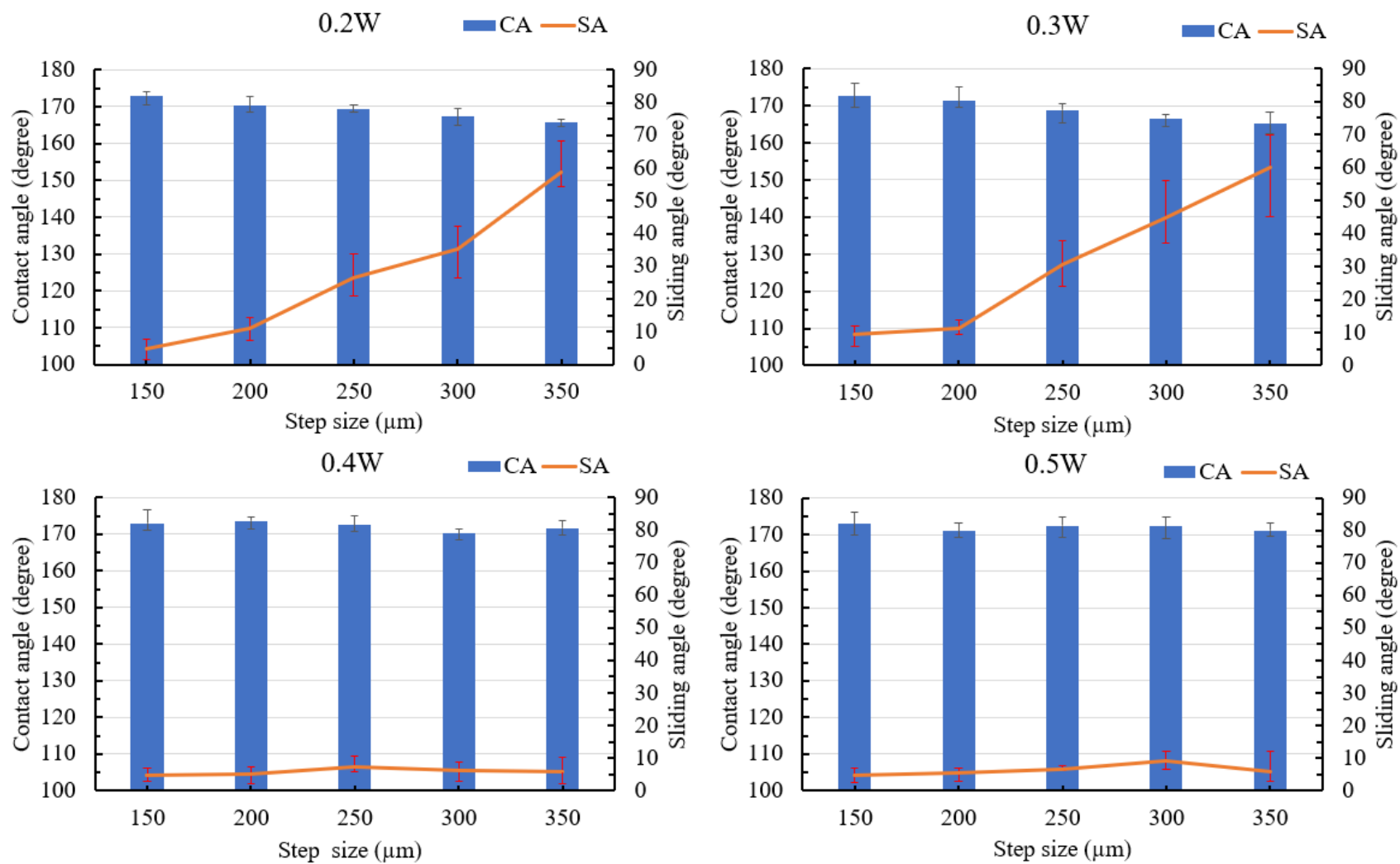


Figure 27. Contact and sliding angle of samples after heat treatment.

### 3.3.2 Transparency

The transmittances of the laser-ablated glass surfaces at different laser powers and step sizes were measured with an ultraviolet-visible-near infrared spectrophotometer in the visible spectrum range from 380nm to 750nm, as shown in Figure 28. As the laser power increased, the transmittance of the fabricated glass decreased because of the increases in burr height and channel depth. As the step size increased, the transmittance of the fabricated glass increased because of the decreased ratio between the fabricated and non-fabricated areas. The highest transmittance was observed in the sample produced with the lowest laser power (0.2W) and the largest step size (350 $\mu$ m); transmittance was higher than 70% in visible light. However, the sample did not have a SA smaller than 10°. Among the samples with a SA smaller than 10°, the transmittance of the sample fabricated with 0.4 W of laser power and a 350 $\mu$ m step size was higher than 60% in visible light.



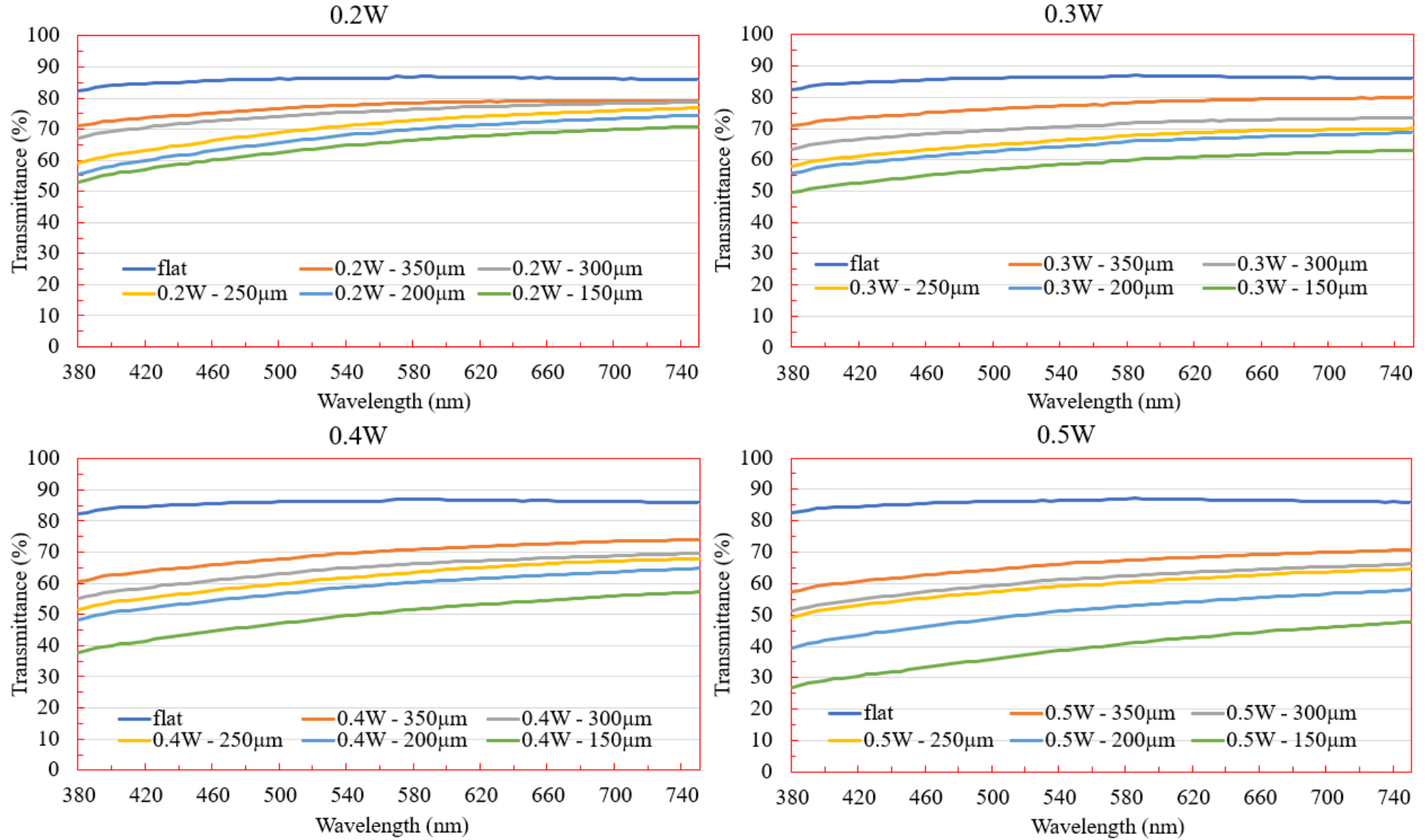


Figure 28. Transmittance results of unprocessed glass and laser-fabricated glass at different laser power and step sizes.

As shown in Figure 29, transmittance differences among samples with different laser powers and step sizes can be clearly observed.

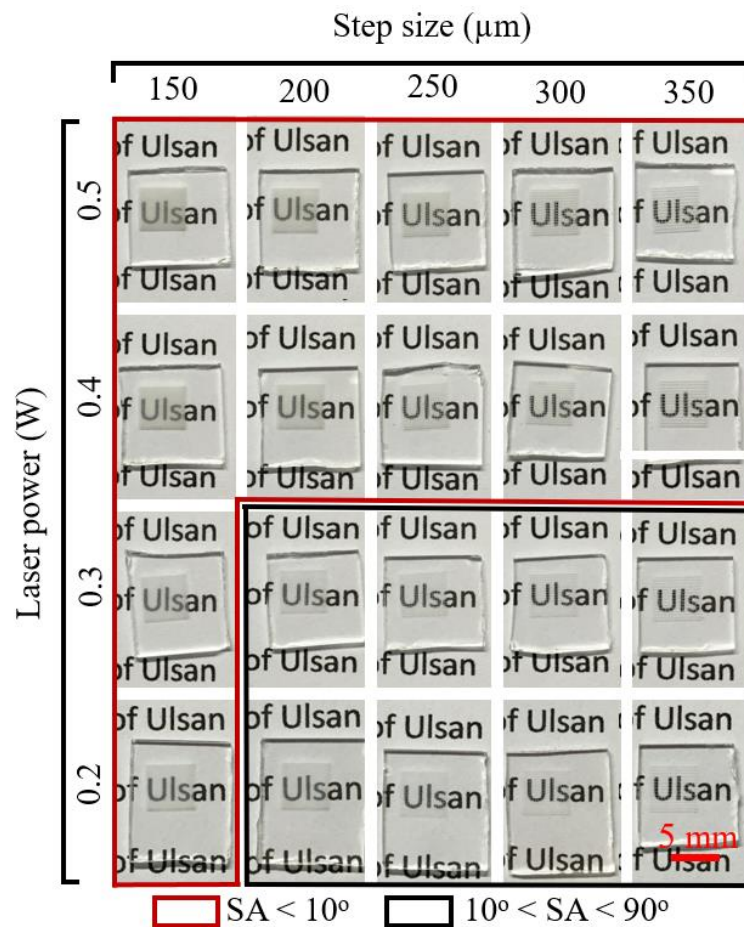


Figure 29. Top view of real images at different step sizes and laser powers.

As could be seen in Figure 30, after the laser fabrication process, the surface became rough with burrs and channels. Therefore, the light could reflect in different directions through the rough glass surface. Besides, as shown in Figure 30, the transparency of the surface fabricated with 0.5W of laser power and a 150 $\mu$ m step size was the lowest. However, the text behind this sample was still readable. At the same laser power of 0.5W, with a step size adjusted to 350 $\mu$ m, the result of such an adjustment is illustrated in the second image in Figure 30. It could be seen that the text behind the fabricated area in the second image appeared more clearly than in the first one. Next, the laser power was

reduced from 0.5W to 0.2W, resulting in the fabricated area showing the highest transparency among the samples, and the text behind the fabricated area was very clearly displayed. Hence, it could be concluded that the change of laser power and step size affects transparency. Besides, as shown in Figure 29, samples fabricated with different laser powers and step sizes can be divided into two groups in the basis of SA results from Figure 5: a group of the samples surrounded by the red line with a SA  $< 10^\circ$  and a group of the samples surrounded by the black line with a SA between  $10^\circ$  and  $90^\circ$ . These results can help other researchers choose superhydrophobic surfaces with different SA values and high transmittance.

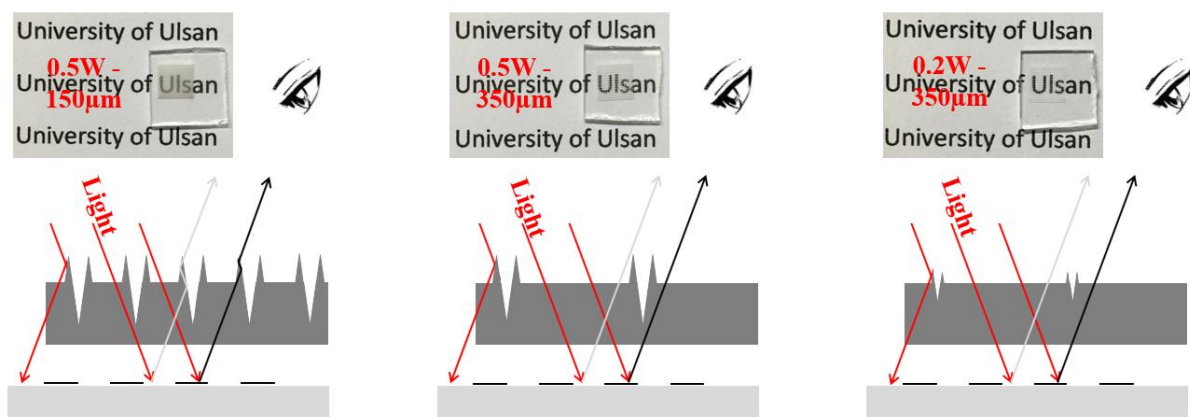


Figure 30. Schematic image of light interactions with different surface structures.

### 3.3.3 Stability and robustness

To check the stability of the fabricated superhydrophobic glass surfaces, the surfaces fabricated at different laser powers, and step sizes were stored in ambient air after heat treatment. The wettability was re-evaluated after 8 weeks to examine the stability of the superhydrophobicity. As shown in Figure 31, all samples maintained their superhydrophobicity. The samples with relatively high SA also showed small changes in SA after 8 weeks, indicating that SA can be controlled with process parameters and used for an extended period.

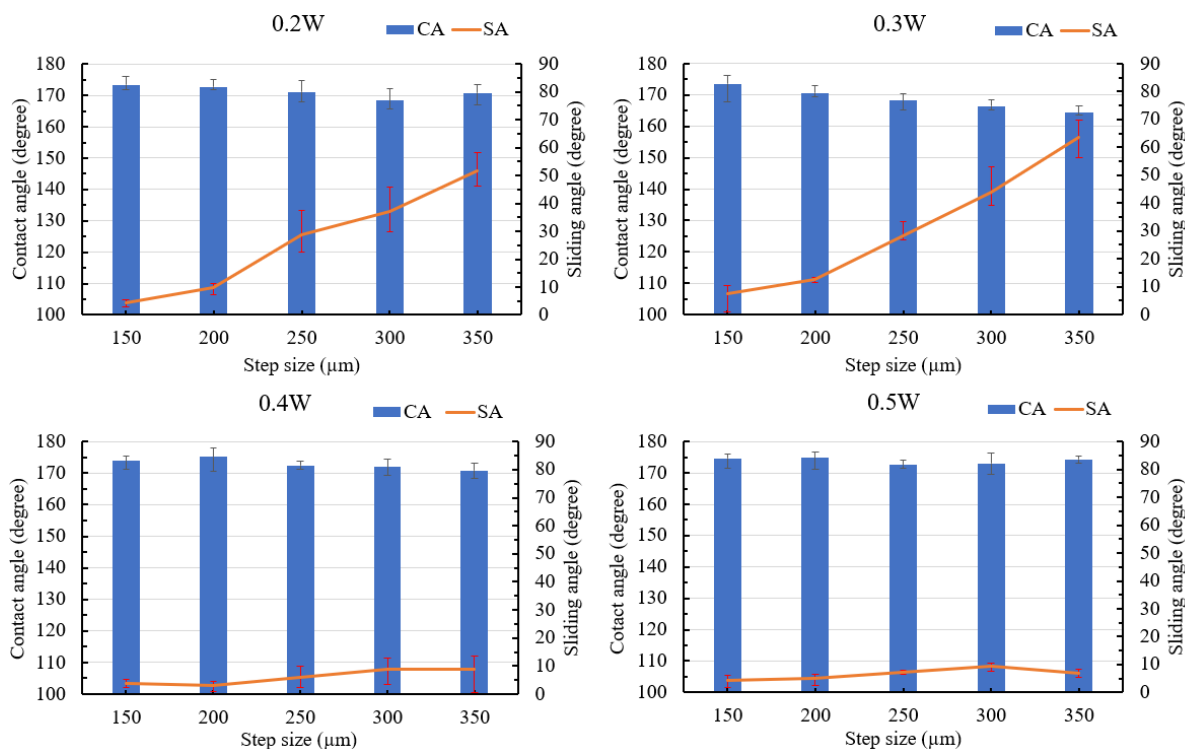


Figure 31. Contact and sliding angle of samples after 8 weeks in ambient air since laser fabrication and surface heat treatment.

The robustness of the superhydrophobicity on the glass surface was checked by an aging and scotch tape test. In the aging test, the samples were put in the ambient air for a long time (8 weeks), the surfaces did not show the decrease in CA but the reduction of SA. For the scotch tape test, as shown in Figure 32a, the samples with 0.4W laser power and 200 $\mu$ m step size were prepared by laser fabrication and heat treatment, and then a tape (3M Scotch Transparent tape 550, Seoul., Korea) was put on these surfaces. A 1kg weight was used for sufficient adhesion, and the tape was removed. This tape test was repeated until four times, and the CA and SA were measured every tape test. As the number of tape tests increased, the SA increased while the CA decreased but higher than 160° as shown in Figure 32b. After the fourth tape test, there was no SA. It means that the robustness of the superhydrophobic glass surface fabricated by the laser and heat treatment could be removed after the four tape tests. Therefore, in the use of this method for making a superhydrophobic glass surface, all samples seemed to be suitable and robust with applications without direct touch of the surface.

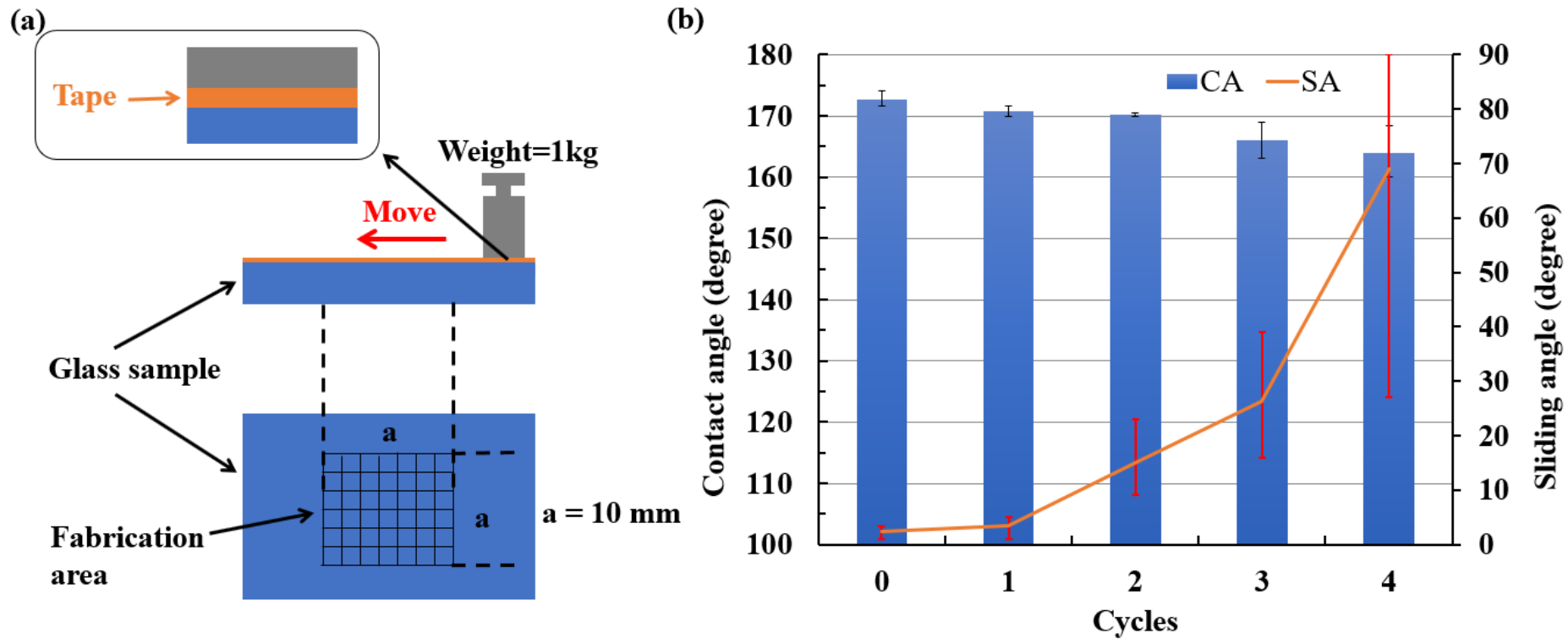


Figure 32. (a) Schematic of the scotch tape test for evaluating the stability and durability of the superhydrophobic glass surface, and (b) CA and SA results on the sample with laser power  $0.4\text{ W}$  -  $200\mu\text{ m}$  step size after the tape test.

## 3.4 Discussion

### 3.4.1 Effect of step size and laser power on wettability and transmittance

It is well known that to make a superhydrophobic surface, a rough surface at micro or nanoscale is necessary. In this study, the rough surfaces were created by laser machining. The change of laser power and step size affected CA and SA as shown in Figure 33a. There were two different groups of surfaces determined by CA and SA results. For the group of the lower laser power (0.2 and 0.3W), increasing the step size decreased the CA and increased SA. However, as shown in Figure 33a, this tendency did not occur in the higher laser power group (0.4 and 0.5W). It meant that the samples with higher laser power (0.4 and 0.5W) have the burr heights bigger than  $2.5\mu\text{m}$ , and there was no significant difference in the CA and SA after changing step size from 150 to  $350\mu\text{m}$ . However, the samples with lower laser power (0.2 and 0.3W) have the burr height smaller than  $1\mu\text{m}$ , and the CA and SA of surfaces showed clearly a downward and upward trend respectively with increasing step size from 150 to  $350\mu\text{m}$ . From this result, it could be concluded that the burr height was an important factor affecting CA and SA. Besides, in the case of the burr height smaller than  $1\mu\text{m}$ , the change of step size also affects CA and SA. At a step size smaller than  $200\mu\text{m}$ , the surface would show SA smaller than  $10^\circ$ . However, the SA increased as the step size increased. Figure 33b shows the transmittances of the samples at the optical wavelengths of 400nm and 700nm. The transmittance increased as the laser power decreased, and the step size increased. These results can provide guidelines for controlling transmission and creating superhydrophobic glass surfaces.

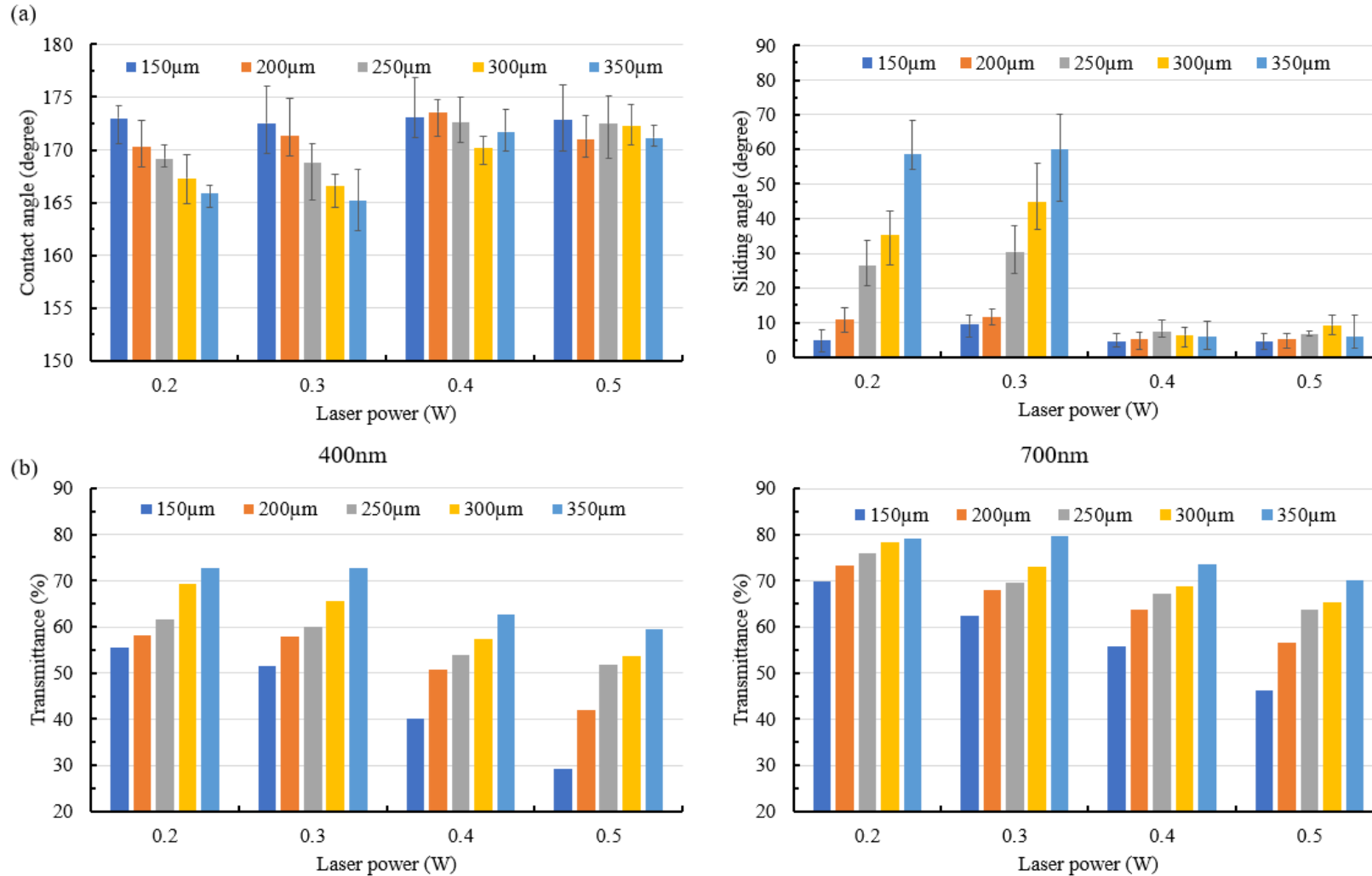


Figure 33. (a) CA and SA results, and (b) transmittance at 400nm and 700 nm of light wavelength at the visible spectrum of all samples with different step sizes and laser power.



### 3.4.2 Mechanism

To make a superhydrophobic surface, a rough surface at the micro or nanoscale and low surface energy materials are required. Rough surface morphology can be seen in Figures 22 - 25. To identify the low surface energy material, surface chemistry was observed.

The crystalline structures of the flat bare glass surface, surface before heat treatment (or laser-fabricated surface), and surface after heat treatment (or samples after laser fabrication and heat treatment) did not change, as shown in the XRD results (Figure 34). However, clear chemical composition changes on the surfaces were observed in the micro-burr area and the area between two fabricated lines, as shown in the EDS results (Table 5). When the chemical composition before and after heat treatment was compared, the ratio of atoms between Si and other elements such as Na, Mg, Al, K, and Ca did not clearly change. However, the ratio of atoms between Si and other elements such as C and O clearly changed after heat treatment. After heat treatment, the ratios of O/Si and C/Si also clearly increased. Carbon, in particular, was newly observed in the area between the two fabricated lines after heat treatment. This suggests that organic materials, including carbon can be attached during heat treatment. In general, organic materials show hydrophobicity. These results were observed on the laser-ablated metallic surface. Through the heat treatment process after laser ablation, the heat treatment could accelerate organic absorption on the surface [20,50,52]. This leads to the surface changing from a hydrophilic to a hydrophobic condition with the low surface energy becoming superhydrophobic.

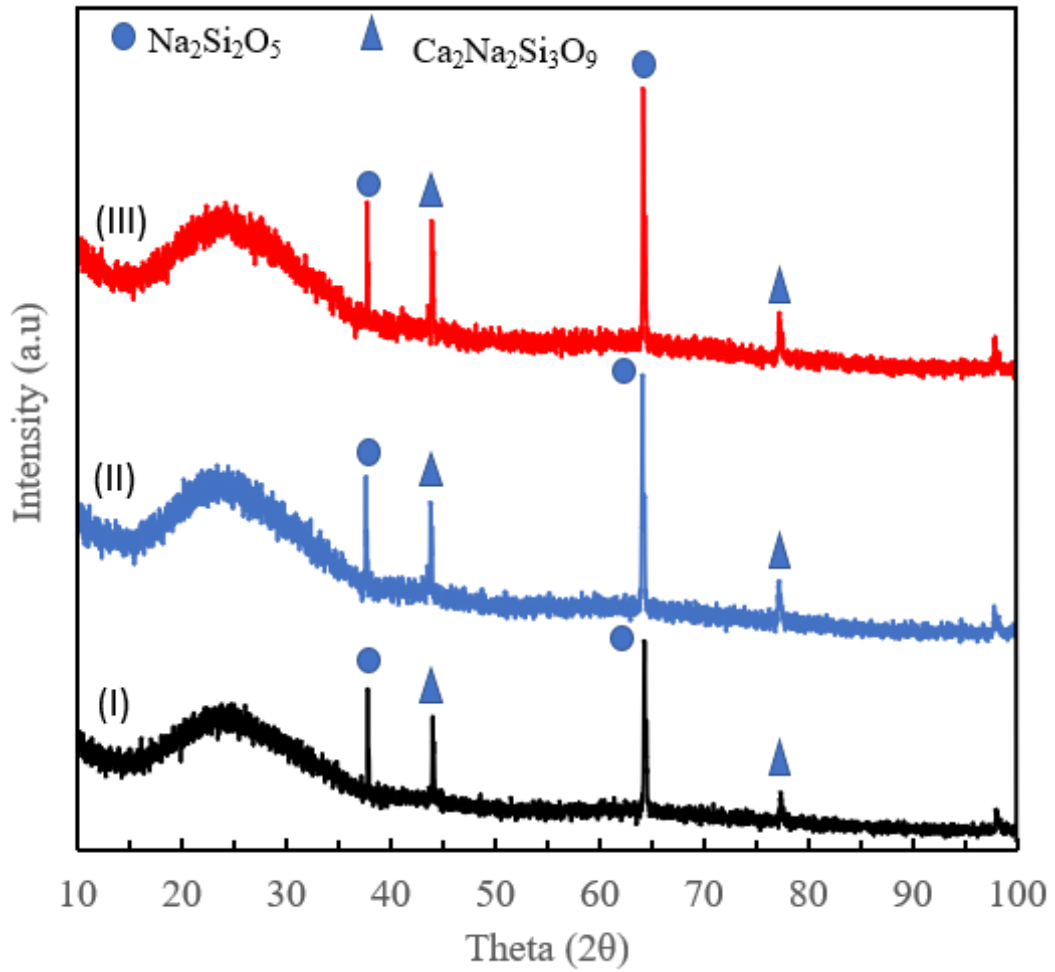


Figure 34. XRD results of soda-lime glass: (I) flat bare glass, (II) laser-ablated glass before heat treatment, and (III) laser-ablated glass after heat treatment.

Table 5. EDS results on burr and non-fabrication area of the soda-lime glass surface.

Element (Atomic %)	Before heat treatment		After heat treatment	
	On burr	On a flat area between two fabricated lines	On burr	On a flat area between two fabricated lines
C	7.47	0.00	8.73	7.35
O	66.31	70.59	69.61	66.35
Na	6.88	5.48	6.36	5.34
Mg	1.33	1.79	1.15	1.58
Al	0.34	0.53	0.27	0.48
Si	16.23	19.70	12.81	17.20
K	0.16	0.14	0.08	0.00
Ca	1.29	1.76	1.01	1.68
C/Si	0.46	0.00	0.68	0.43
O/Si	4.09	3.58	5.43	3.86

The hydrophilic soda-lime glass before the heat treatment and the superhydrophobic soda-lime glass after heat treatment were observed using FTIR spectra, as shown in Figure 35. In the hydrophilic glass, the transmittance peak observed at approximately  $3400\text{ cm}^{-1}$  was assigned to free or adsorbed water. The intensity for the transmittance peaks at  $1413$ ,  $1566$ ,  $1640$ , and  $1723\text{ cm}^{-1}$  correspond to C-H, C=O, molecular water, and C-O bonding, respectively. After heat treatment, the transmittance peaks at  $1295$  with weak C-H bonding became unclear. However, one peak shows an increasing trend after heat treatment at  $1041\text{ cm}^{-1}$ , which can be attributed to mode Si-O-Si vibrations.

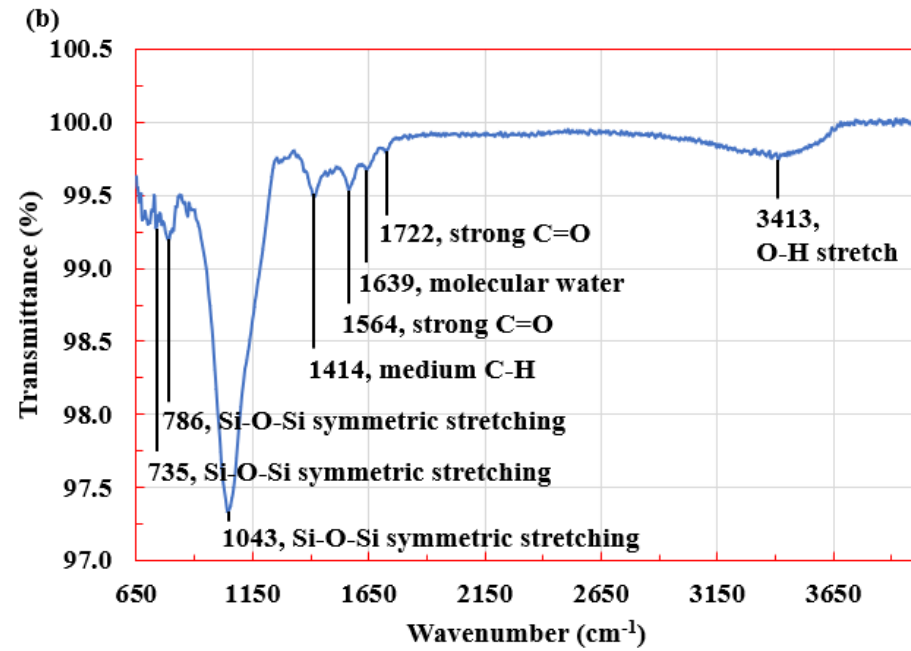
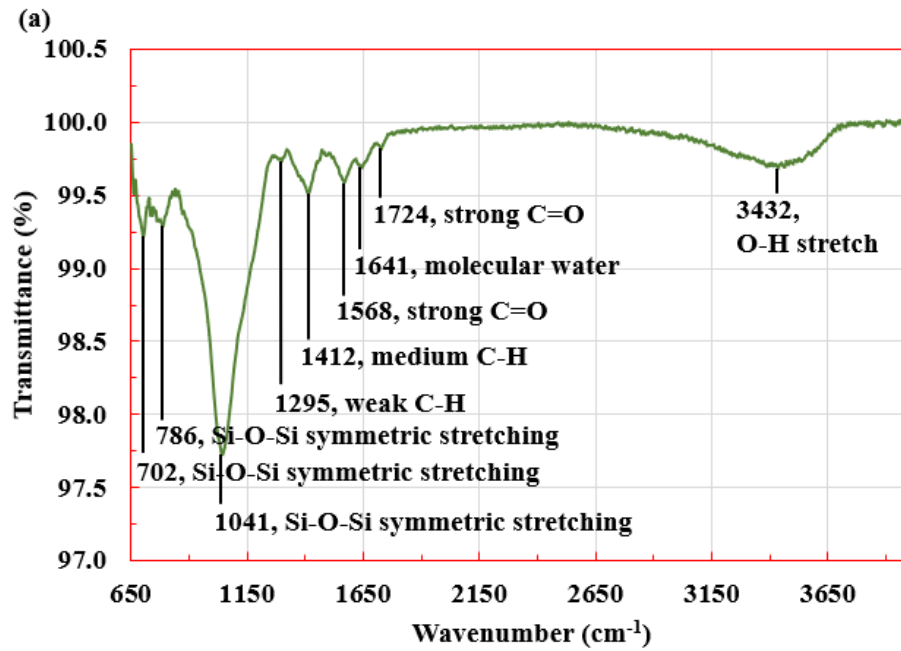
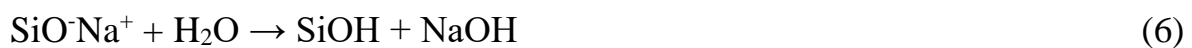
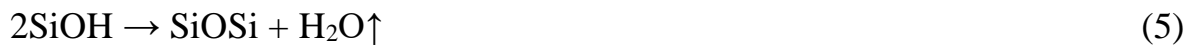


Figure 35. FTIR spectra of soda-lime glass (a) before heat treatment, and (b) after heat treatment.

The laser-ablated glass surfaces before and after heat treatment under the air at 240°C for 48 hours were hydrophilic ( $CA < 90^\circ$ ) and superhydrophobic ( $CA > 150^\circ$ ), respectively. This means that the OH contents on the glass surface may have been decreased by the dehydration reaction of the SiOH group [68]. This can be explained by Equation 5 and the FTIR analysis before and after heat treatment.



SiOH was formed during the laser process by non-bridging oxygen ( $\text{SiO}^-$ ) associated with sodium ions ( $\text{Na}^+$ ) in soda-lime glass reacting with  $\text{H}_2\text{O}$  on the glass surface, as shown in Equations 6 and 7. This reaction is consistent with the XRD comparisons of flat glass, glass after laser, and glass after laser-heat treatment, which shows that the crystalline structure did not change.

### 3.5 Potential applications

The samples fabricated with a 200 $\mu\text{m}$  step size and 0.4W of laser power showed superior superhydrophobic performance (Figure 36). The sample showed low adhesion and bouncing of a water droplet. Samples also exhibited self-cleaning abilities. The surface was covered by a white powder, and the water could trap the powder and roll off with a tilting angle of  $4^\circ$ . In addition, one of the advantages of laser-beam machining is direct patterning. The area near the laser machining can be superhydrophobic after heat treatment, but the non-fabricated area still becomes hydrophilic. Therefore, a laser fabrication area with a certain pattern or shape can control the water-based liquid. Water droplet position control was possible by making a non-fabricated area around the fabricated area. This result can be applied to biomedical applications such as water droplet arrays and cell microarrays [69] on transparent glass.

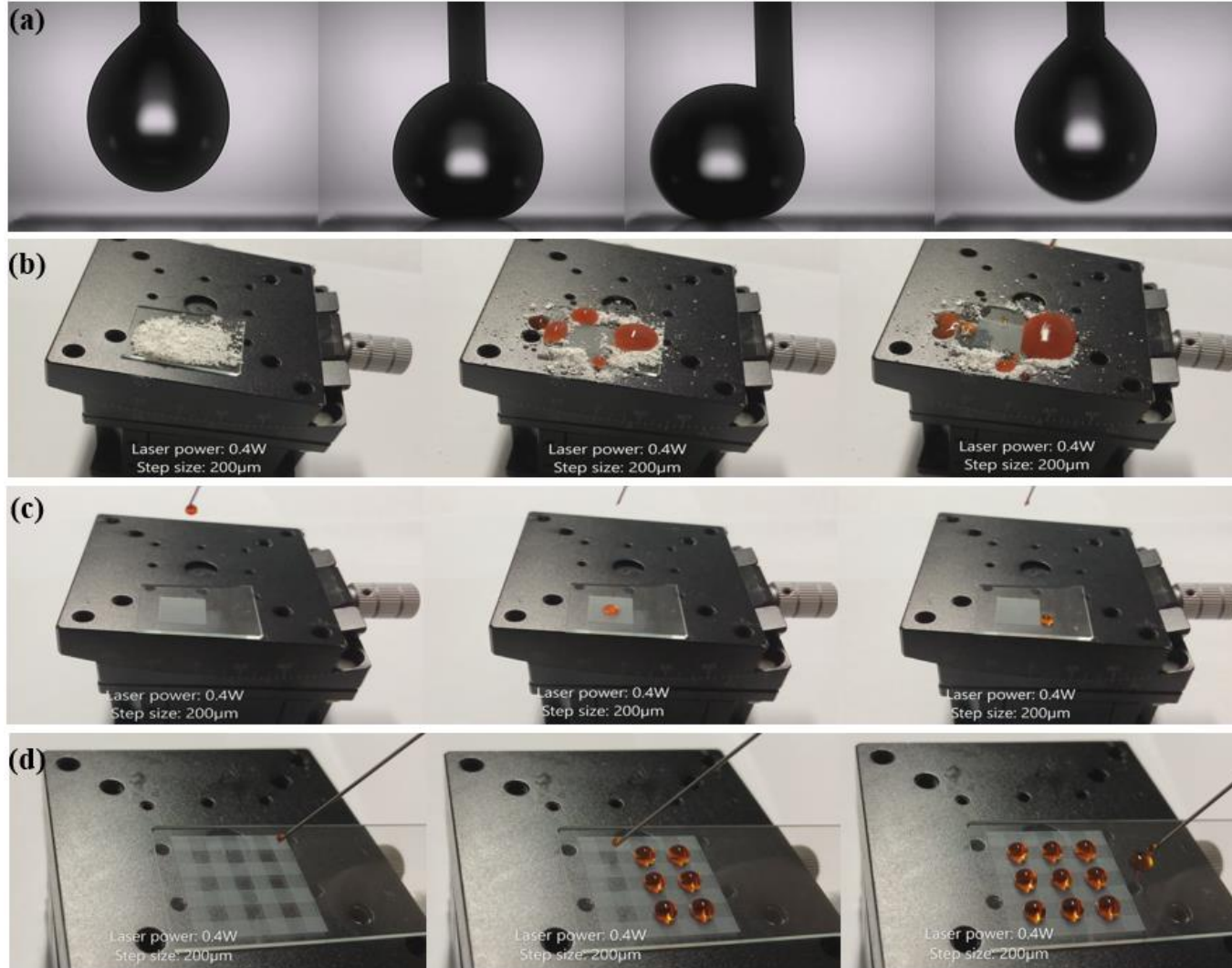


Figure 36. Performance of superhydrophobic glass surface: (a) water adhesion, (b) self-cleaning, (c) water bouncing, and (d) water position.

### 3.6 Summary

Transparent superhydrophobic soda-lime glass can be produced directly and simply by using a nanosecond pulse laser and heat treatment without any chemical coatings. After laser fabrication and heat treatment, the glass samples showed superior superhydrophobicity ( $CA > 170^\circ$ ,  $SA < 10^\circ$ ) and acceptable transmittance over 50% in visible light.

The wettability transition of the laser-ablated glass from hydrophilic to superhydrophobic surface after heat treatment can be explained by the increased carbon (organic absorption) and reduction of the OH group on the glass surface. The fabricated superhydrophobic surface was stable after 8 weeks in ambient air. In addition, the effects of step size and laser power on superhydrophobicity and transparency were investigated. A superhydrophobic surface and superior transmittance were evident at relatively high laser powers (0.4W and 0.5W) and relatively large step sizes (300 $\mu$ m and 350 $\mu$ m) among the experimental process parameters. After reducing the laser power from 0.5W to 0.2W, saw the abilities of the superhydrophobic surface decrease. When the step size increased from 150 $\mu$ m to 350 $\mu$ m with a low laser power (0.2W and 0.3W), the CA decreased slightly, and the SA increased from  $5^\circ$  to  $60^\circ$ . The results of changing process parameters can provide guidelines and a reference for controlling wettability and transparency on glass surfaces. The area near the laser machining can be superhydrophobic after heat treatment, but the non-fabricated area still becomes hydrophilic. The patterned laser-fabrication area and non-fabricated area can control water-based liquids and can be applied to biomedical applications such as water droplet arrays and cell microarrays, especially with transparent glass.

**Chapter 4:**  
**Fabrication**  
**superhydrophobic on metals**  
**and ceramics surface by**  
**using laser beam machining**  
**under silicone oil**



## 4.1 Background

In previous chapters (chapter 2 and chapter 3), laser beam machining and heat treatment were used in fabricating superhydrophobicity on titanium and soda-lime glass materials. However, this method still has a big disadvantage about a long time in heat treatment processes for a hydrophilic surface to become superhydrophobic surface as – 6 hours for titanium and 48 hours for soda-lime glass. And time is the most important factor for any method for making superhydrophobic surface, as well as to apply widely in the industry. Thus, developing a new, faster, and simpler process to fabricate superhydrophobic surfaces with a short time and variety of materials was mentioned in this research. After many experiments, a one-step process has been conducted successfully. This process is simple, one step, fast, friendly with the environment, does not need complicated equipment. This new process using a nanosecond laser beam machining fabricate under silicone oil to make superhydrophobic in a short time. The silicone KF-96 was chosen for the experiment because the chemical structure of silicone oil KF-96 has the hydrophobic group or trimethylsilyl end-groups (-CH<sub>3</sub>).

In this study, the method of using a nanosecond laser beam machining under silicone oil was applied to fabricate a superhydrophobic surface on many materials. For the first example, the copper foil was started investigating the effect of laser parameters and silicone oil on wettability. By using laser beam machining, the parameter as laser power, step size, scan speed was investigated for survey effect of morphology to superhydrophobic surface. Moreover, the effect of silicone oil height and silicone oil viscosity were also investigated. After that, the best condition of laser parameter and silicone oil height was applied in fabricating superhydrophobicity on many materials such as titanium, aluminum, stainless steel, sapphire, soda-lime glass. In addition, using this process to check the fabrication of isotropic and anisotropic surfaces was conducted.

## **4.2 Experiment method**

### **4.2.1 Materials and chemical element**

A copper foil with 0.25mm thickness (99.99% purity, Goodfellow Cambridge Ltd, United Kingdom), titanium sheets (99.5% purity, Nilaco Corporation, Tokyo, Japan) with 0.5mm thickness, soda-lime glass with 1mm thickness (Microscope slides 7101, Hensco Labware Manufacturing, Hangzhou, China), aluminum with 5mm thickness (99.999% purity, The Nilaco Corporation, Japan), stainless steel with 0.5mm thickness (SUS304, The Nilaco Corporation, Japan), and sapphire wafer with 0.45mm thickness ( $\text{Al}_2\text{O}_3$  C-Plane, 4science, Korea) were used in the experiments. Besides, silicone oil was used for making the environment while laser fabricated, and isopropyl alcohol was chosen for cleaning surfaces before and after laser fabrication. For detailed information, four kinds of silicone oil with different viscosities (KF-96-10cs, KF-96-30cs, KF-96-100cs, and KF-96-1000cs) were purchased from Shin-Etsu Chemical Co., Ltd. (Tokyo, Japan). And Isopropyl alcohol (IPA, 99.5%) was bought from Daejung Chemicals & Metals Co., Ltd. (Korea).

### **4.2.2 Fabrication method**

A laser system with a nanosecond laser source (Super Pulse 355-12W, LASERNET Co., Ltd, Korea) was used with a galvanometric scanner system (SCAN cube 10, Scanlab, Germany) as shown in Figure 37a. The laser beam goes from the nanosecond laser source comes directly to the galvanometric scanner. Inside the galvanometric scanner, the SCAN cube has two mirrors to control the direction and scan speed of the laser beam. By adjusting the moving speed and direction moving of these mirrors, the time and direction for laser beam machining fabrication on the surface were controlled. And it can be applied for large areas or difficult shapes for fabrication on a surface with high speed and precision. Besides, Figure 37b also showed the grid-pattern and line-pattern

design for laser beam machining fabrication on the substrate. In this method, the detailed description of the laser beam machining under silicone oil process is shown in Figure 37c. In which, step 1 and step 4 have a mission of cleaning dust or silicone oil before and after laser fabrication with IPA. At step 2, the silicone oil was poured into a glass petri dish with the silicone oil height ranged from 0.25mm to 1mm. At step 3, laser power, scan speed, and step size were adjusted by a computer. After cleaning, the contact angle and sliding angle on sample surfaces were measured by a contact angle meter (SmartDrop SDLab-200TEZD, Femto Fab, Seongnam, Korea). Four samples for each case were creating and for measurement on each sample, the volume of the water drop is 8  $\mu$ L because, with 8 $\mu$ L, the water droplet can easily drop on the surface, while at 7 $\mu$ L the water droplet cannot drop on the surface. Besides, for surface analysis, energy-dispersive X-ray spectroscopy (EDS, a cold FE-SEM, S-4800, Hitachi, Japan), high-resolution X-ray diffraction (XRD, ULTIMA IV, Rigaku, Japan), and Fourier-transform infrared spectroscopy (FTIR, Varian 670-IR, Varian Inc., USA) were used to analyze the chemical composition and crystal structure on the surface.

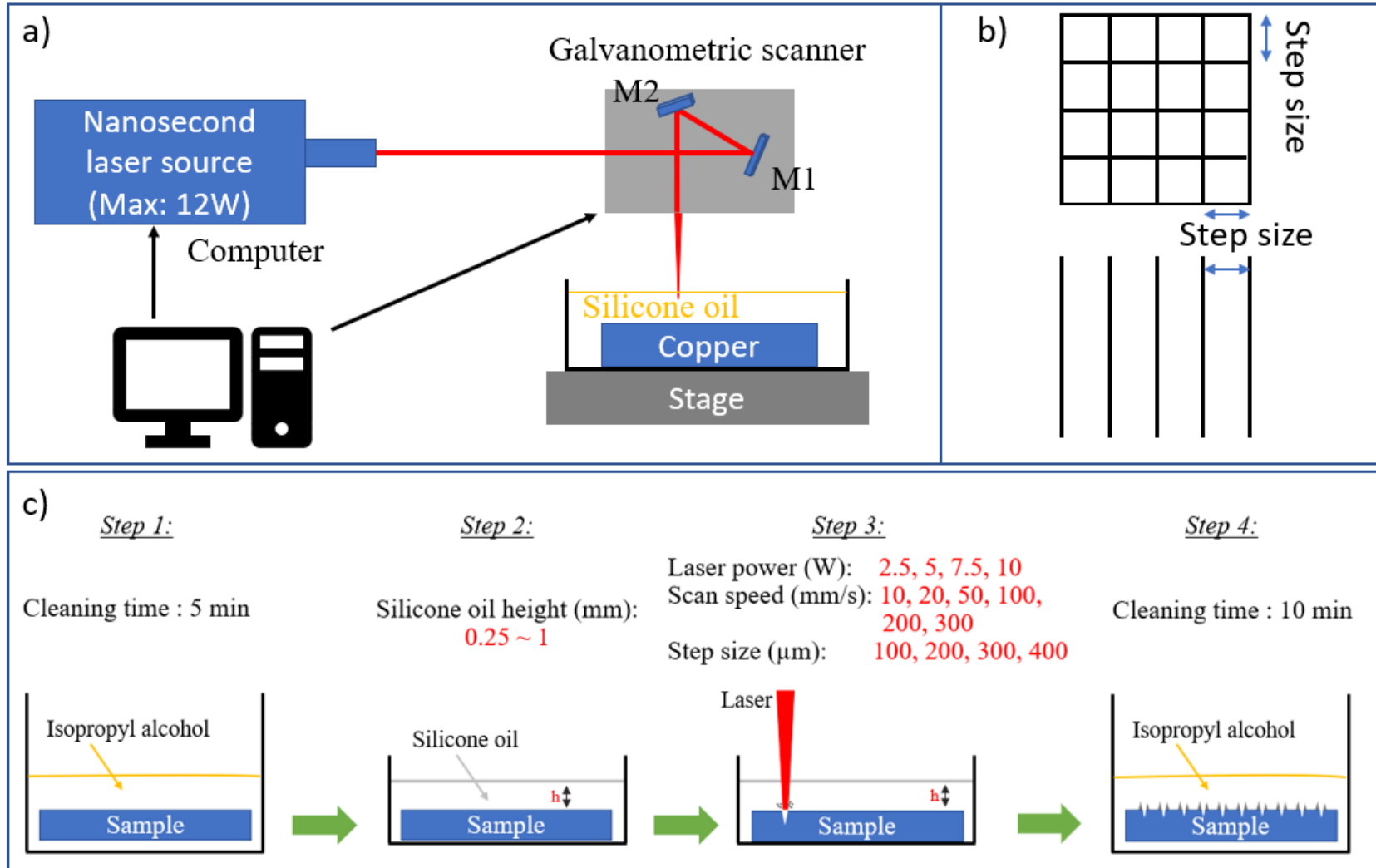


Figure 37. Schematic images of (a) the laser beam machining system, (b) pattern design, and (c) detail process for fabrication of superhydrophobic surface.

## 4.3 Results

### 4.3.1 Surface morphology

A three-dimensional (3D) laser scanning confocal microscope (VK-X200 series, Keyence, Osaka, Japan), and a field emission scanning electron microscopy (FESEM, JSM-6500F, Jeol Co., Tokyo, Japan) were used to analyze the microstructure on the surface after laser fabrication. Figures 38 show the FESEM of grid-pattern at 7.5W laser power, 100 $\mu$ m step size, 10mm/s scan speed, and 0.75mm silicone oil height. As shown in Figure 38, when the laser beam moved on the surface, it created a burr height right next to laser beam movement; meanwhile, the rest are which was located between the two lines of laser beam movement would be a non-fabricated area. Similarly, Figure 39 also showed the 3D confocal microscope image of the copper surface at 7.5W laser power, 10mm/s scan speed, and 0.75mm silicone oil height with step sizes ranged from 100 to 400 $\mu$ m. And the shape of the burr could be observed in Figure 39 and Appendix B.

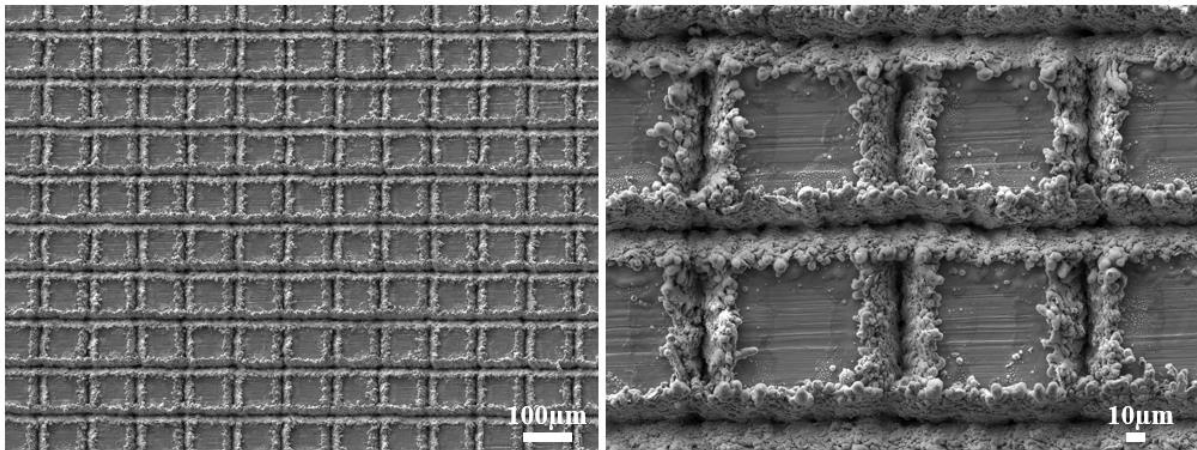


Figure 38. FESEM images of the copper surface at 7.5W laser power, 0.75mm silicone oil height, 100 $\mu$ m step size, and 10mm/s scan speed.

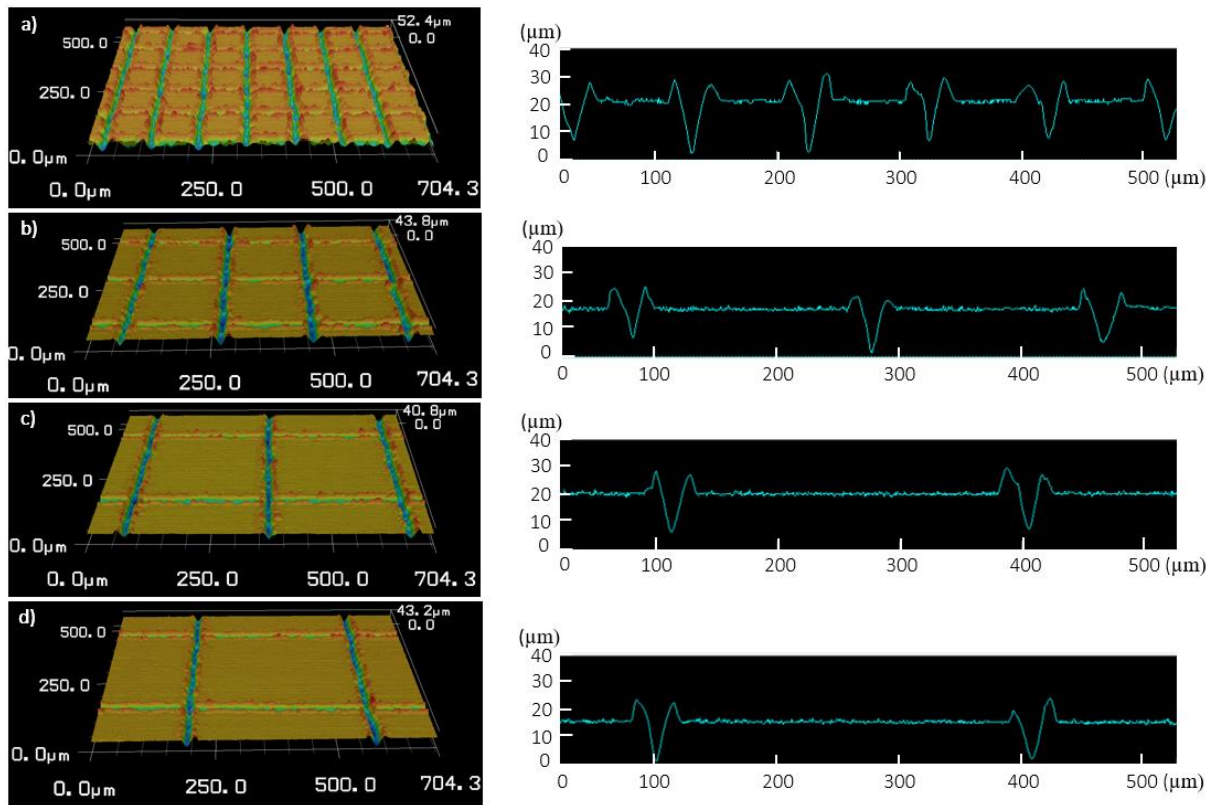


Figure 39. Confocal microscopy images of the copper surface with 10mm/s scan speed, 7.5W laser power, 0.75mm silicone oil height, and different step sizes a) 100, b) 200, c) 300, d) 400 $\mu$ m.

From these confocal microscope images, the average burr height was calculated from 40 points following two-direction x and y as shown in Table 6. Besides the burr height of sample after laser fabricated under silicone oil showed smaller than burr height of sample after laser fabricated in air. That means when laser fabrication under silicone oil, the laser power reduced when going through the silicone oil, which led to the burr height reduction. Moreover, it could be seen the change of burr height when increasing or decreasing one of four values as laser power, step size, scan speed, and silicone oil height one by one. In particular, when the silicone oil height increased the burr height value did not change; meanwhile, the burr height showed a clear increase when raising laser power value and tended to reduce lightly when increasing step size or scan speed.

Table 6. The average of burr height following different conditions.

<b>Laser power: 7.5W</b> <b>Step size: 100<math>\mu</math>m</b> <b>Scan speed: 10mm/s</b> <b>Silicone oil height: ...mm</b>	<b>Silicone oil height</b> <b>(mm)</b>	<b>Burr height</b> <b>(<math>\mu</math>m)</b>
	0.25	7.77
	0.50	7.65
	0.75	7.71
	1.00	7.50
<b>Laser power: ...W</b> <b>Step size: 100<math>\mu</math>m</b> <b>Scan speed: 10mm/s</b> <b>Silicone oil height: 0.75mm</b>	<b>Laser power</b> <b>(W)</b>	<b>Burr height</b> <b>(<math>\mu</math>m)</b>
	2.5	-
	5	6.00
	7.5	7.71
	10	9.35
<b>Laser power: 7.5W</b> <b>Step size: ...<math>\mu</math>m</b> <b>Scan speed: 10mm/s</b> <b>Silicone oil height: 0.75mm</b>	<b>Step size</b> <b>(<math>\mu</math>m)</b>	<b>Burr height</b> <b>(<math>\mu</math>m)</b>
	100	7.71
	200	6.90
	300	6.70
	400	6.25
<b>Laser power: 7.5W</b> <b>Step size: 100<math>\mu</math>m</b> <b>Scan speed: ...mm/s</b> <b>Silicone oil height: 0.75mm</b>	<b>Scan speed</b> <b>(mm/s)</b>	<b>Burr height</b> <b>(<math>\mu</math>m)</b>
	10	7.71
	20	7.16
	50	6.54
	100	4.57
	200	3.25
	300	-

### 4.3.2 Wettability

The CA and SA at the same laser power 7.5W with different values of silicone oil height (0.25, 0.5, 0.75, and 1mm), scan speed (10, 20, 50, 100, 200, 300mm/s), and step size (100, 200, 300, 400 $\mu$ m) were shown in Figure 40. Firstly, at a small silicone oil height - 0.25mm, the superhydrophobic samples were presented at 300 $\mu$ m step size with scan speeds of 10 and 20mm/s. In other cases, the sliding angle cannot be measured (No SA) at a step size of 100 $\mu$ m and 400 $\mu$ m although the value of CA was greater than 150°. Besides, at step size 200 $\mu$ m, when increasing the scan speed from 10 to 100mm/s, the SA also changed from 11 to 85°. Especially, at 200 and 300mm/s scan speed, and step size ranged from 200 to 400 $\mu$ m, the CA was smaller than 150°, and only the CA at 100 $\mu$ m step size showed value greater than 150°, however, all the step size shows No SA. Secondly, at 0.75, and 1mm silicone oil height, the surface showed its superhydrophobicity at 100, and 200 $\mu$ m step size, and from 10 to 50mm/s scan speed. Besides, when increasing the scan speed, the SA changed from SA < 10° to No SA. On the other hand, at the same laser power, when increasing the silicone oil height from 0.25 to 1mm and scan speed from 10 to 300mm/s, at small step size (100, 200 $\mu$ m) the value of CA increased from smaller than 150° to greater than 150°. Hence, when increasing the silicone oil height from 0.5 to 1mm, at 7.5W laser power, the superhydrophobic surface was presented at scan speed ranged from 10 to 50mm/s and at step size of 100 and 200 $\mu$ m. On the other hand, at the scan speed from 100 to 300mm/s, and the step size from 300 to 400 $\mu$ m, the CA was smaller than 140°. And the SA, at 400 $\mu$ m step size, still showed No SA, regardless of ranging silicone oil height from 0.25 to 1mm or any change in other laser parameters. In particular, the detail of CA and SA when changing laser parameters such as laser power, scan speed, step size, and silicone oil height on wettability was shown clearly in Appendix C.



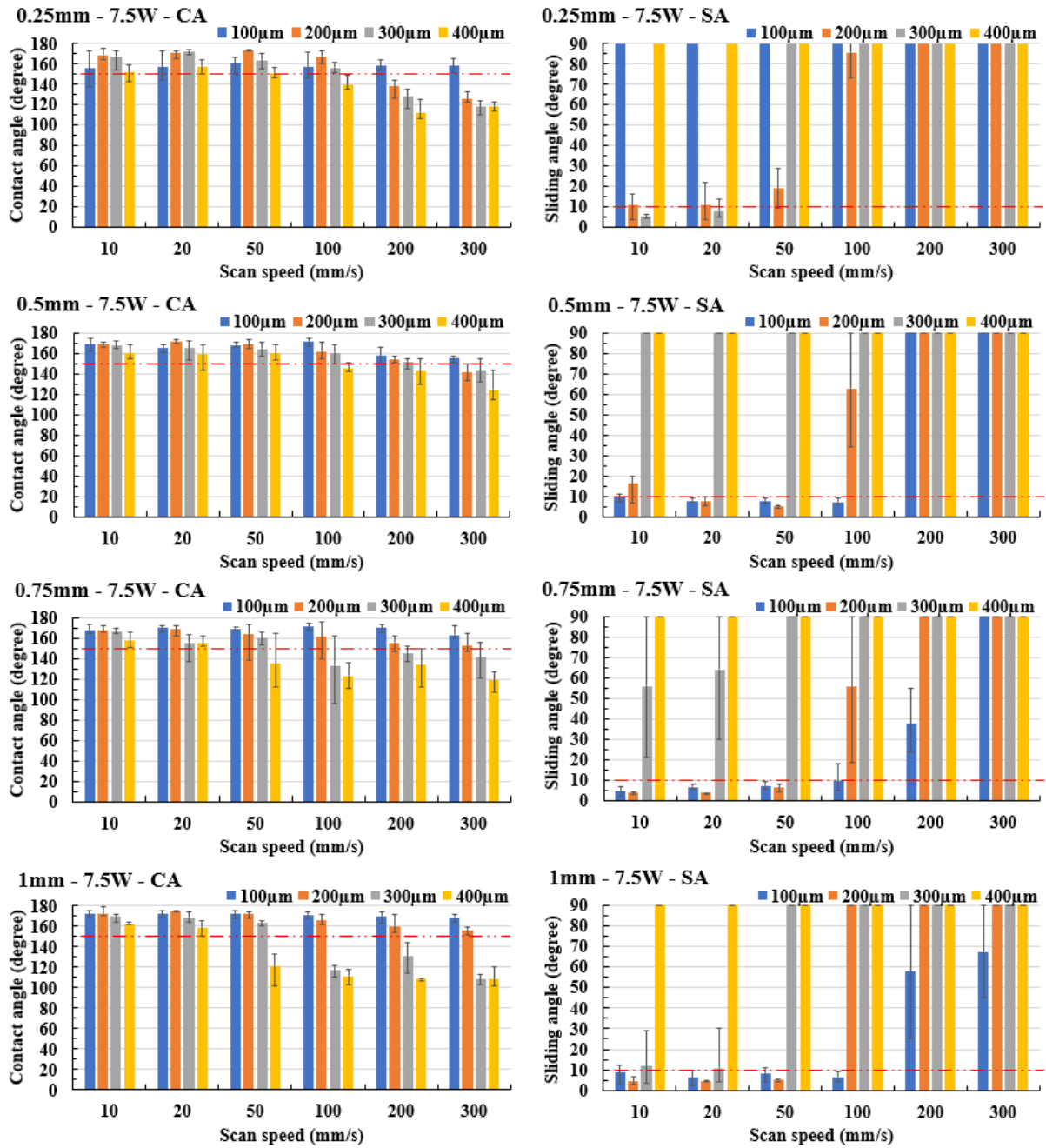


Figure 40. CA and SA at same laser power of 7.5W with different silicone oil height (0.25, 0.5, 0.75, 1mm), step size (100, 200, 300, 400 μm), and scan speed (10, 20, 50, 100, 200, 300mm/s).

Figure 41 described the effect of laser power at the same silicone oil height with different step sizes and scan speeds on the values of CA and SA. For detail, Figure 41 showed the CA and SA at the same silicone oil height – 1mm with different laser power (2.5, 5, 7.5, 10W), step size (100, 200, 300, 400 $\mu$ m), scan speed (10, 20, 50, 100, 200, 300mm/s). At small laser power – 2.5W, the CA was always smaller than 120°. It happened because at low laser power, the laser beam could not go through the 100cs viscosity of silicone oil. Besides, when increasing the laser power from 2.5 to 10W, the CA grew up to 170° with scan speed ranged from 10 to 100mm/s. However, at high scan speed from 100 to 300mm/s, 300 and 400 $\mu$ m step size, laser power from 5 - 7.5W, no experiment result showed a contact angle greater than 150°. At small scan speeds ranged from 10 - 20mm/s, a good superhydrophobic surface with SA smaller than 10° was archived with the step size from 100 to 300 $\mu$ m based on the difference of laser power (7.5 – 10W). The SA also increased up to 90° when changing the scan speed from 10mm/s to 300mm/s. Especially, at 400 $\mu$ m step size, even at a small scan speed of 10mm/s, not any sliding angle was showed.

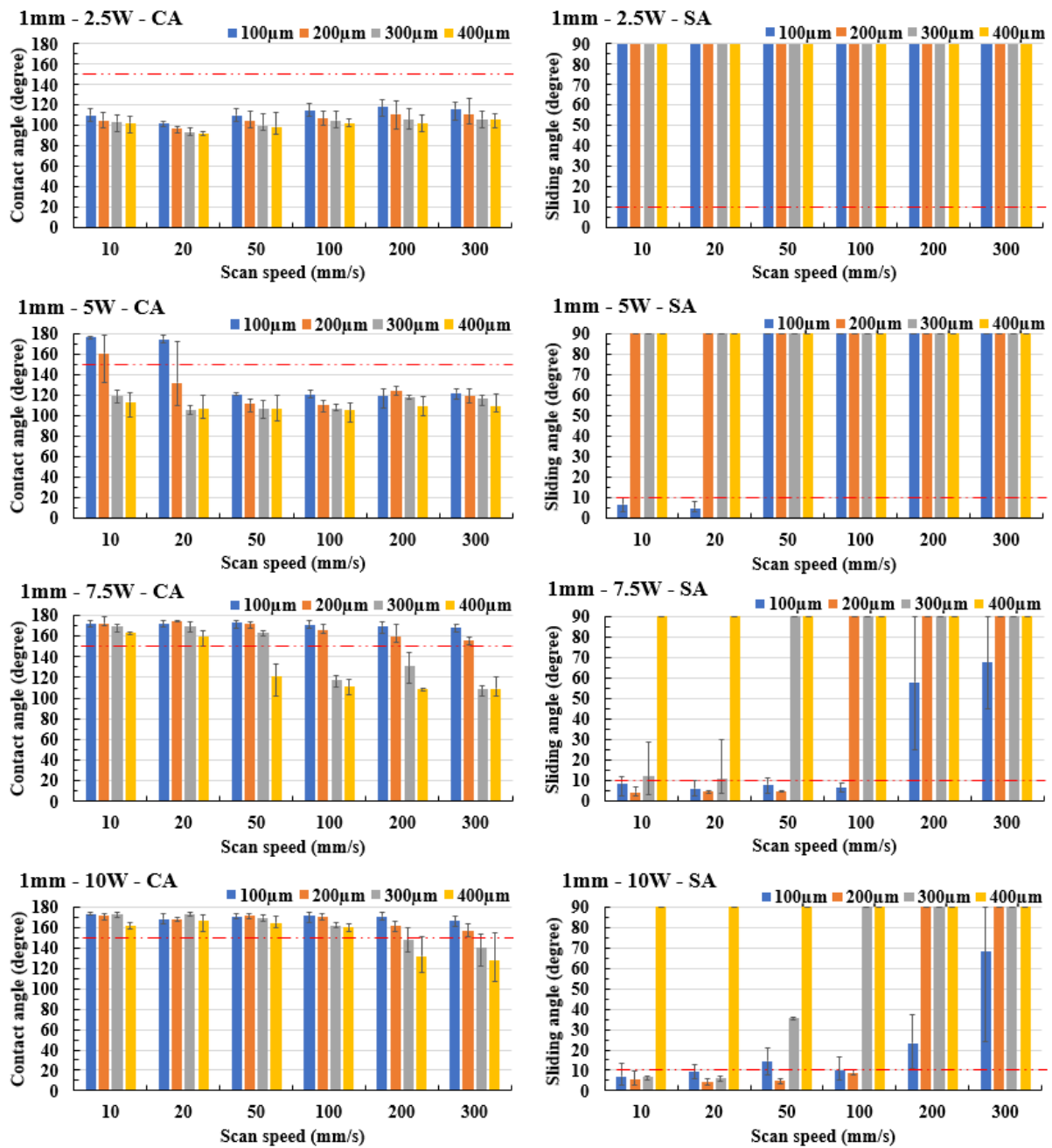


Figure 41. CA and SA at same silicone oil height of 1mm with different laser power (2.5, 5, 7.5, 10W), step size (100, 200, 300, 400μm) and scan speed (10, 20, 50, 100, 200, 300mm/s).

### 4.3.3 Isotropic and anisotropic

As mentioned in Chapter 2, the line pattern on titanium was fabricated by laser beam machining and heat treatment, and it showed the behavior of isotropic and anisotropic based on the value of  $\Delta CA$  ( $\Delta CA < 10^\circ$  called isotropic, and  $\Delta CA > 10^\circ$  called anisotropic). Therefore, in the new process - laser beam machining fabrication under silicone oil, the behavior of isotropic and anisotropic surfaces also was checked. The laser beam fabrication condition with 7.5W laser power, 10mm/s scan speed, 0.75mm silicone oil height, and three values of step size as 100, 200, and 300 $\mu\text{m}$  were used for checking the isotropic and anisotropic wetting state. And the corresponding result of CA and SA were shown in Figure 42. In Figure 42, the difference between parallel and perpendicular directions was shown clearly. At step size 100, and 200 $\mu\text{m}$ , the  $\Delta CA < 10^\circ$ , which meant this surface showed the isotropicity. While at step size 300 $\mu\text{m}$ , the values of  $\Delta CA > 10^\circ$ , that meant this surface showed the anisotropicity. Hence, by using the laser beam machining under silicone oil, the behavior of isotropic and anisotropic wetting states on copper surfaces was presented.

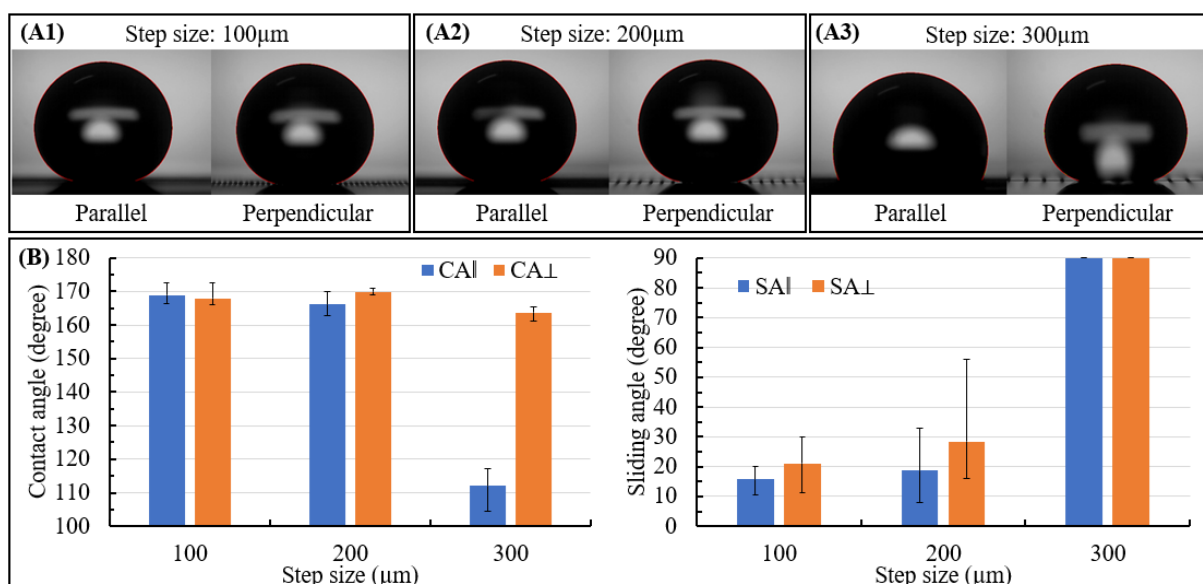


Figure 42. The contact angle and the sliding angle at 7.5W laser power, 100, 200, and 300 $\mu\text{m}$  step size, 10mm/s scan speed, and 0.75mm silicone oil height.

### 4.3.4 Stability and robustness

For stability and robustness test, the step size 100 $\mu$ m, scan speed 10mm/s, the laser power changing from 5 to 10W, and the silicone oil height ranged from 0.5 to 1mm would be used, and because at that condition, the surface showed high CA (CA > 150°) and have SA < 90°.

Firstly, in order to check the stability, the CA and SA of samples after fabrication would be measured. After that, the samples were put in a cabinet with ambient air condition for 80 days. After 80 days the samples were taken out and the measurement of the CA and SA, the detailed result was shown in Figure 43. After 80 days, the values of CA had a light increase in all conditions, while the SA presented a light decrease. That means with the new process, the superhydrophobic surface was created and stable when putting in the air after 80 days.

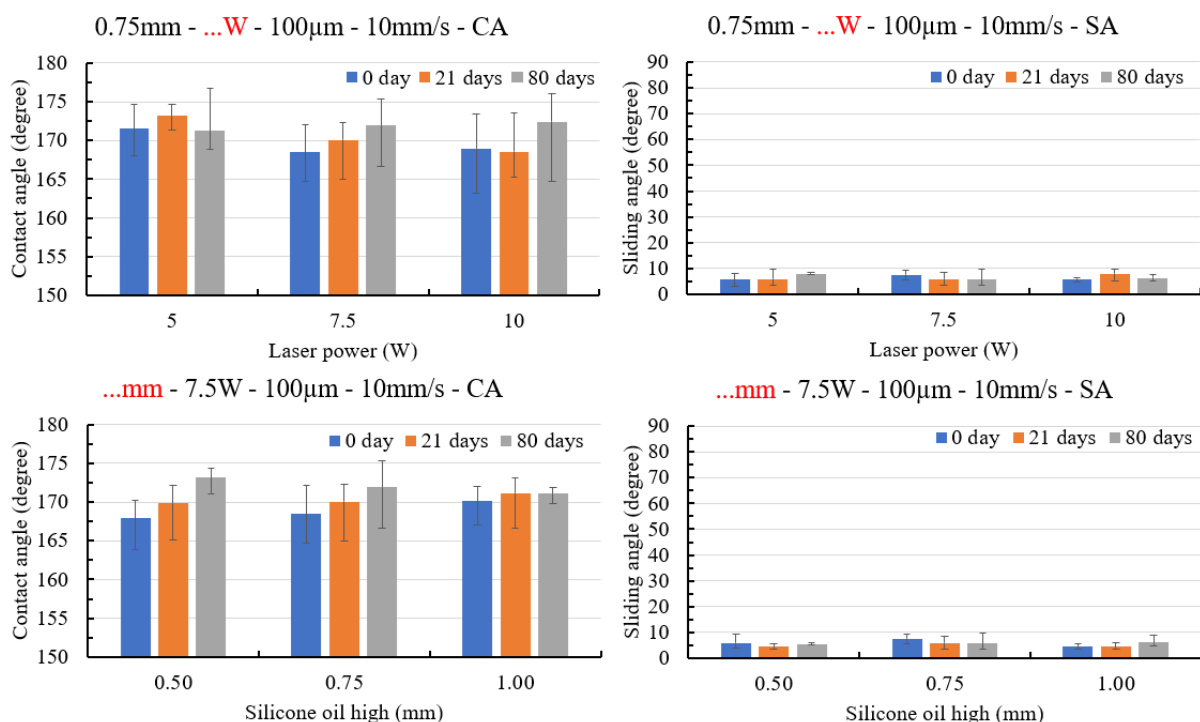


Figure 43. CA and SA after laser fabrication (blue color), after 21 days (orange color), and after 80 days (grey color).

On the other hand, the robustness of the superhydrophobic on the copper surface was checked by a scotch tape test. In the scotch tape test, as shown in Figure 44, the samples were prepared by laser beam machining fabrication under silicone oil, and then a tape (3M Scotch Transparent tape 550, Seoul., Korea) was put on these surfaces. A one-kilogram weight was placed on the copper surface of the adhesive tape, then moved from position 1 to position 2 and then back again, and the tape was removed. This tape test was repeated twenty times, and correspondingly, the CA and SA were measured after every tape test.

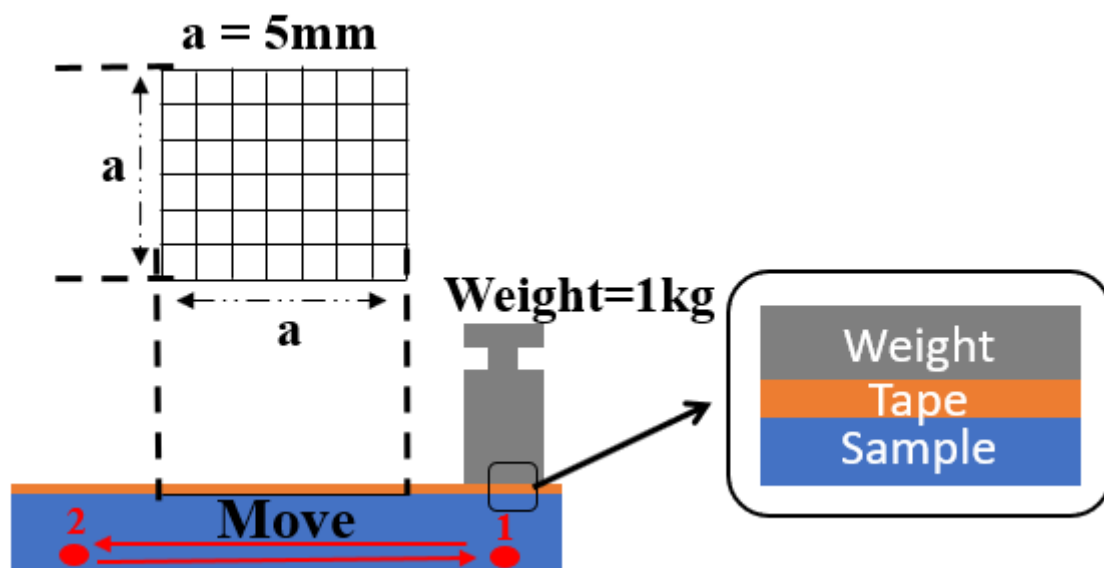


Figure 44. Schematic of the scotch tape test for evaluating the robustness of the superhydrophobic on the copper surface.

For robustness, the tape test proceeded, and the results were shown in Figure 45. After 20 cycles all the samples still show good CA ( $CA > 160^\circ$ ) but have an increase in SA values. At 7.5W laser power, 100 $\mu\text{m}$  step size, and 10mm/s scan speed the SA did not show much considerable difference when the silicone oil height was raised from 0.5 to 1mm. After 4 cycles, the copper surface still showed a superhydrophobic surface ( $CA > 150^\circ$ ,  $SA < 10^\circ$ ) at 7.5W laser power, 100 $\mu\text{m}$  step size, 10mm/s scan speed, and the silicone oil height range from 0.5 to 1mm. However, this situation did not happen when the laser power

was changed. At the same step size  $100\mu\text{m}$ , scan speed  $10\text{mm/s}$ , silicone oil height  $0.75\text{mm}$  the robustness of the surface was obviously different in conditions of small laser power of  $5\text{W}$  and high laser power  $7.5\text{W}$  and  $10\text{W}$ . For  $5\text{W}$  laser power, from the second cycle, the SA already increased to  $35^\circ$ , meanwhile, the SA at  $7.5\text{W}$  and  $10\text{W}$  still showed good superhydrophobic surfaces after 5 cycles. When changing the laser power ( $5 - 10\text{W}$ ) and same other parameters (silicone oil height, scan speed, step size) for fabrication, the condition of lower laser power ( $5\text{W}$ ) creates a superhydrophobic surface with lower robustness than at higher laser power ( $7.5, 10\text{W}$ ). However, the robustness did not change when fabricating at the same laser power ( $7.5\text{W}$ ), step size ( $100\mu\text{m}$ ), scan speed ( $10\text{mm/s}$ ) with different silicone oil heights ( $0.5 - 1\text{mm}$ ). The occurrence of this situation maybe start from the effect of burr height, at  $5\text{W}$  laser power, the experiment gives out the burr smallest burr height in comparison with  $7.5\text{W}$  and  $10\text{W}$  laser power. Besides after 20 cycles of tape test, the burr height of all samples has small reduces.

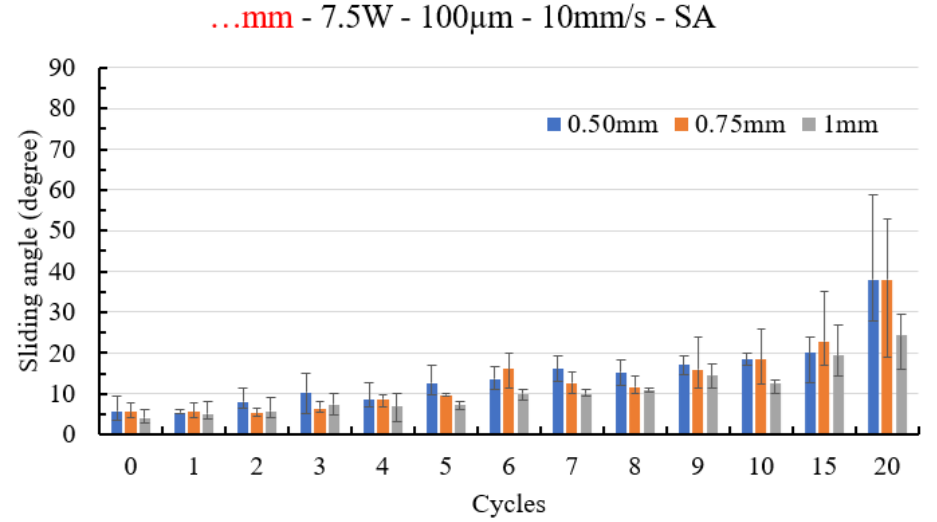
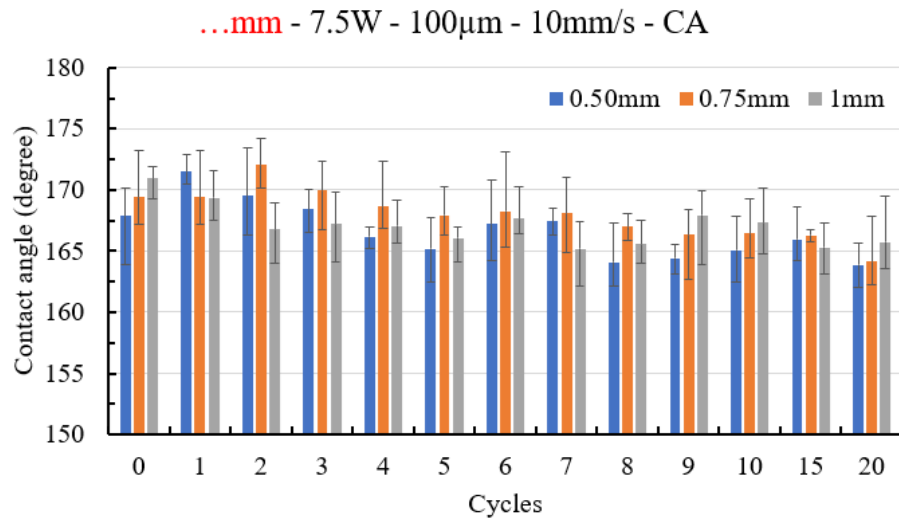
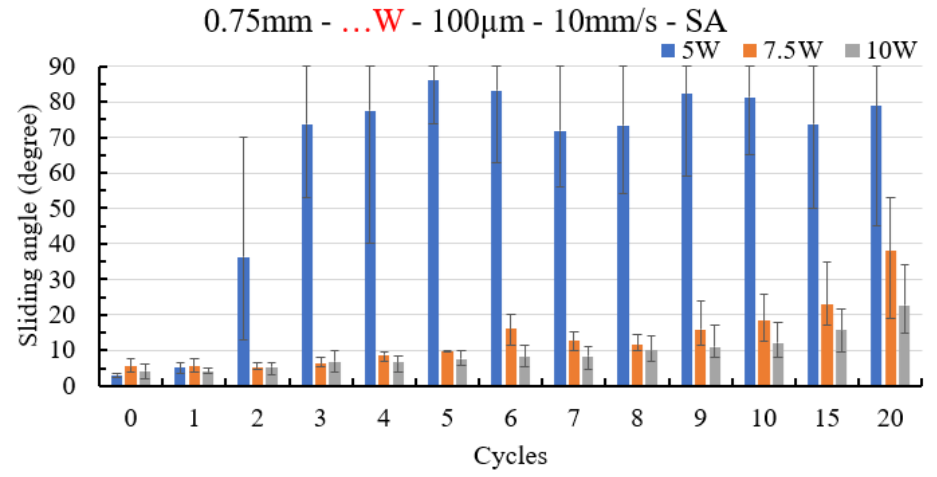
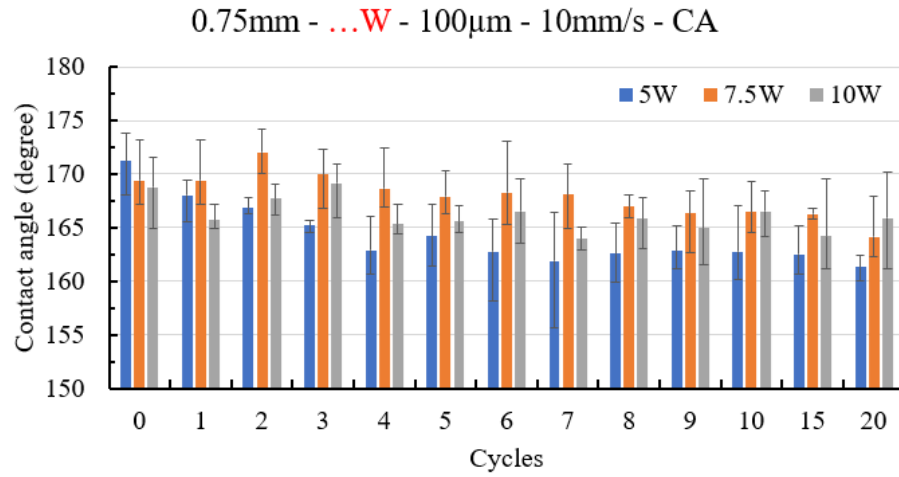


Figure 45. The CA and SA on the superhydrophobic copper surface after twenty cycles of tape test.



## 4.4 Discussion

### 4.4.1 Effect of laser power on wettability

In this study, the effect of silicone oil height, laser parameters (laser power, scan speed), and pattern design (step size) on wettability when using laser beam machining fabrication under silicone oil were investigated. As shown in Table 6, when increasing laser power (2.5 – 10W) or reducing scan speed (300 – 10mm/s), the burr height tended to increase. On the contrary, when the step size increased, which led to the increase of non-fabrication areas, and it made the water droplet easily touch on the non-fabrication areas. As can be seen in Figure 46, increasing laser power or reducing scan speed tends to make the burr height increase. On the other hand, changes in step size make affect the non-fabrication area in direct proportion. That means, when the greater step size is, the bigger the non-fabrication area is, which makes the water droplet can easily touch on the non-fabrication area.

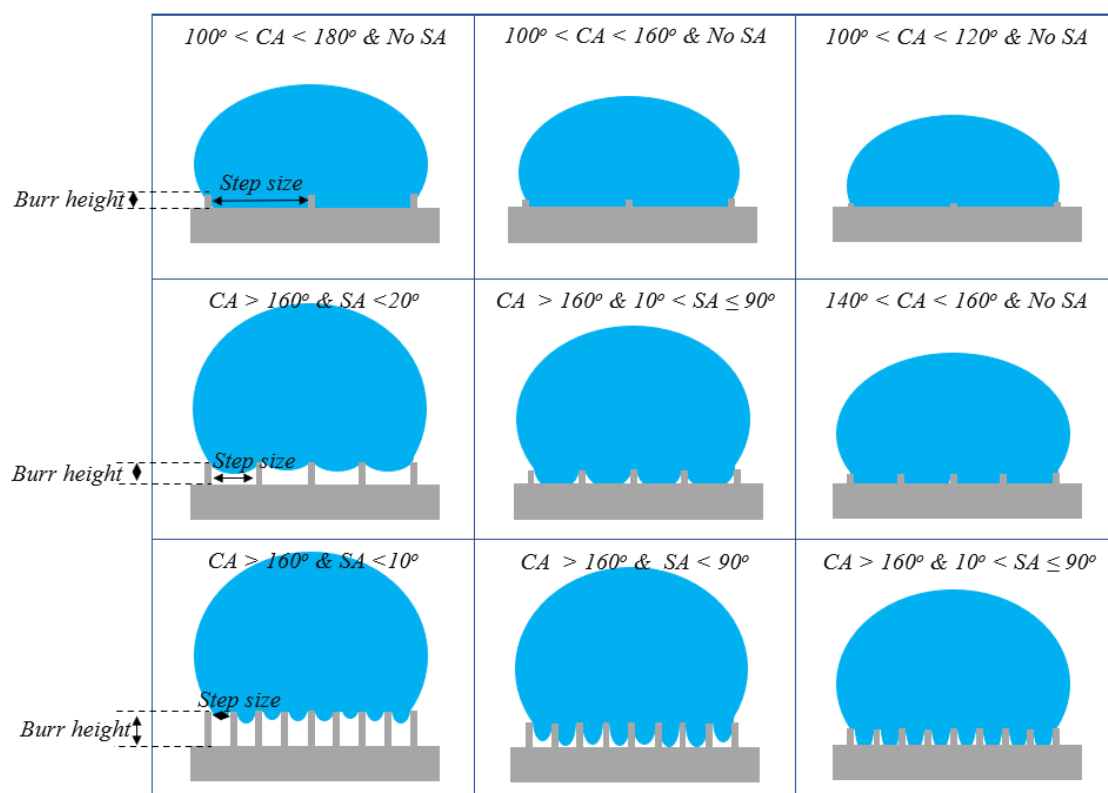
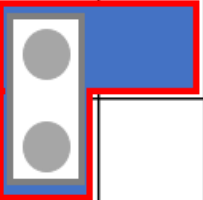
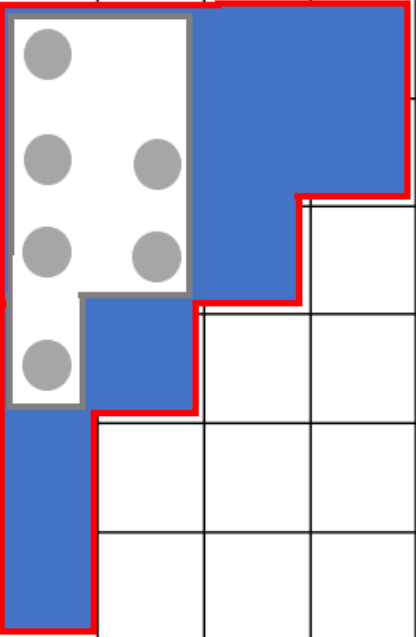
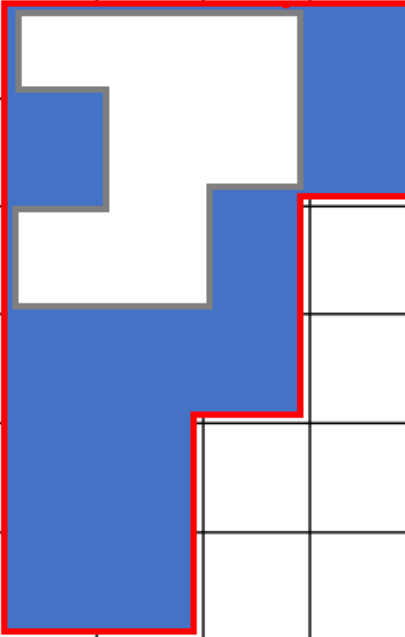


Figure 46. Effect of burr height and step size on wettability.


Using laser beam machining fabrication under silicone oil to create a superhydrophobic surface on copper material with different parameters (laser power, scan speed, step size, and silicone oil height) were investigated. The result was summarized briefly in Table 7 and the full and detailed result was showed Appendix D. As can be seen in Table 7, there are three main areas. The first area or biggest areas, which is blue and bordered with a red line, performed laser parameters suitable for fabricating a copper surface with  $CA > 150^\circ$  with or without SA upon silicone oil height (0.5 – 1mm) and laser power (5 – 10W). The second area, which is white and surrounded by grey color. In this area, the CA was greater than  $150^\circ$  and the SA is smaller than  $90^\circ$  with different silicone oil height and laser power. Lastly, the area shaped as a grey circle showed a laser parameter suitable for fabricating a superhydrophobic surface. As a result in Table 7, researchers can get a brief and general overview of the effect of laser parameters such as laser power, scan speed, step size on CA and SA on the copper surface when using laser beam machining fabrication under silicone oil, after that, find out the fastest way to create the superhydrophobic surface. For example, as shown in Table 7, the laser power of 5W and any value of silicone oil height from 0.5 to 1mm, at step size  $100\mu\text{m}$  and scan speed range from 10 to 20mm/s would be the best condition to fabricate superhydrophobic surface by laser beam machining. Meanwhile, the condition of  $200\mu\text{m}$  step size and 10mm/s scan speed, the experiment only gave out a high CA ( $CA > 150^\circ$ ). Besides, when increasing laser power from 5 to 7.5W, the area has  $CA > 150^\circ$  increase and the values of laser parameter that can fabricate superhydrophobic surface increase as well. Furthermore, based on the time for laser fabricate as shown in Table 8, the best condition for the fabricated superhydrophobic copper surface for short time (a few seconds) is 7.5W laser power,  $100\mu\text{m}$  step size, 100mm/s scan speed, or  $200\mu\text{m}$  step size and 50mm/s scan speed.

Table 7. The distribution of CA and SA following the change of laser power, step size, and scan speed.

0.5 - 1mm	Laser power (W)	5				7.5				10			
	Step size ( $\mu\text{m}$ )	100	200	300	400	100	200	300	400	100	200	300	400
Scan speed (mm/s)	10												
	20												
	50												
	100												
	200												
	300												

$CA > 150^\circ$  &  $SA \leq 90^\circ$  (SA =  $90^\circ$  mean No SA)

$CA > 150^\circ$  &  $SA < 90^\circ$



$CA > 150^\circ$  &  $SA < 10^\circ$

Table 8. Time for laser fabrication with a 5x5mm<sup>2</sup> area.

Step size (μm)		100	200	300	400
Scan speed (mm/s)	10	51.1	26.1	18.1	14.1
	20	25.6	13.1	9.1	7.1
	50	10.4	5.3	3.7	2.9
	100	5.3	2.7	1.9	1.5
	200	2.7	1.4	1.0	0.8
	300	1.9	1.0	0.7	0.6

#### 4.4.2 Effect of viscosity on wettability

In this research, the silicone oil KF-96 with viscosity 100cs was chosen for all experiments. However, the oil with different viscosity maybe affects the fabrication process so a survey of the effect of viscosity is necessary. The different viscosity of a liquid can easily understand as the speed of this liquid when moving on the surface. It means, for the same distance from A to B the low viscosity (ex: 10cs) can go to B earlier than the high viscosity (ex: 30, 100, 1000). And when using laser beam machining fabrication under silicone oil, at the same laser power and silicone oil height, if the viscosity of silicone oil increases the laser's ability to pass through will decrease. Thus, in this study, 4 kinds of viscosities were chosen as 10, 30, 100, and 100cs. And the laser beam machining will fabricate under silicone oil with process parameters as 7.5W laser power, 100μm step size, 10mm/s scan speed, and 0.75mm silicone oil height, the copper surfaces still showed superhydrophobic surface as in Figure 47.

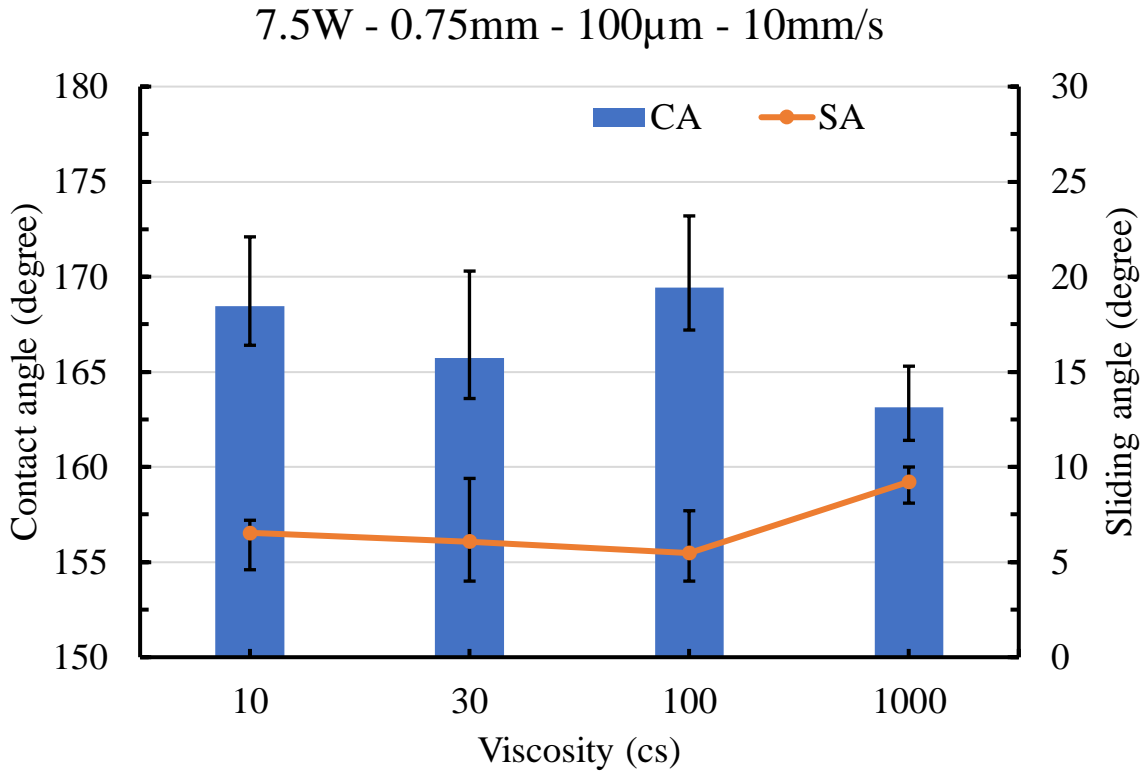


Figure 47. The values of CA and SA following the increase of viscosity of silicone oil by using laser beam machining fabrication under silicone oil with 7.5W laser power, 100 $\mu$ m step size, 10mm/s scan speed, and 0.75mm silicone oil height.

#### 4.4.3 Wettability with different materials

Copper was the first material that was used to investigate the influence of parameters (laser power, scan speed, step size, silicone oil height) in the fabrication process. Besides, to check the wetting ability of different materials, a laser beam fabrication under silicone oil was conducted. With the 5W laser power, 100 $\mu$ m step size, 10mm/s, 0.75mm silicone oil height, all metallic materials (copper, aluminum, titanium, stainless steel) can become superhydrophobic, detailed as shown in Figure 48a. While, at the same parameter condition sapphire showed the CA smaller than 150°, and glass could not be fabricated because the surface was broken when using the lower speed. To find out the best parameter for fabricating superhydrophobic surfaces on metals and

ceramics, a reduction in parameter values among silicone oil height, laser power, scan speed, step size is necessary, but in this case, the silicone oil height is fixed at 0.75mm and only laser parameter will be adjusted. Besides, with ceramic materials, only increasing or decreasing laser power is not enough to create superhydrophobic surfaces. For example of sapphire material, it needs to reduce the scan speed; as a result, with 10W laser power, 5mm/s scan speed, 100 $\mu$ m step size, and 0.75mm silicone oil height superhydrophobicity is created on the sapphire surface. On the other hand, for glass material, due to its characteristics, all increases in step size, scan speed, and laser power are needed. In detail, the 10W laser power, 200 $\mu$ m step size, 50mm/s scan speed, and 0.75mm silicone oil height were applied to fabricated glass superhydrophobic surface. In addition, Figure 48b about the bouncing effect on different materials is clear evidence for the superhydrophobicity of the above materials.

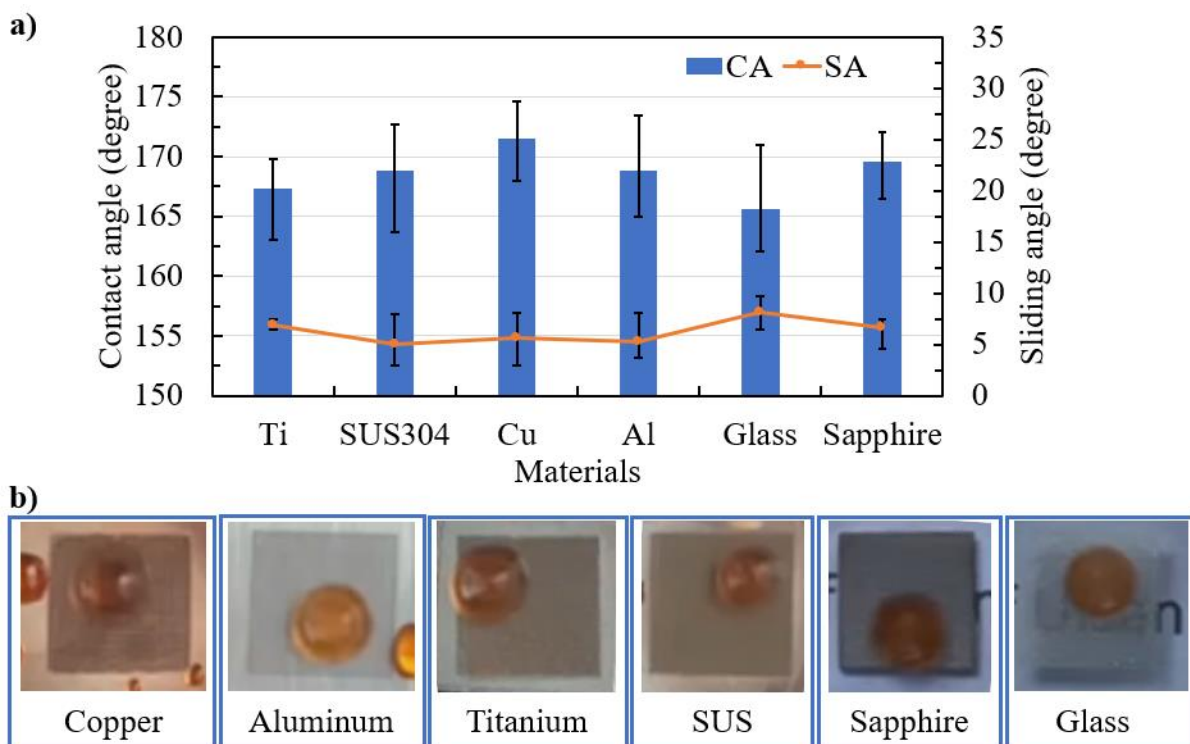


Figure 48. a) CA and SA of a superhydrophobic surface by using laser fabrication under silicone oil with different materials, and b) water bouncing on a different superhydrophobic surface.

#### **4.4.4 Compare the robustness between new process and post-process**

The comparison of robustness between post-process (laser and heat treatment) with the new process (laser beam machining under silicone oil) was conducted by tape test. The result was shown in Figure 49. The parameter was chosen at 7.5W laser power, 100 $\mu$ m step size, and scan speed 10mm/s for both cases. For the new process, the surface will be fabricated in one process under silicone oil height changing from 0.5 to 1mm; meanwhile, for post-process, the surface will be fabricated with many steps in this comparison, the result of using temperature at 150°C and heat treatment time for 12, 18 hours taken from another research [70] would be used. After 5 cycles, all cases showed high contact angle (> 160°), however, the SA presents differently between the two processes. In a post-process, from 1 cycle, the SA already increased with 12 or 18 hours of heat treatment, however, with longer heat treatment time (18 hours), the samples show better results than shorter heat treatment time (12 hours). However, with the new process, the results showed robustness better than post-process because after 5 cycles the samples still show a superhydrophobic surface.

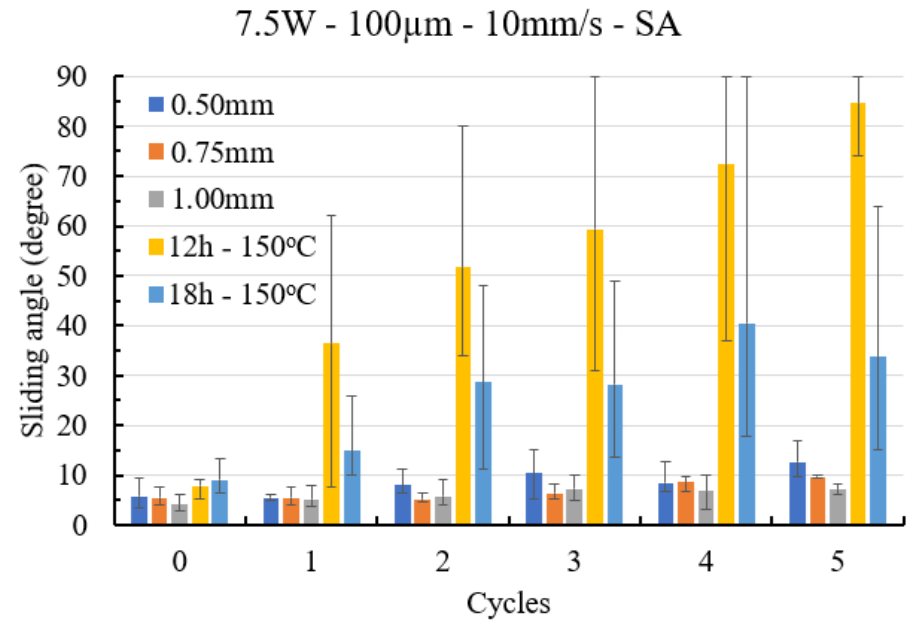
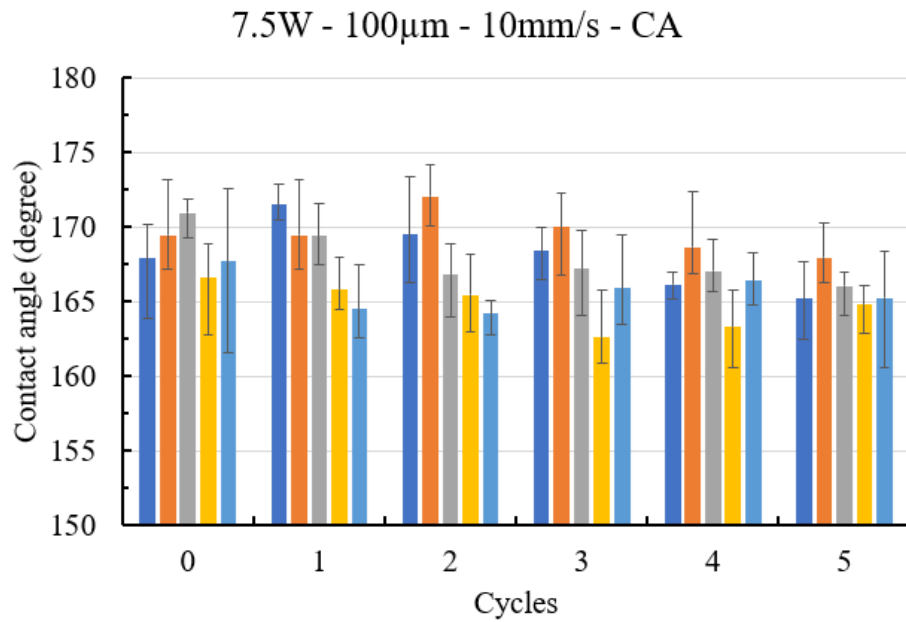


Figure 49. Compare the CA and SA of superhydrophobic copper surface between new process (laser beam machining under silicone oil), and post-process (laser and heat treatment) after 5 cycles tape test.



#### 4.4.5 Mechanism

The reason for the wetting change from hydrophilic to superhydrophobic surface on copper by using laser beam fabrication under silicone oil could be interpreted by investigation of the surface. The fabricated paths make a clear grid pattern on the copper surfaces as shown in Figures 38 – 39, 50, and Appendix B. And through Figure 50, the clear difference of surface between laser fabrication in air and under silicone oil was observed. With laser beam fabrication under silicone oil, the silicone oil has mission as an environment rich hydrophobic group (-CH<sub>3</sub>) and protects the surface during fabrication, that is when laser beam moving on the surface, the removed materials will not stick to the un-fabrication areas. And when laser fabrication in air, the removed materials can easily attach to the surface as shown in Figure 50.

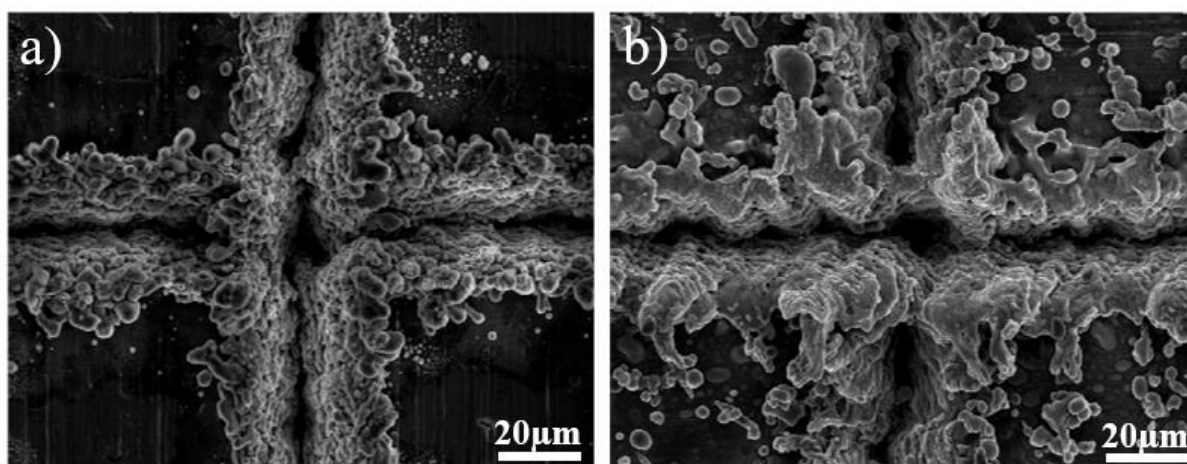


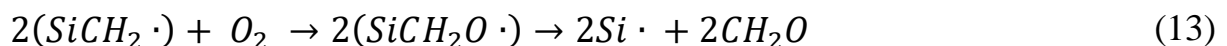
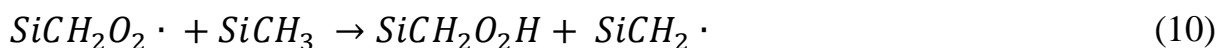
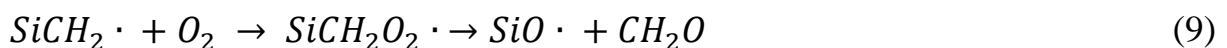
Figure 50. FESEM of copper surfaces with (a) laser under silicone oil, and (b) laser in air.

Through XRD results, after the fabrication process by using a laser beam, a metal oxide peak appear on the surfaces of the metals as shown in Figure 51. For detail, with copper and titanium, the structure during laser fabrication in the air (or only laser) and laser fabrication under silicone oil have different. While sapphire did not show any difference in structure between unfabricated, only

laser, and laser under silicone oil. The mechanism for copper, titanium and sapphire surface to change from hydrophilic to superhydrophobic will happen because of an increase of carbon element and the appearance of the new element silicon, which is presented through EDS results as shown in Table 9.

The carbon element will come from organic adsorption, and its appearance on the surface when laser fabrication under silicone oil because the silicone oil has rich organic adsorption (-CH<sub>3</sub>). To confirm this mechanism, FTIR analysis was conducted as shown in Figure 52. Laser beam fabrication under silicone oil samples has increased the hydrophobic group when comparing with the only laser. The appearance of the strong hydrophobic group (-CH<sub>3</sub>) appears on the surface and the Si-O-Si, which is formed from the siloxy group generated in equation (9) reaction with the silyl groups in equation (12), and (13) lead to the surface become superhydrophobicity.

When laser-ablated in silicone oil environment, with high energy or high temperature at the laser beam, will interact with the silicone oil, the oxidation of silicone oil starts as oxygen attacks the methyl groups. And a chain reaction of oxidation begins with the equations below:



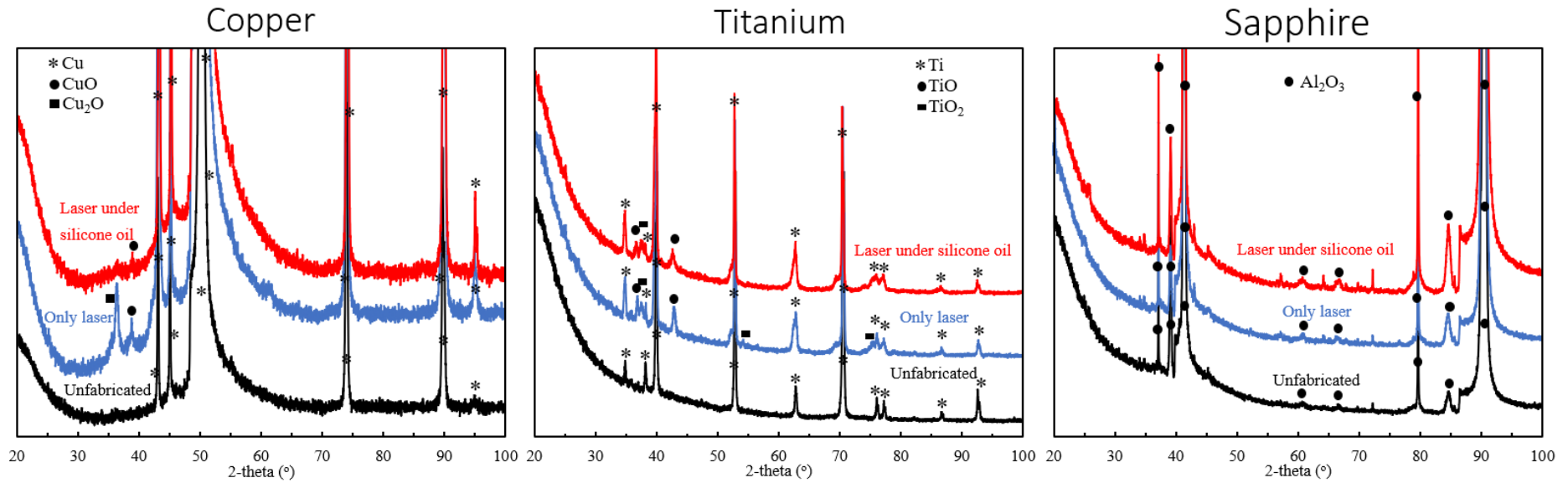


Figure 51. XRD results on unfabricated, only laser, and laser under silicone oil with Copper, Titanium, and Sapphire.

Table 9. EDS results of copper, titanium, and sapphire materials.

	Copper	Fabrication method			Titanium	Fabrication method			Sapphire	Fabrication method		
		(0)	(1)	(2)		(0)	(1)	(2)		(0)	(1)	(2)
Element (Atomic %)	Cu	100	88.80	72.70	Ti	100	59.28	40.71	Al	41.49	33.60	31.23
	O	-	10.70	10.30	O	-	39.41	54.09	O	58.51	62.90	58.60
	C	-	0.50	13.20	C	-	1.31	3.22	C	-	3.40	7.23
	Si	-	-	3.80	Si	-	-	1.97	Si	-	-	2.93

Note: (0) Unfabricated

(1): Only laser

(2): Laser under silicone oil

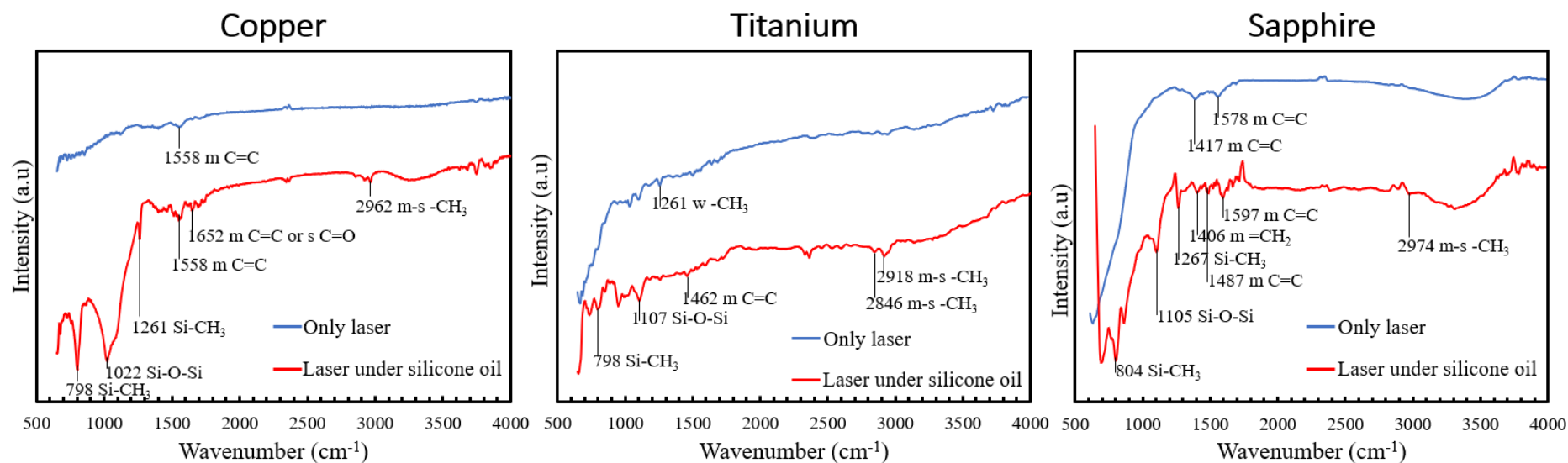


Figure 52. FTIR spectra of the only laser, and laser under silicone oil with Copper, Titanium, and Sapphire.

## 4.5 Potential applications

The superhydrophobic surfaces demonstration about fabrication by using laser beam machining under silicone oil at 0.75mm silicone oil height, 100 $\mu$ m step size, 10mm/s scan speed, and 7.5W laser power was shown in Figure 53. The sample presented low adhesion with a 7 $\mu$ L volume of a water droplet and the bouncing effect of a water droplet with the copper surface tilted at an angle of 4°, and 10cm height from the needle to the surface. Samples also exhibited self-cleaning abilities. First, the surface was tilted at an angle of 4°, and then a water droplet from 10cm height to the surface, the water droplet could trap the white powder covering in the surface and roll-off the surface. In addition, one of the advantages of laser-beam machining is direct patterning, so the area where the laser beam passed can become superhydrophobic after laser beam machining under silicone oil, but the non-fabricated area still becomes hydrophilic. Therefore, a laser fabrication area with a typical pattern or shape can control the water-based liquid as shown in Figure 54.

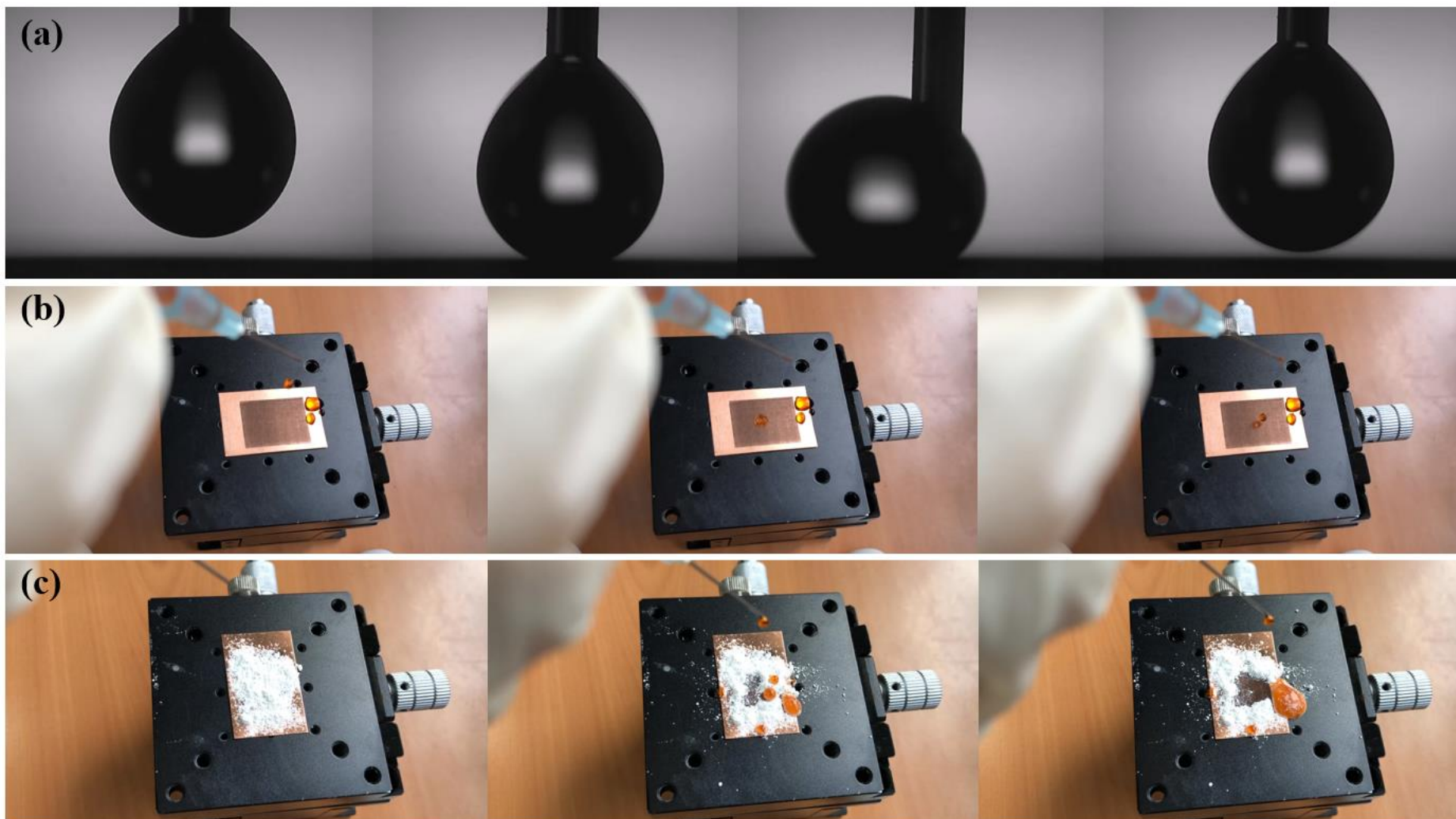


Figure 53. Performance of superhydrophobic copper surface: (a) water adhesion, (b) water bouncing, (c) self-cleaning.

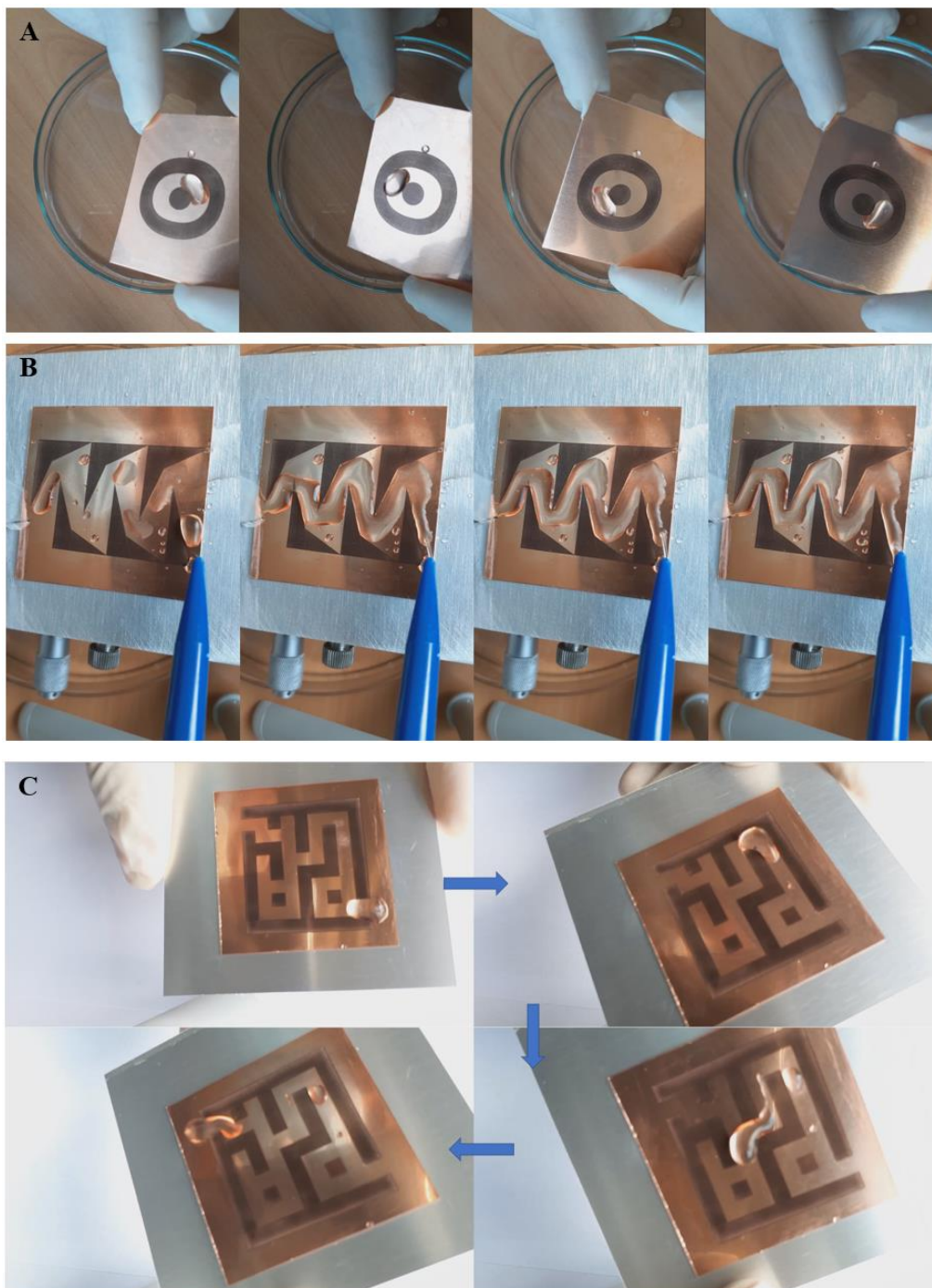


Figure 54. Controlling of water moving following different shapes.

## 4.6 Summary

A simple, fast, one-step process by using laser beam machining under silicone oil was developed. With this process, many materials can be changed from hydrophilic to superhydrophobic surfaces in a short time (few minutes). Besides, laser beam machining under silicone oil process has more advantages than laser and heat treatment process such as saving time, getting high robustness. Effect of changing parameters such as silicone oil height, laser power, scan speed, and step size on the values of CA and SA was also mentioned. These results will be helpful for other researchers in choosing a good fabrication condition to make a superhydrophobic surface in a short time. For example, metals (titanium, copper, aluminum, stainless steel) surface can become superhydrophobic by using nanosecond laser fabricate under silicone oil at 5W laser power, 10mm/s scan speed, 100 $\mu$ m step size, and 0.75mm silicone oil height. While, with ceramics (glass, sapphire) the condition for fabrication superhydrophobic will be different specific for sapphire is 10W - 5mm/s - 100 $\mu$ m - 0.75mm and for glass is 10W - 50mm/s - 200 $\mu$ m - 0.75mm. On the other hand, the effect of silicone oil viscosity is also presented when the conditions for fabrication superhydrophobic surface were 7.5W laser power, 0.75mm silicone oil height, 100 $\mu$ m step size, and 10mm/s scan speed. And when the silicone oil height ranged from 0.5 to 1mm, at high laser power (0.75 and 1W) the superhydrophobic surface can be created at 100 $\mu$ m step size and scan speed from 10 - 20mm/s. Besides, at a big step size from 300 - 400 $\mu$ m and scan speed from 200 - 300mm/s the samples would not show superhydrophobicity (CA < 150° and SA < 10°). In addition, using this new process, the isotropic and anisotropic were presented at the same laser power (7.5W), scan speed (10mm/s), silicone oil height (0.75mm), and different step size (100, 200 $\mu$ m for isotropic, and 300 $\mu$ m for anisotropic).



# **Chapter 5:**

# **Conclusion**

This thesis is started with laser beam machining and heat treatment process for creating a superhydrophobic surface on titanium and glass. This post-process was chosen because it is simple, does not require complicated equipment, does not require chemicals. However, the results of this process point out that the time for heat treatment increases from a few hours (6 hours with titanium) to several days (2 days with glass) so that the sample's surface changes from hydrophilic to superhydrophobic. This is the main reason for the effort to develop and research a new simple process to generate a superhydrophobic surface in a short time with only several seconds or minutes. This new, simple, and fast process use laser beam machining under silicone oil for the fabrication of superhydrophobic surfaces on many substrates. Besides, the effect of changing laser power, step size in both processes was investigated. However, for the new process, more parameters affect fabrication processes such as scan speed, and silicone oil height, the silicone oil viscosity. Besides, the surface robustness of samples fabrication by the new process was compared with the post-process which used laser and heat treatment by a tape test. The key findings in each chapter were summarized below:

(1) A superhydrophobic surface on titanium was fabricated by using laser machining and heat treatment without chemical or complex equipment. The effects of laser power, step size, and pattern design (line or grid) on wettability were investigated. The grid pattern showed better CA and SA than the line pattern at the same condition for fabrication. In line-patterned samples, the critical step size for the surface changing from isotropic wetting state to anisotropic wetting state was reduced from a large to smaller step size when decreasing laser power. For grid-patterned samples when decreasing laser power the critical step size for the lotus effect and petal effect region was reduced. The obtained results could provide a useful guide to select proper parameters to fabricate desired superhydrophobic surfaces. For a high-quality

superhydrophobic surface and with isotropic behavior, the grid pattern was a good candidate. To make a superhydrophobic surface with strong anisotropic behavior to control the water direction, the line pattern is preferred.

(2) Using laser beam machining and heat treatment process for fabricating superhydrophobicity on soda-lime glass was reported for the first time. The glass samples showed good superhydrophobicity ( $CA > 170^\circ$ ,  $SA < 10^\circ$ ) with acceptable transmittance (over 50% in visible light) after post-process. However, the heat treatment time in post-process takes a very long time – 48 hours, which is a disadvantage of this process. On the other hand, the effect of laser power and step size on wettability was presented. Besides, the wettability transition of the glass samples from hydrophilic to superhydrophobic surface after heat treatment can be explained by the increased carbon (organic absorption) and reduction of the OH group on the glass surface. With these results, it can provide guidelines and a reference for controlling wettability and transparency on glass surfaces

(3) A simple, fast, one-step process using nanosecond laser beam machining under silicone oil was developed. With this process, many materials surfaces can be changed from hydrophilic to superhydrophobic surfaces in a shorter time than the post-process. The advantage of laser beam machining under silicone oil in comparison with laser and heat treatment is a short time and single process. The values of CA and SA following the change of parameter processes such as silicone oil height, laser power, step size, and scan speed were reported. These results will be helpful for other researchers in choosing the good condition to making a superhydrophobic surface in a short time. Besides with metallic materials as titanium, copper, aluminum, stainless steel by using laser fabricate under silicone oil at 5W laser power, 10mm/s scan

speed, 100 $\mu$ m step size, and 0.75mm silicone oil height, the samples become superhydrophobic after fabrication. And at conditions for fabrication superhydrophobic surface as 7.5W laser power, 0.75mm silicone oil height, 100 $\mu$ m step size, and 10mm/s scan speed, the effect of silicone oil viscosity is also presented. At high laser power (0.75 and 1W) the superhydrophobic can be created with 100 $\mu$ m step size and scan speed change from 10 - 20mm/s. However, at a big step size from 300 - 400 $\mu$ m and scan speed from 200 - 300mm/s the samples did not show superhydrophobicity (CA < 150°). In addition, by using this process, the isotropic and anisotropic surfaces also were fabricated.

## Reference

1. S. Das, S. Kumar, S. K. Samal, S. Mohanty, and S. K. Nayak, *Ind. Eng. Chem. Res.* **57**, 2727 (2018).
2. B. Y. A. B. D. Cassie and S. Baxter, *Physics* (College. Park. Md). 546 (1944).
3. R. N. Wenzel, *Ind. Eng. Chem.* **28**, 988 (1936).
4. T. Young, *Philos. Trans. R. Soc. London* **95**, 65 (1805).
5. S. Nishimoto and B. Bhushan, *RSC Adv.* **3**, 671 (2013).
6. X. Yao, Y. Song, and L. Jiang, *Adv. Mater.* **23**, 719 (2011).
7. J. Chen, Z. Luo, Q. Fan, J. Lv, and J. Wang, *Small* **10**, 4693 (2014).
8. A. H. A. Lutey, L. Gemini, L. Romoli, G. Lazzini, F. Fuso, M. Faucon, and R. Kling, *Sci. Rep.* **8**, 1 (2018).
9. H. Li, Y. Li, and Q. Liu, *Nanoscale Res. Lett.* **8**, 183 (2013).
10. J. Ge, Y. Si, F. Fu, J. Wang, J. Yang, L. Cui, B. Ding, J. Yu, and G. Sun, *RSC Adv.* **3**, 2248 (2013).
11. P. Zhang and F. Y. Lv, *Energy* **82**, 1068 (2015).
12. J. P. Lee, S. Choi, and S. Park, *Langmuir* **27**, 809 (2011).
13. V. A. Ganesh, H. K. Raut, A. S. Nair, and S. Ramakrishna, *J. Mater. Chem.* **21**, 16304 (2011).
14. C. Dong, Y. Gu, M. Zhong, L. Li, K. Sezer, M. Ma, and W. Liu, *J. Mater. Process. Technol.* **211**, 1234 (2011).
15. D.-M. Chun, C.-V. Ngo, and K.-M. Lee, *CIRP Ann. - Manuf. Technol.* **65**,

519 (2016).

16. Y. Tuo, H. Zhang, W. Rong, S. Jiang, W. Chen, and X. Liu, *Langmuir* **35**, 11016 (2019).

17. C. Juan Yang, X. Song Mei, Y. Ling Tian, D. Wei Zhang, Y. Li, and X. Ping Liu, *Int. J. Adv. Manuf. Technol.* **87**, 1663 (2016).

18. G. Kwak, M. Seol, Y. Tak, and K. Yong, *J. Phys. Chem. C* **113**, 12085 (2009).

19. J. Yong, F. Chen, Q. Yang, U. Farooq, and X. Hou, *J. Mater. Chem. A* **3**, 10703 (2015).

20. C. V. Ngo and D. M. Chun, *Adv. Eng. Mater.* **20**, 1 (2018).

21. C.-V. Ngo and D.-M. Chun, *Appl. Surf. Sci.* **409**, 232 (2017).

22. Z. Yang, Y. L. Tian, C. J. Yang, F. J. Wang, and X. P. Liu, *Appl. Surf. Sci.* **414**, 313 (2017).

23. H. Yan, M. R. B. Abdul Rashid, S. Y. Khew, F. Li, and M. Hong, *Guangdian Gongcheng/Opto-Electronic Eng.* **44**, 587 (2017).

24. Z. Yang, Y. Tian, Y. Zhao, and C. Yang, *Materials (Basel)*. **12**, (2019).

25. Y. Jiao, C. Li, S. Wu, Y. Hu, J. Li, L. Yang, D. Wu, and J. Chu, *ACS Appl. Mater. Interfaces* **10**, 16867 (2018).

26. J. Long, Z. Cao, C. Lin, C. Zhou, Z. He, and X. Xie, *Appl. Surf. Sci.* **464**, 412 (2019).

27. R. Jagdheesh, M. Diaz, S. Marimuthu, and J. L. Ocaña, *Appl. Surf. Sci.* **471**, 759 (2019).

28. P. Fu, X. Shi, F. Jiang, and X. Xu, *Appl. Surf. Sci.* **501**, 1 (2020).

29. C. Yang, X. Jing, F. Wang, K. F. Ehmman, Y. Tian, and Z. Pu, *Appl. Surf. Sci.* **497**, (2019).
30. A. He, W. Liu, W. Xue, H. Yang, and Y. Cao, *Appl. Surf. Sci.* **434**, 120 (2018).
31. Y. L. Zhan, M. Ruan, W. Li, H. Li, L. Y. Hu, F. M. Ma, Z. L. Yu, and W. Feng, *Colloids Surfaces A Physicochem. Eng. Asp.* **535**, 8 (2017).
32. C. V. Ngo and D. M. Chun, *Appl. Surf. Sci.* **435**, 974 (2018).
33. J. Long, M. Zhong, H. Zhang, and P. Fan, *J. Colloid Interface Sci.* **441**, 1 (2015).
34. Y. Shi, Z. Jiang, J. Cao, and K. F. Ehmman, *Appl. Surf. Sci.* **500**, (2020).
35. J. Huang, S. Wei, L. Zhang, Y. Yang, S. Yang, and Z. Shen, *Materials (Basel)*. **12**, (2019).
36. P. Gregorčič, B. Šetina-Batič, and M. Hočevar, *Appl. Phys. A Mater. Sci. Process.* **123**, 1 (2017).
37. D. Wang, X. Wang, X. Liu, and F. Zhou, *J. Phys. Chem. C* **114**, 9938 (2010).
38. Z. Lian, J. Xu, P. Yu, Z. Yu, Z. Wang, and H. Yu, *Met. Mater. Int.* (2019).
39. P. Hauschwitz, R. Jagdheesh, D. Rostohar, J. Brajer, J. Kopeček, P. Jiříček, J. Houdková, and T. Mocek, *Mater. Lett.* **256**, (2019).
40. R. Jagdheesh, P. Hauschwitz, J. Mužík, J. Brajer, D. Rostohar, P. Jiříček, J. Kopeček, and T. Mocek, *Appl. Surf. Sci.* **493**, 287 (2019).
41. J. Long, Q. Weng, W. Hong, Z. Cao, P. Zhou, and X. Xie, *Exp. Therm. Fluid Sci.* **103**, 9 (2019).

42. I. Etsion, *J. Tribol.* **127**, 248 (2005).
43. A. Riveiro, A. L. B. Maçon, J. del Val, R. Comesaña, and J. Pou, *Front. Phys.* **6**, (2018).
44. B. S. Yilbas, M. Khaled, N. Abu-Dheir, N. Aqeeli, and S. Z. Furquan, *Appl. Surf. Sci.* **286**, 161 (2013).
45. X. Liu, P. K. Chu, and C. Ding, *Mater. Sci. Eng. R Reports* **47**, 49 (2004).
46. M. T. Mohammed, Z. A. Khan, and A. N. Siddiquee, *Procedia Mater. Sci.* **6**, 1610 (2014).
47. I. Inagaki, T. Takechi, Y. Shirai, and N. Ariyasu, *Nippon Steel Sumitomo Met. Tech. Rep.* **106**, 22 (2014).
48. T. Jiang, J. Koch, C. Unger, E. Fadeeva, A. Koroleva, Q. Zhao, and B. N. Chichkov, *Appl. Phys. A Mater. Sci. Process.* **108**, 863 (2012).
49. S. Z. Wu, J. N. Wang, L. G. Niu, J. Yao, D. Wu, and A. W. Li, *Appl. Phys. Lett.* **98**, 8 (2011).
50. S. Moradi, N. Hadjesfandiari, S. F. Toosi, J. N. Kizhakkedathu, and S. G. Hatzikiriakos, *ACS Appl. Mater. Interfaces* **8**, 17631 (2016).
51. M. H. M. A. Shibraen, H. Yagoub, X. Zhang, J. Xu, and S. Yang, *Appl. Surf. Sci.* **370**, 1 (2016).
52. T. H. Dinh, C. V. Ngo, and D. M. Chun, *Nanomaterials* **8**, (2018).
53. C. V. Ngo and D. M. Chun, *CIRP Ann.* **67**, 571 (2018).
54. Y. Lin, J. Han, M. Cai, W. Liu, X. Luo, H. Zhang, and M. Zhong, *J. Mater. Chem. A* **6**, 9049 (2018).



55. D. M. Chun, G. Davaasuren, C. V. Ngo, C. S. Kim, G. Y. Lee, and S. H. Ahn, *CIRP Ann. - Manuf. Technol.* **63**, 525 (2014).
56. X. Chen, J. Wen, J. Zhou, Z. Zheng, D. An, H. Wang, W. Xie, R. Zhan, N. Xu, J. Chen, J. She, H. Chen, and S. Deng, *J. Opt. (United Kingdom)* **20**, (2018).
57. A. K. VARSHNEYA and J. C. MAURO, *Inorganic Glasses* (2019).
58. P. Dimitrakellis, A. Travlos, V. P. Psycharis, and E. Gogolides, *Plasma Process. Polym.* **14**, 1 (2017).
59. S. Sutha, S. Suresh, B. Raj, and K. R. Ravi, *Sol. Energy Mater. Sol. Cells* **165**, 128 (2017).
60. L. Zhang, C. H. Xue, M. Cao, M. M. Zhang, M. Li, and J. Z. Ma, *Chem. Eng. J.* **320**, 244 (2017).
61. S. Zhao, J. Zhao, M. Wen, M. Yao, F. Wang, F. Huang, Q. Zhang, Y. B. Cheng, and J. Zhong, *Langmuir* **34**, 11316 (2018).
62. B. Wang, Y. Hua, Y. Ye, R. Chen, and Z. Li, *Appl. Surf. Sci.* **426**, 957 (2017).
63. L. B. Boinovich, A. G. Domantovskiy, A. M. Emelyanenko, A. S. Pashinin, A. A. Ionin, S. I. Kudryashov, and P. N. Saltuganov, *ACS Appl. Mater. Interfaces* **6**, 2080 (2014).
64. K. J. Bachus, L. Mats, H. W. Choi, G. T. T. Gibson, and R. D. Oleschuk, *ACS Appl. Mater. Interfaces* **9**, 7629 (2017).
65. J. Zhi and L. Z. Zhang, *Appl. Surf. Sci.* **454**, 239 (2018).
66. S. Stroj, S. Kasemann, M. Domke, G. Piredda, J. Zehetner, and V. Matylitskaya, *Appl. Surf. Sci.* **420**, 550 (2017).
67. T. Son, E. Yang, E. Yu, K. H. Oh, M. W. Moon, and H. Y. Kim, *J. Mech. Sci.*

Technol. **31**, 5407 (2017).

68. S. Takeda, K. Yamamoto, Y. Hayasaka, and K. Matsumoto, *J. Non. Cryst. Solids* **249**, 41 (1999).

69. E. Ueda and P. A. Levkin, *Adv. Mater.* **25**, 1234 (2013).

70. C. V. Ngo and D. M. Chun, *Adv. Eng. Mater.* **1701086**, 1 (2018).

# Appendices

## Appendix A: Credits & Copyright Permissions

Notes on Copyright Licenses for Reproduction of Text and Figures in this Thesis

### ***Chapter 1:***

For reproducing those figures that have appeared in the following publication with credit to other sources, permission has also been sought from the respective sources.

### ***Chapter 2***

The text excerpts and the figures presented in Chapter Two are reproduced with permission from the following article:

The-Hung Dinh, Chi-Vinh Ngo, and Doo-Man Chun, “*Controlling the Wetting Properties of Superhydrophobic Titanium Surfaces Fabricated by UV Nanosecond-Pulsed Laser and Heat Treatment*”, *Nanomaterials* 2018, 8, 766.

### ***Chapter 3***

The text excerpts and the figures presented in Chapter Three are reproduced with permission from the following article:

The-Hung Dinh, Chi-Vinh Ngo, and Doo-Man Chun, “*Direct laser patterning for transparent superhydrophobic glass surfaces without any chemical coatings*”, *Applied Physics A* 126, 462 (2020).

## Appendix B: The confocal microscope of samples when using laser beam machining under silicone oil

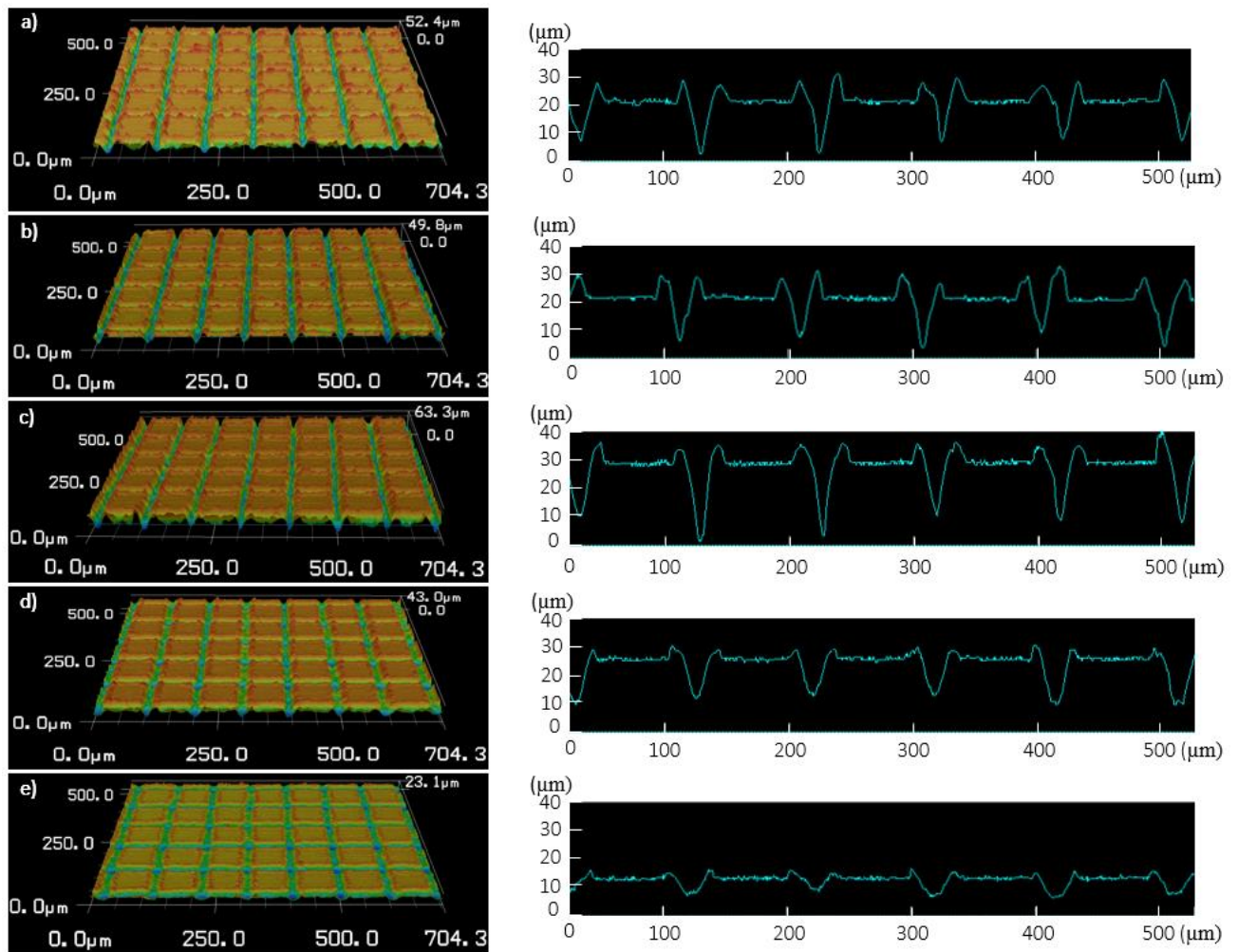


Figure 55. Confocal microscopy images of the samples at 7.5W laser power, 100µm step size, 0.75mm silicone oil height and different scan speeds a) 10, b) 20, c) 50, d) 100, and e) 200mm/s.

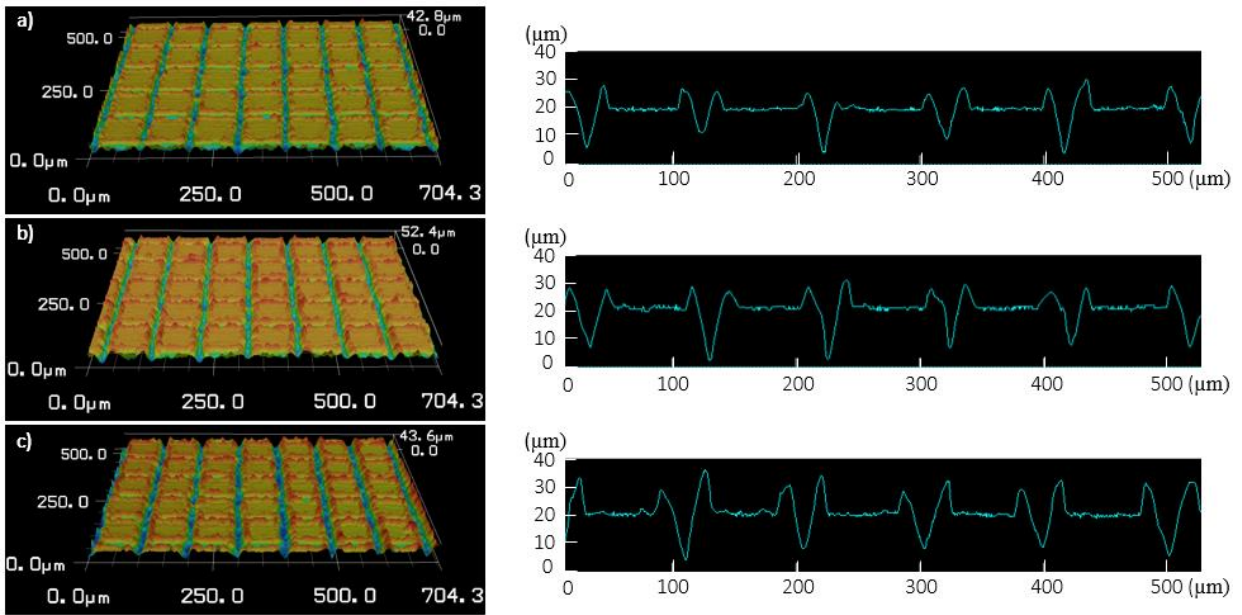


Figure 56. Confocal microscopy images of the samples at 10mm/s scan speed, 100µm step size, 0.75mm silicone oil height, and different laser powers a) 5, b) 7.5, and c) 10W.

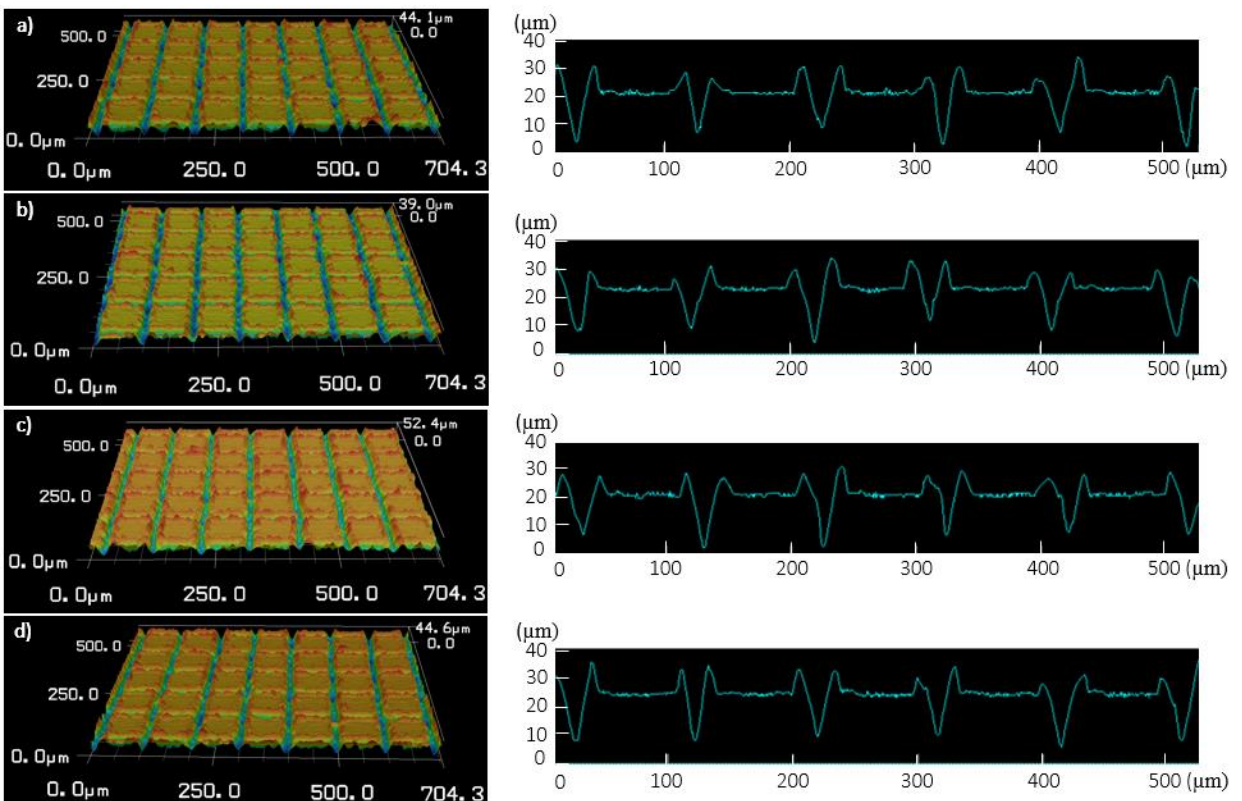


Figure 57. Confocal microscopy images of the samples at 10mm/s scan speed, 7.5W laser power, 100µm step size, and different silicone oil heights a) 0.25, b) 0.5, c) 0.75, and d) 1mm.

## Appendix C: Contact angle and the sliding angle at different parameters

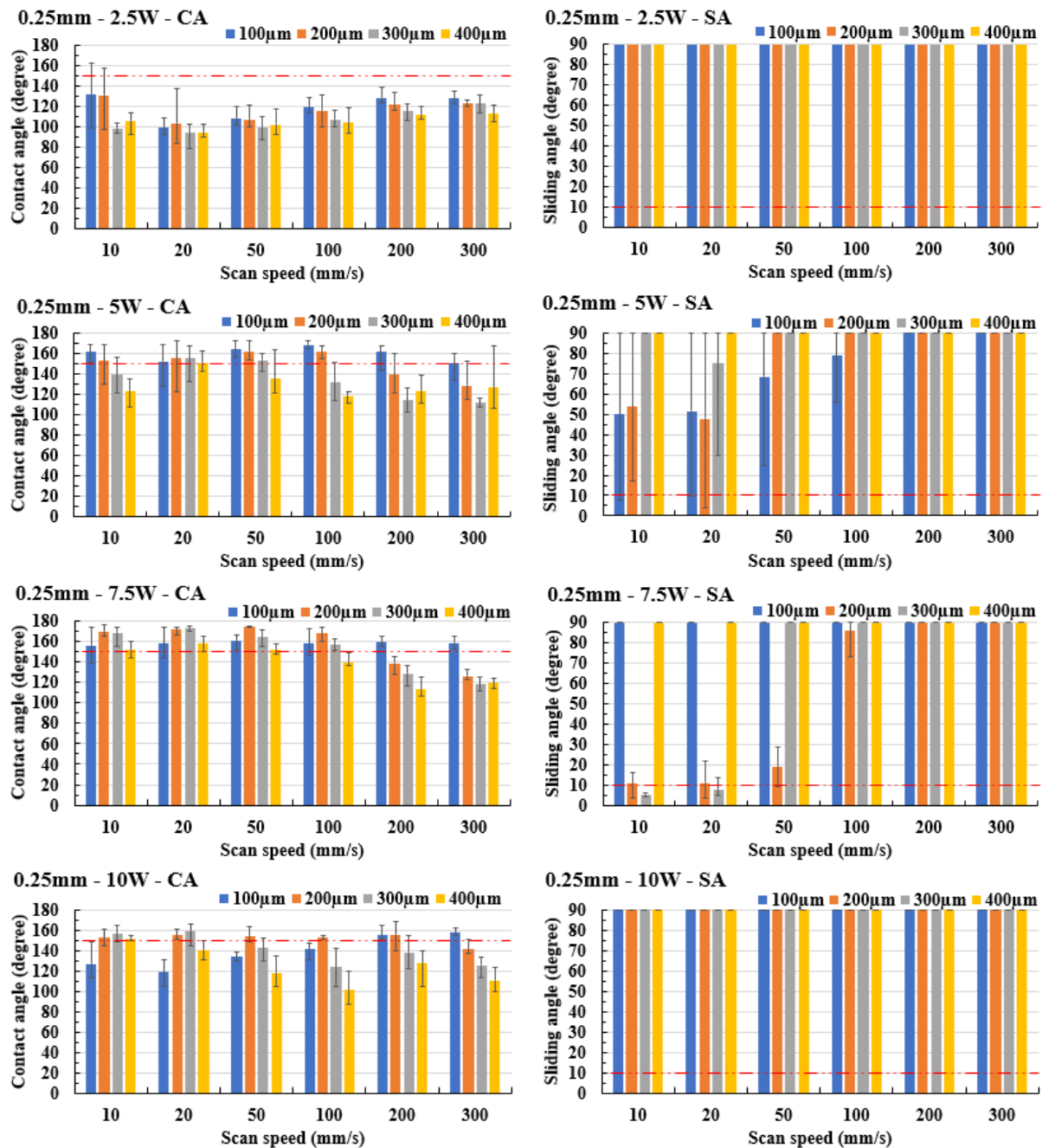


Figure 58. CA and SA on copper surfaces at 0.25mm silicone oil height with different laser power (2.5, 5, 7.5, 10W), step size (100, 200, 300, 400μm), and scan speed (10, 20, 50, 100, 200, 300mm/s).

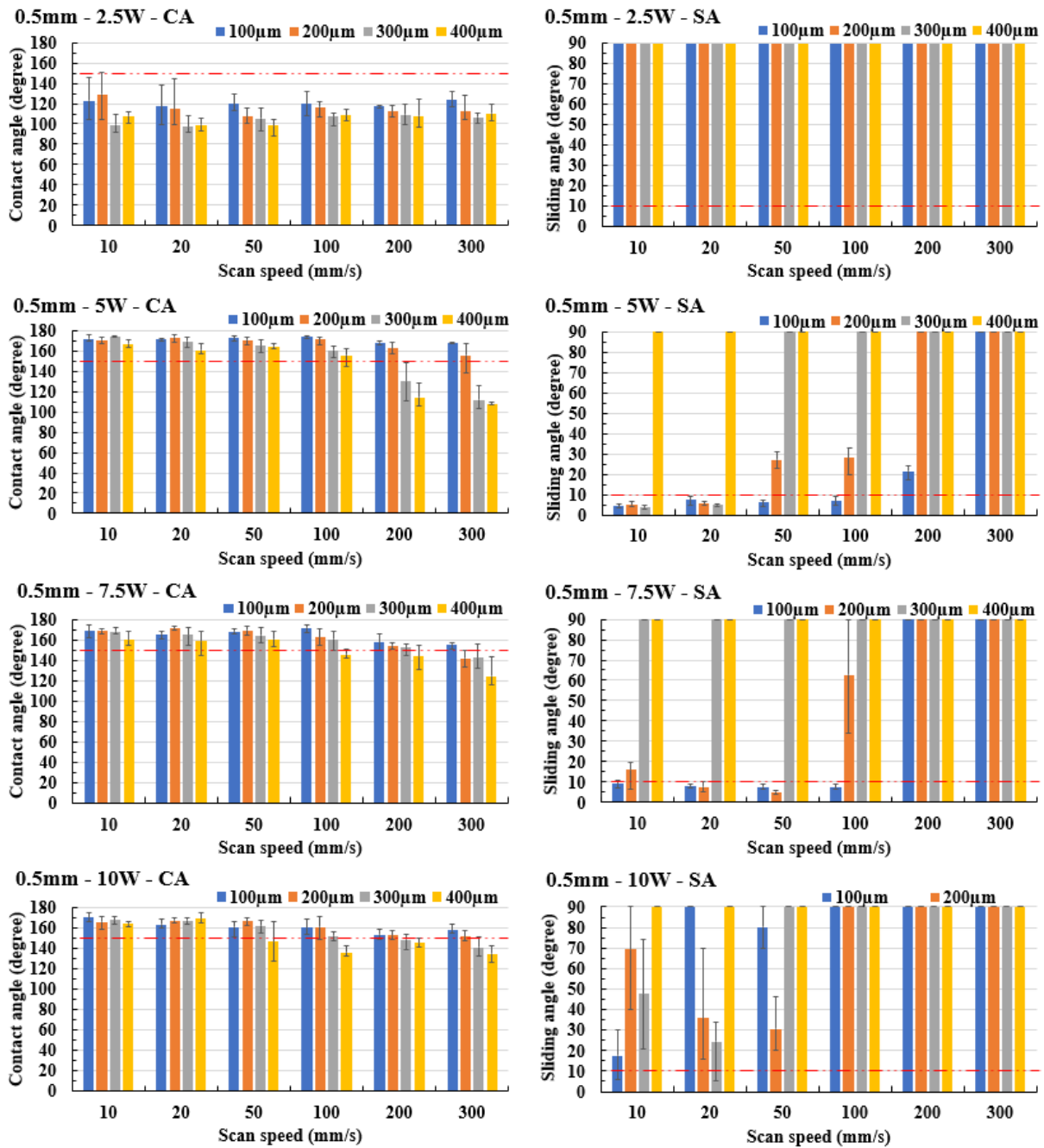


Figure 59. CA and SA on copper surfaces at 0.5mm silicone oil height with different laser power (2.5, 5, 7.5, 10W), step size (100, 200, 300, 400 μm), and scan speed (10, 20, 50, 100, 200, 300mm/s).

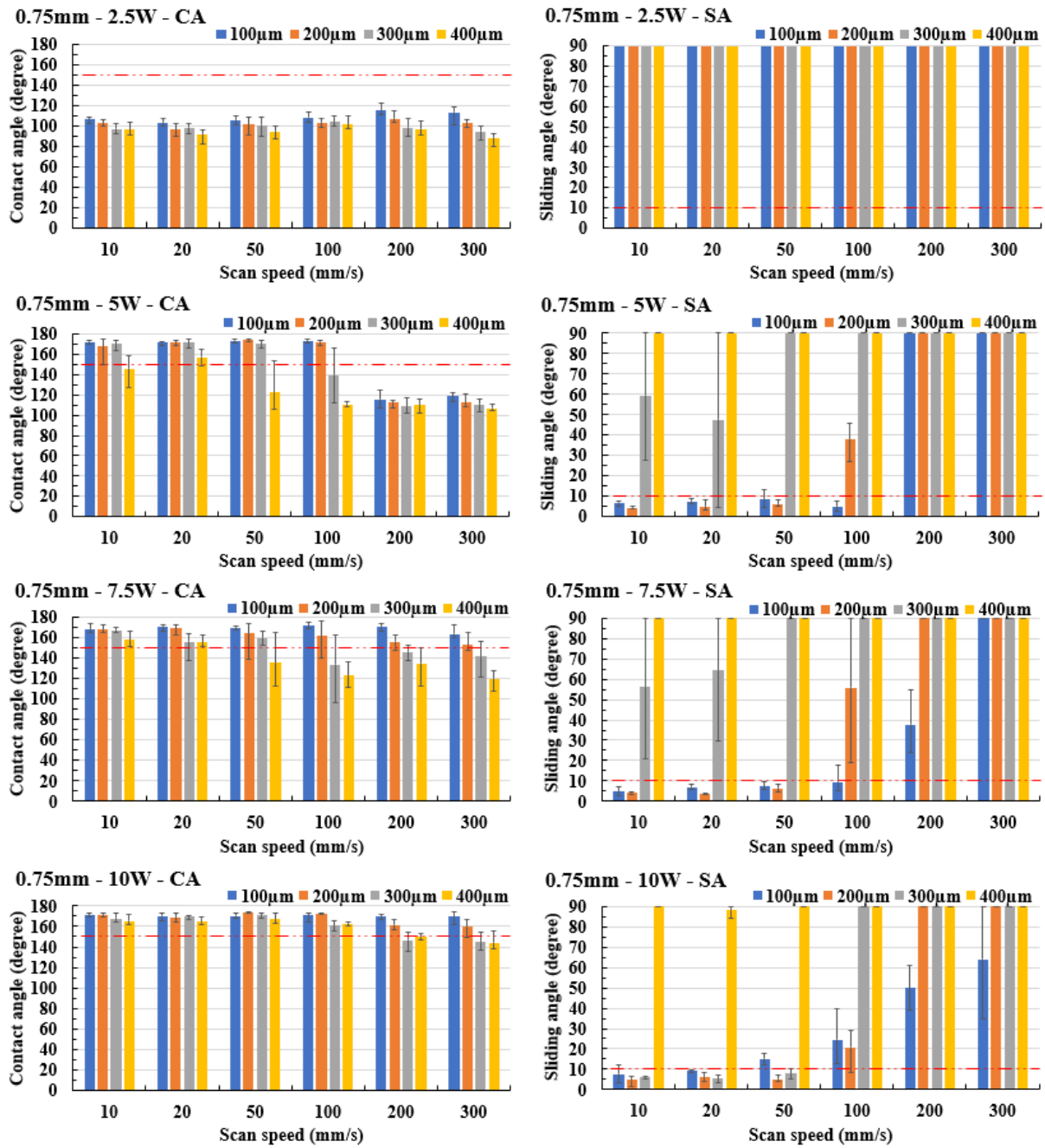


Figure 60. CA and SA on copper surface at 0.75mm silicone oil height with different laser power (2.5, 5, 7.5, 10W), step size (100, 200, 300, 400μm), and scan speed (10, 20, 50, 100, 200, 300mm/s).



## Appendix D: Summary CA and SA of samples when using laser beam machining under silicone oil

Table 10. The presence of CA and SA following the change of laser power (2.5, 5, 7.5, 10W), step size (100, 200, 300, 400 $\mu$ m), scan speed (10, 20, 50, 100, 200, 300mm/s), and silicone oil height (0.5, 0.75, 1mm).

0.5 - 1mm	Laser power (W)	2.5				5				7.5				10			
	Step size ( $\mu$ m)	100	200	300	400	100	200	300	400	100	200	300	400	100	200	300	400
Scan speed (mm/s)	10																
	20																
	50																
	100																
	200																
	300																

*Silicone oil height:*

			0.5mm
			0.75mm
			1mm

